Design of a Subsonic Wind Tunnel for Academic Activities

Jaime Iriarte Martínez
María Nicolle Gómez

Advisor:
Ph. D. Adriana Gómez Gómez
Coadvisor:
Engineer Simón Plata

Mechanical Engineering Program
Electronic Engineering Program
Department of Civil and Industrial Engineering
Faculty of Engineering and Science
Pontificia Universidad Javeriana
Santiago de Cali, Colombia
2025

Santiago de Cali, 6 de julio de 2025

Declaración de obra original

Nosotros, Jaime Iriarte Martínez y María Nicolle Gómez declaramos lo siguiente:

Hemos leído el Acuerdo 535 de 2010 del Consejo Directivo de la Pontifica Universidad Javeriana. «Política de Propiedad Intelectual» y la Normatividad Nacional relacionada al respeto de los derechos de autor. Este anteproyecto representa nuestro trabajo original, excepto donde hemos reconocido las ideas, las palabras, o materiales de otros autores.

Cuando se han presentado ideas o palabras de otros autores en proyecto de grado, hemos realizado su respectivo reconocimiento aplicando correctamente los esquemas de citas y referencias bibliográficas en el estilo requerido

Hemos obtenido el permiso del autor o editor para incluir cualquier material con derechos de autor (por ejemplo, tablas, figuras, instrumentos de encuesta o grandes porciones de texto).

Por último, hemos sometido esta disertación a la herramienta de integridad académica, definida por la universidad.

Atentamente,

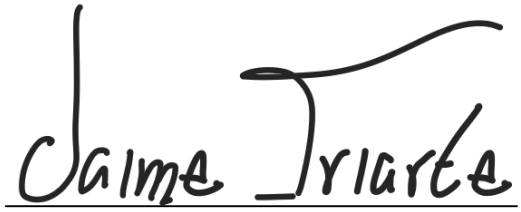

Jaime Iriarte Martínez

María Nicolle Gómez

Abstract

Practical laboratories have proven to be an essential educational resource to demonstrate concepts through hands-on experiments. Therefore, Pontificia Universidad Javeriana – Cali is committed to the development of infrastructure for their teaching process, where students can carry out practical learning experiences. This project aims to design a subsonic wind tunnel as a piece of laboratory equipment for educational purposes to carry out activities in the fluid mechanics field. In addition, this work presents an integration with an Open-loop Control and Data Acquisition (CDAQ) system to regulate airflow speed and measure key variables, such as, temperature, dynamic pressure, and airflow speed in the test section. Thus, a Pitot tube system and Pt100 temperature transmitter were implemented and evaluated through practical tests in a real-size wind tunnel provided by the collaboration between Pontificia Universidad Javeriana – Cali (PUJ-Cali) and Universidad Autónoma de Occidente (UAO).

Keywords: Wind tunnel, Open-loop control, practical laboratories, Computer Aided Design, Programmable Logic Controller.

Contents

List of figures

List of tables

1. Introduction

The integration of hands-on activities from engineering education has become critical to enhance students' training and effectively prepare them for real-world challenges. It is imperative for students to conceptualize theoretical criteria, given that deep teaching approaches lead to better learning outcomes, as a consequence of this, students can achieve the conception of what is studied; that is, it refers to general processes of thought and reasoning about how knowledge is acquired [1].

For this reason, for the specific case of the study of the fluid mechanics, it makes sense to instruct guided practical activities in order to consolidate knowledge. Some authors propose conceptions such as: apply, understand, and see in a new way [1]. Therefore, this project aims to design a wind tunnel that promotes learning by allowing the development of practical activities for engineering students of the *Pontificia Universidad Javeriana Cali.*

A wind tunnel is a piece of equipment specially designed to create a controlled environment in which air can be sucked in or blown to create a regulated airflow. It is a facility used in engineering to study the behavior of objects in the airflow, thus simulating the atmospheric conditions to which an object may be subjected in reality, and the characteristics of the flow can be measured using specialized instruments [2].

This project presents the mechanical design and the electronic implementation of a subsonic wind tunnel intended for academic use, developed through the collaboration between Pontificia Universidad Javeriana – Cali (PUJ-Cali) and Universidad Autónoma de Occidente (UAO). The design not only focuses on the geometric configuration of the tunnel but also integrates a fully functional Control and Data Acquisition (CDAQ) system. This system is fundamental to ensure controlled airflow conditions and accurate measurement of key variables such as temperature, pressure, and flow velocity within the test section. The implementation features an open-loop control scheme operated which allow the user to set target speeds. Finally, the electronic system was also implemented and evaluated through practical tests in a real-size wind tunnel provided by UAO.

2. Theoretical framework

2.1 Definition of a wind tunnel

A wind tunnel is a specialized equipment designed to create a controlled environment into which air can be sucked or blown to create a controlled flow of air. The main goal is to achieve a specific speed and flow pattern, and then observe the behavior and effects of an immersed object. Therefore, the wind tunnel has a transparent window in the test section to see through it. Thus, the simulation allows the identification and measurement of flow characteristics such as temperature, pressure, and velocity [2].

2.2 Wind tunnel classification

Some criteria are used to classify wind tunnels. However, for this project, the most relevant are the path followed by the drawn air and the maximum speed reached by the air.

2.2.1 Classification by circuit type: Open or closed-circuit wind tunnel

In this classification, wind tunnels are divided depending on the circuit flow of air created, so there are open wind tunnels and closed wind tunnels.

Open-circuit wind tunnels draw in air from the surrounding environment, pass it across the test area, and then return it to the surrounding environment. One inherent limitation of this system is its lower efficiency due to the constant loss of air in each cycle. This configuration can also be constructed by blowing the air instead of drawing it, however, this change could hinder getting a laminar flow. A representation of this configuration is shown in Figure 1.

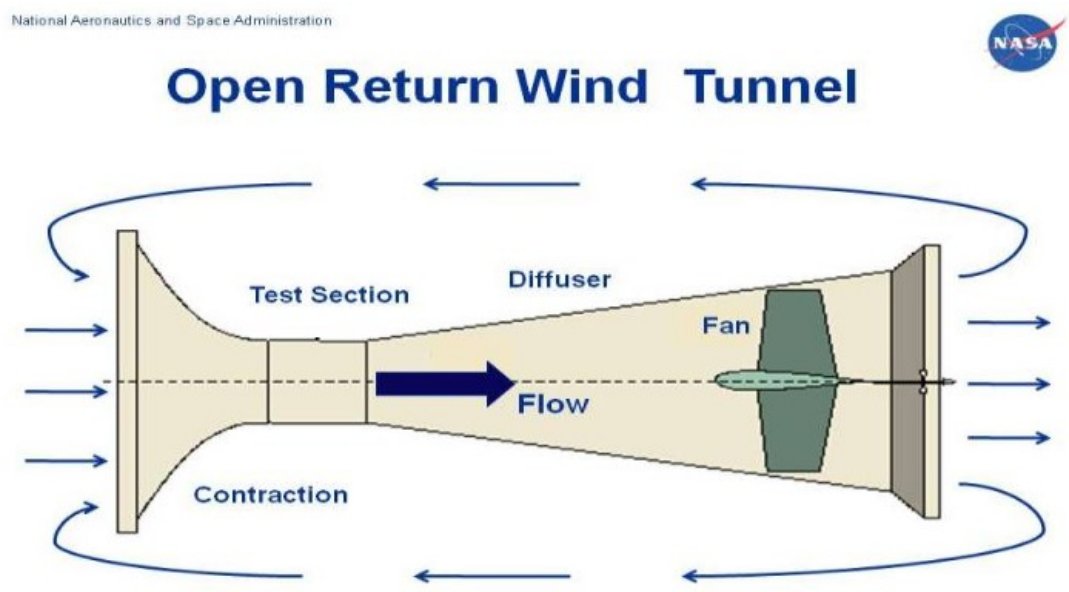

Figure 1. Representation of an open-circuit wind tunnel and its sections, also known as open-return, wind tunnel (from NASA) [2].

Closed-circuit wind tunnels keep the same air circulating, so there is no need to draw air from the surroundings or return it to the environment during operation. This configuration allows the control of variables such as the pressure and the air quality. It also offers higher efficiency through the reuse of the same air volume. However, this increases the fabrication costs. A representation of this configuration is shown in Figure 2.

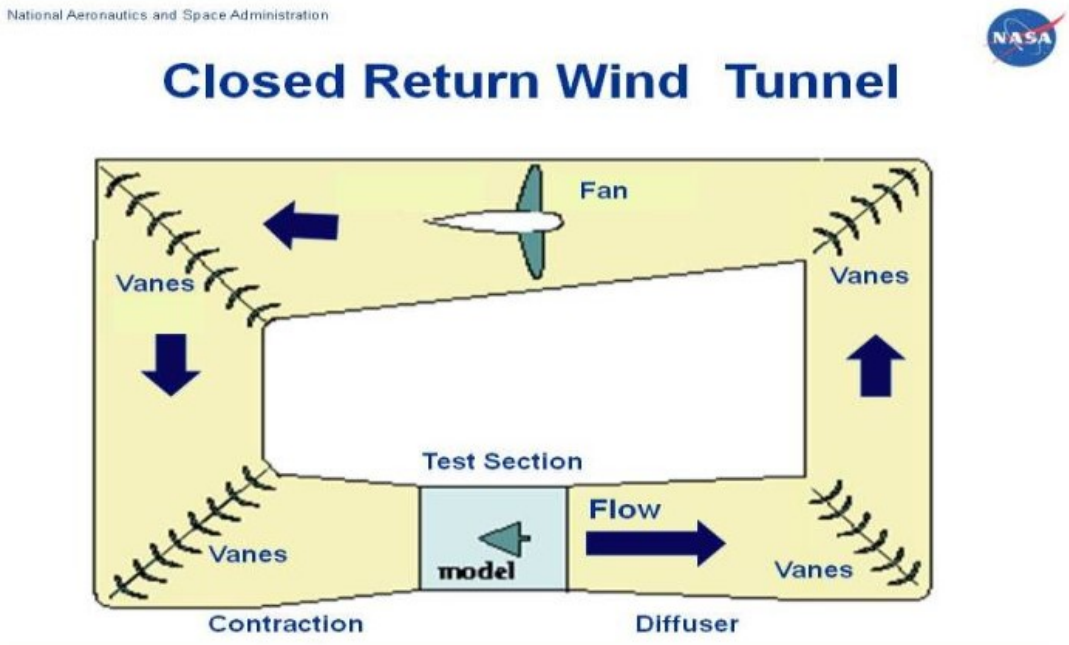

Figure 2. Representation of a closed-circuit wind tunnel and its sections, also known as closed-return, wind tunnel (NASA) [2].

2.2.2 Classification by maximum achieved speed

This criterion categorizes the wind tunnels according to the maximum airflow velocity. Thus, the ratio between the fluid speed and the speed of sound is used to classify them. This ratio is called the Mach number (M) in honor of the physicist Ernst Mach. Considering that the speed of the sound in air at room temperature is approximately 343 m/s, the values M<1 denote the wind tunnels in a subsonic regime, and M>1 in a supersonic regime. The summary of this classification is shown in Table 1.

Table 1. Classification of flows based upon their Mach numbers (taken from [2]).

Range of the Mach number, M	Name of flow, or conditions
M<1	Subsonic
M=1, or near 1	Transonic
1<M<3	Supersonic
3<M<5	High supersonic
M>5	Hypersonic
M>> 5	High Hypersonic

2.3 Nature of the flow

The fluid regime achieved inside the wind tunnel is also an important feature. The regime flow can be laminar or turbulent, the first one is characterized by smooth streamlines and highly ordered motion; otherwise, the turbulent regime is distinguished by velocity fluctuations and a highly disordered motion. In addition, any region in which the flow fluctuates between laminar and turbulent flows before it becomes fully turbulent is called the transition zone, and it is determined by numerous factors including geometry, surface roughness, flow velocity, surface temperature, and fluid type [3].

This phenomenon can be observed injecting some dye streaks into the flow in a glass pipe, as the British engineer Osborne Reynolds (1842–1912) did over a century ago [3]. Figure 3a shows a representation of the laminar regime, and Figure 3b shows the turbulent regime.

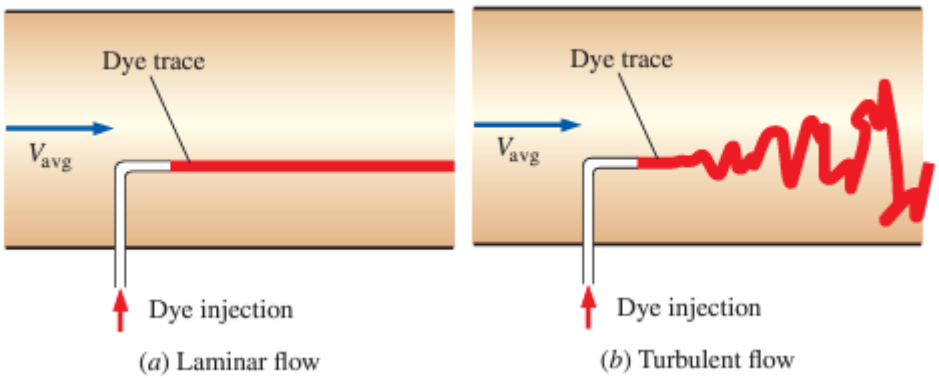

Figure 3. Motion representation of (a) laminar flow, and (b) turbulent flow.

2.3.1Reynolds Number

Osborne Reynolds also discovered, after several experiments, that the flow regime depends primarily on the ratio of inertial forces to viscous forces. This ratio is called the Reynolds number and is expressed for internal flow in a circular pipe as [3]:

$$Re = \frac{Inertial\ forces}{Viscous\ forces} = \frac{V_{avg} \cdot D}{v} = \frac{\rho \cdot V_{avg} \cdot D}{\mu} \qquad \text{Equation 1}$$

Reynolds number is a dimensionless quantity where $V_{avg} =$ average flow velocity (m/s), $D =$ characteristic length of the geometry (diameter for circular pipes, in m), and $v = \frac{\mu}{\rho} =$ kinematic viscosity of the fluid ($^{m^2}/_{s}$).

For flow through noncircular pipes, the characteristic length of the geometry (D) is defined for the hydraulic diameter (D_h), as shown in Equation 2:

$$D_h = \frac{4 \cdot A_c}{p} \qquad \text{Equation 2}$$

where A_c is the cross-sectional area of the pipe and p is its wetted perimeter.

This means that for smalls Reynolds numbers the viscous forces are large enough to control the inertial forces, therefore the fluctuation of the fluid is dominated and keeps it "in line", thus the flow is laminar. On the other hand, the turbulent case is observed for large Reynolds numbers when the inertial forces overcome the viscous forces, thus this latter cannot prevent the random fluctuation of the fluid.

The Reynolds number at which the flow undergoes from laminar transition to turbulence is referred to as the critical Reynolds number Re_{cr}. This parameter's value varies depending on the geometrical configuration and flow characteristics. In the case of internal

flow within a circular pipe, the acknowledged critical Reynolds number stands at $Re_{cr} = 2300$ [3].

As mentioned before, the transition between laminar and turbulent regime is determined by different factors; however, in a controlled space under practical conditions, the flow in a circular pipe is [3].

$R_e \leq 2300$	Laminar Flow
$2300 \leq R_e \leq 4000$	Transitional flow
$R_e \geq 4000$	Turbulent flow

2.4 The Bernoulli equation

"The Bernoulli equation is an approximate relation between pressure, velocity, and elevation, and is valid in regions of steady, incompressible flow where net frictional forces are negligible" as shown in Equation 3 [3]:

$$\frac{P_1}{\rho} + \frac{V^2{}_1}{2} + gz_1 = \frac{P_2}{\rho} + \frac{V^2{}_2}{2} + gz_2 \qquad \text{Equation 3}$$

Where, P/ρ as flow energy, $V^2/_2$ as kinetic energy, and gz as potential energy.

This equation considers the viscous effects are negligible because of the small impact compared to inertial, gravitational, and pressure effects. Due to this consideration, the equation cannot be used within regions of high viscosity or where the flow is not steady. However, it can be used in some regions to determine theoretically the pressure drop and velocity variation in the different sections of the wind tunnel circuit.

The Bernoulli equation relates the energy of the flow along a streamline. Therefore, during the flow, the energy can vary the proportion among flow, kinetic, and potential energy. To observe this in terms of pressure, Equation 3 is multiplied by the density ρ, as shown in Equation 4.

$$P + \rho\frac{V^2}{2} + \rho gz = Cons\tan t\ (along\ a\ streamline) \qquad \text{Equation 4}$$

Each term represents a kind of pressure:

- P is the static pressure in which there is not any dynamic effect incorporated.
- $\rho\, V^2/2$ is the dynamic pressure; it represents the increase in pressure when the moving fluid is stopped isentropically.

- ρgz is the hydrostatic pressure term; its value depends on the selected reference level; it explains the elevation effects due to the weight of the fluid on the pressure. Since it is just a reference level this is not pressure in a real sense.

A graphic representation of these terms is shown in Figure 4:

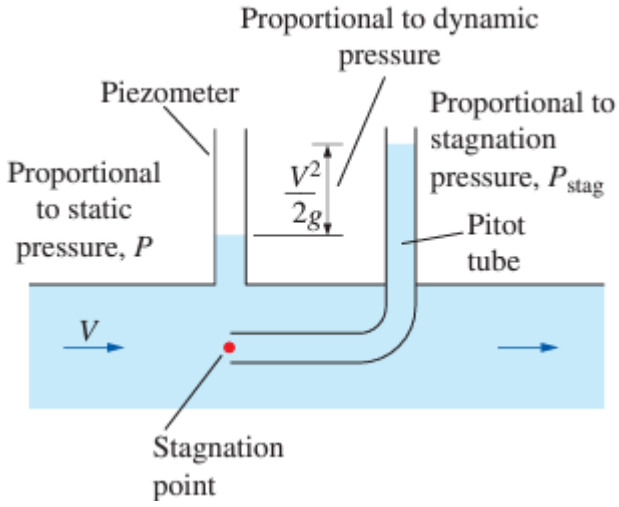

Figure 4. The static, dynamic, and stagnation pressures measured using piezometer tubes [3].

On the other hand, the sum of the static and dynamic pressure is called the stagnation pressure P_{stag}, and it is expressed as shown in Equation 5:

$$P_{stag} = P + \rho\frac{V^2}{2} \qquad \text{Equation 5}$$

The stagnation pressure is the pressure at a point where the fluid is brought to a complete stop isentropically. This is extremely useful because when the stagnation and static pressures are read at a specified location, the fluid velocity at that location is calculated from Equation 6.

$$V = \sqrt{\frac{2 \cdot (P_{stag} - P)}{\rho}} \qquad \text{Equation 6}$$

2.5 Theory of boundary layer

This theory says the molecular air layer directly in contact with the surface remains attached to it. Then, as the distance from the surface increases, the layers move further apart from each other, increasing their velocity to the point where the air layer velocity is equal to the free stream velocity. The boundary layer thickness is simply defined as δ, the distance from the point of zero velocity to the point where the velocity reaches 99% of the free stream velocity. A simple representation of the velocity is shown in Figure 5, the velocity of the air layer that touches the surface is considered zero.

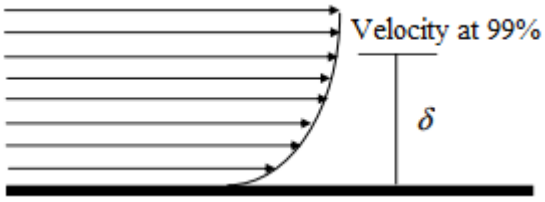

Figure 5. Behavior of the velocity in the boundary layer

The boundary layer divides the flow in two regions, inside of the layer the viscosity fluid causes viscous shearing forces. However, outside of this region, the velocity remains constant in the radial direction, and the frictional effects are negligible. Notice that inside of the boundary layer is not possible to use the Bernoulli equation due to viscous effects, however, outside of this region the viscosity is negligibly small compared to inertial, gravitational, and pressure effects, so Equation 3 can be used.

The boundary layer has a significant property. Through this, the pressure in the free air stream is transmitted to the contact surface, allowing the measurement of the velocity since the static pressure can be measured.

2.6 Important parameters for model similarity and dimensionless numbers

There are fundamental principles to model low-speed aerodynamic flows, these are three: (1) conservation of mass, (2) force and motion, which are related by Newton's Second Law, and (3) energy exchanges which are governed by the First Law of Thermodynamics [4]. In addition, properties such as density, velocity, pressure, strain rate, internal energy, and viscosity of fluids suffer variations due to changes in pressure and temperature, then a body that is moved in a fluid experience forces due to these properties. Therefore, it is important to mention these forces:

$$Inertial\ force = \rho l^2 V^2 \quad \text{Equation 7}$$

$$Viscous\ force = \mu V l \quad \text{Equation 8}$$

$$Gravity\ force = \rho l^3 g \quad \text{Equation 9}$$

$$Elastic\ force = \rho a^2 l^2 \quad \text{Equation 10}$$

Where ρ is the density, l is a characteristic dimension of the phenomenon, V is the velocity, g is the acceleration of gravity and a is the velocity of the mechanical waves in the fluid which is related to the elasticity of the fluid.

The conduction of experiments with scale models is the main activity of the wind tunnels; thus, it is necessary to transform Equation 7, Equation 8, Equation 9, and Equation 10 dimensionless ratios that can be effectively used to predict large-scale behavior. Dividing

the inertia force (Equation 7) by each of the others (Equation 8, Equation 9, and Equation 10) gives three force ratios that are the most relevant expressions of the dimensionless coefficients to study wind tunnels.

$$Reynolds\ number = \frac{Inertia\ force}{Viscous\ force} = \frac{\rho V l}{\mu} \qquad \text{Equation 11}$$

$$Mach\ number = \frac{Inertia\ force}{Elastic\ force} = \frac{V}{a} \qquad \text{Equation 12}$$

$$Froude\ number = \sqrt{\frac{Inertia\ force}{Gravity\ force}} = \sqrt{\frac{V^2}{lg}} \qquad \text{Equation 13}$$

Note that the Reynolds number (Equation 11) and Mach number (Equation 12) have been discussed previously to classify the velocity and flow regime. However, these appear again as dimensionless coefficients because they are the most important similarity parameters for experiments in which the model remains stationary during data collection. On the other hand, the Froude number (Equation 13) is important for flows in which there is a free surface, such as flow in open channels. The Froude number will also arise as an important similarity parameter if there are unsteady boundary conditions; however, this number will not appear if the fluid body forces are neglected [3], [4].

Therefore, the dimensionless numbers arise as parameters of similarity between models.

> *"…The nondimensional functions for fluid velocity components, pressure coefficient, density, viscosity, and temperature will then be the same for the model and the full-scale flows. In turn the force and moment coefficients will be the same for the model and full-scale flows" [4].*

2.7 Loss coefficient, pressure loss, head loss, and power required for flow

The loss in a section is defined as the mean loss of total pressure sustained by the stream in passing through the particular section. The definition of **loss coefficient** K_L is given in dimensionless form by the ratio of the pressure loss ΔP_L in the section to the dynamic pressure $\frac{1}{2}\rho \cdot V^2$ at the entrance to the section, as shown in Equation 14.

$$K_L = \frac{\Delta P_L}{\frac{1}{2}\rho \cdot V^2} \qquad \text{Equation 14}$$

In practical cases, it is convenient to rewrite the pressure in terms of $\Delta P = \rho g h$ (from fluid statics). By substituting this expression into Equation 14 and isolating h, it is possible to determine the equivalent fluid column height, known as the **head loss** h_L , as shown in Equation 15.

$$h_L = K_L \cdot \frac{V^2}{2g} \qquad \text{Equation 15}$$

Along a pipe there are losses due to friction, which cause **pressure drops** that are represented also as ΔP_L. To calculate the pressure drops in a section, there are several formulas. This work proposes to work with the Darcy-Weisbach model which allows the evaluation of pressure drops for several conditions: laminar or turbulent flow, smooth or rough surfaces, circular or noncircular pipes, horizontal or inclined pipes of constant cross-sectional area, as shown Equation 16 [3]. In addition, the head loss of this pipe section is expressed by Equation 17.

$$\Delta P_L = f \frac{L}{D_h} \frac{\rho V_{avg}^2}{2} \qquad \text{Equation 16}$$

$$h_L = \frac{\Delta P_L}{\rho g} = f \frac{L}{D_h} \frac{V_{avg}^2}{2g} \qquad \text{Equation 17}$$

Where $\frac{\rho V_{avg}^2}{2}$ is the dynamic pressure, f is the friction factor, L is the length of the section where the pressure drop is to be calculated and D_h is the hydraulic diameter. By comparing Equation 15 and Equation 17, it can be seen that for a duct with constant cross-sectional area, such as the test section, the local section loss coefficient is related to the friction factor by Equation 18.

$$K_L = f \frac{L}{D_h} \qquad \text{Equation 18}$$

The friction factor depends on the Reynolds number R_e and can be calculated by an iterative algorithm purposed by Prandtl equation. It starts by setting an initial value of f far away, such as $f = 1$ .Then, Equation 19 is iterated about 5 times leading this result to convergence. [3].

$$f = \left[2 \cdot Log_{10}\left(R_e \cdot \sqrt{f}\right) - 0.8\right]^{-2}$$ Equation 19

It is relevant to identify the power required to maintain the flow. Therefore, once the pressure drop is known, the **required pumping power** $\dot{W_{pump}}$ to overcome the pressure loss is determined from Equation 20 and Equation 21 [3].

$$\dot{W_{pump}} = \dot{V}\ \Delta P_L$$ Equation 20

$$\dot{V}\ = V_{avg}\ A_c$$ Equation 21

Where V_{avg} is the average flow velocity, A_c is the cross-sectional area of the pipe, $\dot{V}$ is the volume flow rate.

2.8 Sensors & variable measurements

In wind tunnels, the data acquisition stage plays a crucial role in obtaining detailed information about the behavior of the test model. In the test section, different specialized measurement tools are employed to capture and record accurate data on the airflow and aerodynamic forces acting on the model. Among the sensors used are pressure transducers to measure pressure distributions, anemometers to characterize the flow velocity profile, aerodynamic balances, load cells to measure aerodynamic forces, pressure microphones for aerodynamic noise studies, and so on. In addition, temperature sensors are used to monitor the thermal conditions of the flow and the wind tunnel environment. This range of sensors allows accurate and reliable data to be obtained during the model in aerodynamic testing.

To determine the flow characteristics, it is necessary to define the type of variables to be studied, and thus define the measuring instruments which are strategically located in the test section. Their calibration is crucial to ensure the accuracy and reliability of measurements.

This project just considers the measure of flow speed, temperature, and pressure inside the tunnel. Therefore, it is proposed deepen in this measurement sensors.

A relevant characteristic of the flow is its velocity, which can be calculated by the difference between its stagnation pressure P_{stag} and its static pressure P in a point, as shown in Equation 6. This can be measured with a Pitot tube, which consists of two small tubes, one of them with a frontal orifice (which measures the stagnation pressure) and the

other one with lateral orifices (which measures the static pressure). Figure 6 shows a schematic of this device.

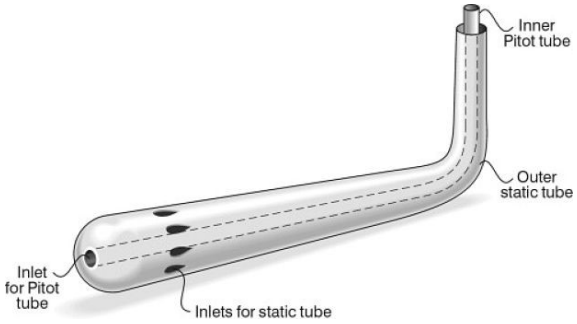

Figure 6. Pitot tube

Another way to characterize the flow velocity profile is by using anemometers:

- Anemometers provide data on the speed and direction of flow at different locations within the wind tunnel, the anemometer is equipped with cups or propellers attached to a central shaft that rotates in the fluid (Figure 7). This rotation activates a tiny electric generator that facilitates an accurate measurement, allowing the user to visualize how the air velocity is distributed around the model [5].

Figure 7. Rotating cup anemometers [1]

[1] Image obtained from "https://www.matecmedicion.com.ar/producto/anemometro-de-copelas-an-1-con-indicacion-digital-y-alarmas/" Matec Medición srl, anemometer with digital display and alarms.

For the study variable "pressure", it is common to find the following measuring instrument:

- Pressure transducers: the operation of this device is based on the conversion of physical pressure into a measurable electrical signal. By means of various principles such as variable resistance, capacitance and piezoelectric effect, pressure distributions on the surface of the model can be measured, shows the operation in Figure 8. These measurements are essential for understanding how airflow interacts with the geometry of the model and generate crucial information about downforce at different points [5].

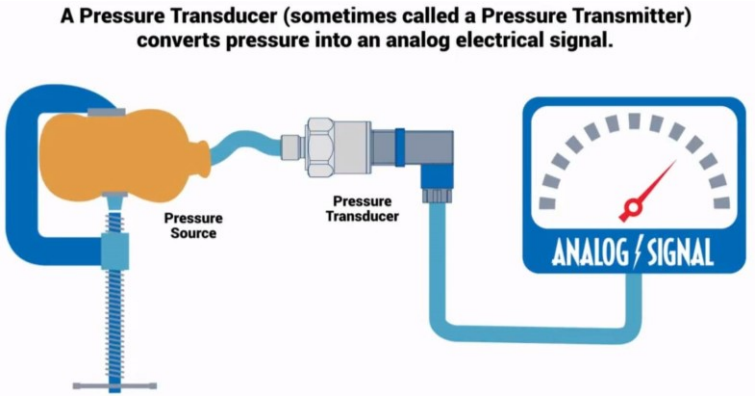

Figure 8. Pressure transducer[2]

Temperature is another variable that can be studied in the wind tunnel, the commonly used measuring instrument is the hot wire anemometer.

- Hot wire anemometer: A normal thermal anemometer measures the velocity of the fluid by detecting changes in heat transfer using a small, electrically heated sensor (a wire or thin film) exposed to the fluid under study (see Figure 9).

[2] Image obtained from "https://www.omega.com/en-us/resources/pressure-transducers-how-it-works" Omega Engineering, Inc.

Figure 9. Hot wire anemometer[3]

[3] Image obtained from "https://www.directindustry.es/prod/sefram-instruments/product-7902-2277957.html" VirtualExpo Group

3. Estate of art

Aerodynamic research has been crucial in the development and advancement of space and aeronautical exploration. One of the pillars of this research is the wind tunnel, an essential tool that allows simulating airflow conditions on scale models and aerodynamic components. At the heart of this technology is a deep understanding of the fundamental principles of fluid mechanics and aerodynamics. Some of the main and most important wind tunnels that exist internationally are shown in Table 2.

The trisonic wind tunnel is capable of operating across the three main flow speed classifications: subsonic, sonic, and supersonic, allowing aerodynamic tests to be conducted under any of these regimes within a single facility. Thanks to its design, which incorporates variable-geometry nozzles and adjustable control systems, this type of tunnel enables the analysis of a wide range of flow phenomena, from laminar behavior to the formation of shock waves and compressibility effects.

Table 2. Major International Wind Tunnels

Description	**Location**	**Type**		**Size (Test volume)**	**Type of flow**
		Open	**Closed**		
NASA Langley Transonic Dynamics Tunnel (DTT)[4]	Hampton, Virginia, United States		X	36,7 m^3	Transonic

[4] Data obtained from the "https://www.nasa.gov/image-article/transonic-wind-tunnel-nasa-langley/" information of Transonic Wind Tunnel at NASA Langley.

Description	Location	Type		Size (Test volume)	Type of flow
		Open	Closed		
Wind Tunnel of the German Institute for Aerodynamics and Space Propulsion (DLR)[5]	Göttingen, Germany		X	-	Trisonic
U.S. Air Force High Speed Wind Tunnel (Arnold Engineering Development Complex, AEDC)[6]	Tullahoma, Tennessee, United States		X	18,9 m^3	Supersonic / High Hypersonic
European Transonic Wind Tunnel (ETW)	Colonia, Germany		X	11,025 m^3	Transonic & Subsonic
European Space Agency (ESA) Wind Tunnel	Noordwijk, South Holland, Netherlands		X	1,35 m^3	Supersonic
Delft University of Technology (TU Delft) High Speed Wind Tunnel	Delft, South Holland, Netherlands	X		5,6 m^3	Subsonic

[5] Data obtained from the "https://www.dlr.de/en/research-and-transfer/research-infrastructure/trisonic-wind-tunnel-tmk" Principal web site to Deutsches Zentrum für Luft- und Raumfahrt e.V.

[6] Data obtained from the "https://www.arnold.af.mil/About-Us/Fact-Sheets/Display/Article/409293/propulsion-wind-tunnel-facility/" this wind tunnel are in the arnold air force.

3.1 Antecedents

The wind tunnels presented in the following table play a fundamental role in the research and development of new technologies and in the training of professionals in engineering. Table 3 shows the main characteristics of wind tunnels in Colombia, including their location, description, specific applications, and owner.

- Industrias Metalúrgicas La Macarena Ltda: This company's activity in the calibration of dryer fans may require airflow simulations and testing, which could potentially involve the use of wind tunnels for performance evaluation and optimization.

- Laboratorio de Aeronáutica Universidad de San Buenaventura: This laboratory be engaged in activities related to aerodynamics and airflow testing, which could involve the use of wind tunnels for research and practical experiments in the field of aeronautics.

- Universidad Nacional (Medellin): The wind tunnel at Universidad Nacional is used for testing purposes and airflow simulations, contributing to research and practical activities in the field of aerodynamics.

- Universidad Nacional (Bogotá): Is used for subsonic airflow simulations, playing a vital role in both academic research and hands-on engineering applications in aerodynamics.

- Universidad de los Andes: The testing area with removable walls at Universidad de los Andes could be used for practical experiments and airflow simulations, contributing to research and activities in the field of aerodynamics and engineering.

- U.I.S. Bucaramanga: The wind tunnel at U.I.S. Bucaramanga is used for various evaluations, including range hood assessments, which may involve airflow simulations and testing for practical applications in engineering and environmental studies.

- U. Tecnológica de Pereira: The wind tunnel is utilized for practical activities related to air conditioning practices, specifically focusing on the recommended air velocities for evaporators.

- Universidad del Valle: The activities at Universidad del Valle related to fluid and thermal practices, particularly in simulating ambient airflow for spray applications, may require the use of wind tunnels for practical experiments and research.

- Spraying Systems de Colombia S.A: The activities at Spraying Systems de Colombia S.A. related to simulating ambient airflow for spray applications may involve the use of wind tunnels for practical experiments and research in the field of fluid mechanics.

- Universidad Autónoma de Occidente: The activities related to studying aerodynamic forces on a wing foil NACA-2412 may involve the use of wind tunnels for practical experiments and research in the field of aerodynamics.

Table 3. Wind tunnels in the country (Modified from [6]).

Owner	Purpose	Additional information	Location
Industrias Metalúrgicas La Macarena Ltda.	Calibration of dryer fans	-	Risaralda
Laboratorio de Aeronáutica Universidad de San Buenaventura	For simulations in AAAcad (CAD program) and Aerocad (CAD program)	-	Bogotá
Universidad Nacional	Ergonomic Simulation Module	Length 6m , Circular section 0.3048m diameter. Max. speed 7m/s	Medellín
Universidad Nacional	-	Length 3.2m, Octagonal cross-section 0.65 diameter. Max. speed 12m/s	Bogotá

Owner	Purpose	Additional information	Location
Universidad de los Andes	Testing area with windows and all its walls are removable	Length 1.2m, Cross Section Rectangular 0.4 1x 0.43m Max Speed 27m/s	Bogotá
U.I.S. Bucaramanga	Equipment Conditioned for All Types of Range Hood Evaluations	Length 3.5m, circular cross-section: 0.3m diameter Max. speed 5.6m/s	Bucaramanga
U. Tecnología de Pereira	Air conditioning practices, the recommended velocity for air in evaporators is 2-3 m/s.	Length 2.27m, Rectangular cross-section: 0.26x 0.26m Max speed 2.6m/s	Pereira
UPB	Fluid and thermal practices.	Length 5.120m, Circular cross-section: 0.5 diameter Max. speed 10m/s	-
Universidad del Valle	Fluid and thermal practices.		Cali
Spraying Systems de Colombia S.A.	Simulate ambient airflow for spray applications.	Rectangular cross-section: 2 x 2 ft, its speed can be adjusted from approximately 5 ft/s to 200 ft/s (1.5 to 60 m/s)	Bogotá
Univeridad Autonoma de Occidente	Studying aerodynamic forces on a wing foil NACA-2412	Rectangular test section : 0.4 m wide and 0.27 m high, and a length of 1.0 m. speed between 2 and 19 m/s	Cali

A significant technological increase in wind tunnels has been observed, thus allowing the development of simulations with greater precision, and facilitating the possibility of applying these studies in different fields. The growing need for improvements drives the development of tests that allow different situations to be simulated, such as:

- Wind tunnel for high Reynolds numbers: Initially, wind tunnels operated under normal atmospheric conditions, however, the results did not match the Reynolds data and numbers of the full-scale aircraft. Therefore, the specific solution was to increase the pressure to a value greater than the standard and the density, for this reason it is necessary to increase the Reynolds number [7].
- Free Flight Wind Tunnel: Traditionally, in wind tunnels, aircraft models are attached to supports to measure aerodynamic forces, however, it limits the ability to accurately simulate the real flight, restricting the behavior of the prototype. For this reason, we have opted for electronic transmission through different cables and processing units attached to the model, this allows to obtain data without the interference of supports, simulating with high accuracy the behavior of the sample during its operation [7].
- Environmental Wind Tunnel: Their primary aim is to examine flows proximate to architectural structures, alongside assessing static and dynamic loads impacting buildings. Additionally, they undertake investigations encompassing topics such as soil erosion and air pollution. These wind tunnels are crafted to replicate the Earth's boundary layer, typically with a thickness of 304.80 meters to 609.60 meters [4].

3.2 Normative

The regulations that academic laboratories must comply with are regulated by different entities such as the Ministry of Education and the Colombian Institute of Technical Standards and Certification (ICONTEC). These regulations are crucial to ensure the safety, quality, and effectiveness of laboratory activities within educational institutions.

The Colombian Technical Standard NTC 4595 establishes specific guidelines for the planning and design of academic facilities and environments in Colombia, with the main objective of improving the quality of educational service. This standard focuses on ensuring that facilities are adequate and safe, and adapted to local, regional, and national conditions. In addition, it has a strong focus on environmental sustainability, promoting designs that minimize operating costs and environmental deterioration.

4. Problem statement

The teaching of engineering can be a struggle for both teachers and students; for this reason, there are tools that seek to support this training process. Among the most relevant are practical activities, which have proven to be an essential educational resource for didactic and dynamic learning where experimentation and analysis of results are materialized. Some authors consider that an essential part of engineering learning takes place in the workshop, resulting in an optimal way to synthesize the topics covered in theoretical lectures [8]. Therefore, it is of utmost importance to carry out experimentation from the early days of classes, unlike the traditional classroom where students acquire knowledge passively [1].

Moreover, the didactics of fluid mechanic sciences in engineering can be challenging in the educational field, underscoring the importance of having a meticulously designed set of experimental tasks to achieve effective learning in this area. In the specific context of the *Pontificia Universidad Javeriana Cali* (*PUJ-Cali*), for example, some related subjects, such as heat transfer, it is currently limited to a set of lectures. Hence, there is also an opportunity to support the development of practical experiences in some other related areas of fluid mechanic [7].

In the current market, there are equipment options available for conducting laboratory practices across various fields. However, it should be noted that they can be expensive, not only in terms of initial acquisition but also in relation to their long-term maintenance, with an approximate cost ranging from $50,000 to $100,000[7] USD. Furthermore, when opting for commercial equipment, there is a limitation in the ability to make significant modifications to adapt them to the diverse needs that may arise in the educational setting. This constraint on flexibility restricts the potential for students to fully engage and explore, as they are unable to experiment with specific adjustments that could enrich their practical learning experiences.

[7] Data obtained from the "*Centro de Automatización y Procesos*" CAP in PUJ Cali.

Consequently, with calculations and simulations, this project speculates how the design of a wind tunnel would be, such that allow the development of practical activities for engineering students at *Pontificia Universidad Javeriana Cali?*

5. Justification

Throughout teaching and learning history, the academic field has seen and registered the relationship between hands-on during the academic process with proven learning systems. Engineering programs are not the exception; as a practical profession, educational institutes aim to prepare students for practice situations of engineering; therefore, instructional laboratories have been an essential part of undergraduate and graduate studies [1].

The construction of laboratories corresponding to the topics taught in this discipline is crucial to provide students with the opportunity to apply the theoretical concepts acquired, thus strengthening their understanding, skills, and going beyond to gain knowledge in a practical learning environment, which is a fundamental competence of engineers [1]. In fact, some research made by Shiavi and Brodersen [9]. reveals that laboratory work is considered by engineering students as the preferred environment for learning instead of attending lectures.

Moreover, research has identified six essential functions of experimental work. Indeed, the Laboratory Development Committee of the Commission on Engineering Education reported the main functions and objectives of this type of activity are [2]:

- Familiarization
- Model identification
- Validation of assumptions
- Prediction of the performance of complex systems
- Testing for compliance with specifications
- And exploration for new fundamental information

Emphasizing the importance of these functions and objectives, Ernst [10]. states that: "The role of the undergraduate instructional laboratory is to teach student engineers to perform these six functions. Hence the primary goal of undergraduate laboratories is to inculcate into the student the theory and practice of experimentation. This includes instrumentation and measurement theory." A wind tunnel is such an instrument that could comply with what was previously mentioned.

Therefore, this project intends to design one of these devices for educational purposes, to provide a piece of laboratory equipment in the *PUJ-Cali* capable of demonstrating concepts of fluid mechanics. This device will address the educational process of engineering students and boost the use of academic laboratories as a didactic tool for learning, involving activities of analyzing samples in a controlled flow environment under low-speed conditions. The anticipated impacts for the students include: reinforcement of theoretical knowledge through experimentation, development of practical and technical skills, and encouragement of innovation since access to this experimental facility promotes applied research, supporting student-led design projects, simulations, and prototype validations. Moreover, it will broaden the pool of practical laboratory activities for the student community that has taken related subjects to this area, which has reached an average of 443 members every semester, with a report of 3549 participants who have taken such subjects from 2019 to 2021 in PUJ Cali, according to internal data obtained from the Engineering and Sciences Faculty[8].

This project is suitable for integration into various engineering subjects, for example:

- Fluid Mechanics: Experiments involving pressure and velocity measurements, flow regime analysis (laminar vs. turbulent), and application of Reynolds number and Bernoulli's equation.
- Heat Transfer: Analysis of convective heat exchange with airflow across surfaces.
- Mechanical Design: Structural modeling, selection of materials, CAD development, and performance testing of scale models under controlled airflow conditions

This is aligned with the criteria for ABET certification, which includes an ability to develop and conduct appropriate experimentation, analyze and interpret data, and use engineering judgment to draw conclusions.

[8] Internal report of PUJ Cali students who have taken the courses: *Análisis de Estructuras, Diseño I, Diseño II, Diseño Integrad. de Producto I, Diseño Integrad. de Producto II, Estructuras, Estructuras Metálicas, Máquinas Térmicas y de Fluidos, Materiales de Constr. Altenat, Mecánica de Fluidos, Proyecto de Diseño I, Proyecto de Diseño II, Termodinámica, Transferencia de Calor*.

6. Objectives

6.1 General objective

- Design a wind tunnel to carry out academic activities for engineering students at *Pontificia Universidad Javeriana Cali*

6.2 Specific objective

1. Define the wind tunnel engineering specifications by researching literature and interviewing stakeholders.
2. Determine the embodiment design by defining the wind tunnel configuration.
3. Specify the detailed design of the required tunnel sections and fan power to maintain the flow speed through calculations and software tools.
4. Design the control of the air-flow speed and data acquisition system of variables such as temperature and pressure, using off-the-shelf software and hardware
5. Validate the fulfillment of the technical requirements through software or a practical test.

7. Methodology

Based on the exploration carried out, the C.D.I.O methodology is proposed to meet the expected specific objectives. This methodology consists of four stages: Conceive – Design – Implement – Operate, as shown in Table 4 detailed by Crawley, Malmqvist, Ostlund, and Brodeur, in the book "Rethinking engineering education: the CDIO approach" [11]. However, the scope of this project only covers the conceiving, designing, and implementing phases.

Table 4. Details of the tasks: conceiving, designing, implementing, and operating phases [11].

Conceive		Design		Implement		Operate	
Mission	Conceptual Design	Preliminary Design	Detailed Design	Element Creation	Systems' Integration & Test	Lifecycle Support	Evolution
• Business Strategy • Technology Strategy • Customer Needs • Goals • Competitors • Program Plan • Business Plan	•Requirements • Function • Concepts • Technology • Architecture • Platform Plan • Market Positioning • Regulation • Supplier Plan • Commitment	• Requirements Allocation • Model Development • System Analysis • System Decomposition • Interface Specifications	• Element Design • Requirements Verification • Failure & Contingency Analysis • Validated Design	• Hardware Manufacturing • Software Coding • Sourcing • Element Testing • Element Refinement	• System Integration • System Test • Refinement • Certification • Implementation Ramp-up • Delivery	• Sales & Distribution • Operations • Logistics • Customer Support • Maintenance & Repair • Recycling • Upgrading	• System Improvement • Product Family Expansion • Retirement

Supported by this methodology, the first specific objective covers the requirements, the second objective refers to the preliminary design, the third and fourth objectives develop the detailed design, and finally, the fifth objective belongs to the implementation stage.

7.1 Definition of the wind tunnel engineering specifications

This section presents the initial activities of the design process, aimed at defining the engineering specifications of the wind tunnel. In order to identify the most relevant functional and technical attributes for this type of equipment in academic contexts, interviews with stakeholders (see Appendix 1) and exhaustive literature reviews were carried out, including specialized books, scientific articles, and academic databases (ScienceDirect, Scopus, EBSCO, ProQuest, IEEE, and so on). Additionally, previous undergraduate thesis projects were consulted as methodological and conceptual references for this work [4], [5], [6], [7], [12].

The identified characteristics were consolidated in a table and classified as either "Necessary" or "Optional" in order to prioritize them according to how indispensable they were to meeting the design expectations.

7.2 Embodiment design

The embodiment design stage is one of the most important design processes considering that it requires the detailing of concepts and needs. "The embodiment design consists of two major phases: design configuration and analysis of the design" [13].

At this stage, it is essential to translate the previously defined specifications into technical solutions that integrate all relevant aspects of the wind tunnel system, ensuring its feasibility and alignment with the identified requirements. This phase requires careful consideration of functional aspects, structural constraints, operational conditions, and practical implications of each design decision. The first step in the design configuration consists in selecting the type of wind tunnel. In Section 2.2.1, the different types of wind tunnels were classified (open-circuit and closed-circuit). Therefore, in the tunnel configuration selection process, the characteristics of both layouts were evaluated. This comparation (see Table 7) is supported by lower construction cost (as detailed in Section 4), simpler design, the interview outcomes, and ease of integration with observation windows and measurement, which align effectively with the operational characteristics of the open-circuit wind tunnel.

In the second step, analysis of the design, each of the sections that compose the wind tunnel was determined, this is part of the System Decomposition suggested by the C.D.I.O. methodology in the Preliminary Design stage. This analysis involved dividing the tunnel into its main sections: settling chamber (with honeycomb and screens), contraction, test section, diffuser and fan. Based on this, the main function of each segment was

identified, to later consider its aerodynamic effect on airflow, limitations and wind tunnel operation mode.

7.3 Detailed design of the required tunnel sections and fan power

7.3.1 Test section selection

The test section, where the test models are placed, is the most important part of a wind tunnel. Thus, it will be the first part to be designed, its shape and size will be decisive for the development of the tunnel. The most common test section types, based on the cross-section geometry are: square, rectangular and circular. In addition, regardless of the choice, it is suggested a transparent material for the section to observe the flow behavior.

In order to determine the most suitable cross-sectional shape for the test section, seven features were compared. Then, based on literature review [4], [5], rectangular, octagonal, and circular test section shapes were scored on a 0-2 scale according to their performances in each defined feature, where "0" means low performance, "1" medium performance, and "2" high performance.

7.3.2 Detailed design of the wind tunnel sections

Based on the desired attributes and the selected wind tunnel configuration, the specific design of the tunnel sections was determined, starting with determining the dimensions of the test section. Next, the diffuser section was designed to reduce the downstream flow velocity at the test section. Finally, the dimensions of the contraction and settling chamber sections were calculated taking into account the fluid mechanics theory to ensure a uniform flow in the test section.

Subsequently, in order to know the total loss of the system, the loss coefficient in each tunnel section is calculated. Then, this value is used to evaluate the required fan power to maintain the flow speed. Based on this, a commercial fan was selected and included in the general assembly.

7.3.3 3D Modeling

Once the dimensions of each section were calculated, the SolidWorks (SolidWorks Corp, USA, Waltham) software was used to model all the parts of the tunnel, as well as the assembly. Finally, the materials were determined considering the required properties for

each part. A bill of materials (BOM) is included in the assembly drawing that includes all the components required for manufacturing. The selection of materials was made with the help of a comparative table.

7.4 Control and data acquisition (CDAQ) system design

An open-loop control and data acquisition system were developed capable of satisfying the design attributes identified in section 9.1 related to the Conceptual Design stage (see Table 5). Based on this, the system should:

- Measure the air temperature inside the test section
- Measure the air velocity inside the test section
- Control the airflow speed

In order to translate these attributes into engineering specifications, the variables to be measured and controlled were first characterized. This enabled the definition of their operational ranges.

Then, the operation of the CDAQ system is described. This included a graphical representation of the system, illustrating the system components and their connections.

Finally, the system components were summarized in a table and a detailed operating description of each component was provided. The selection of these was carried out by prioritizing the resources available at PUJ-Cali and Universidad Autónoma de Occidente (UAO), who contributed to this project by providing equipment and laboratory facilities for the development of this design. For this reason, the Allen-Bradley Micro850 PLC and the Allen-Bradley PanelView 800 HMI from PUJ-Cali were selected as the system controller and the user interface monitor, respectively. In addition, a Siemens Micromaster variable frequency driver (VFD) was provided by the UAO as fan motor driver. On the other hand, some sensors —such as pitot tube system (with differential pressure sensor) and Pt100 RTD temperature transmitter— were chosen based on the fulfillment of the technical requirements. The entire components were summarized in a table, followed by a description of their operation.

7.5 Validation of the fulfillment of technical requirements

- For the fluid simulation, the designed 3D model was imported into SolidWorks. Then, a turbulence model was proposed to capture turbulent flow behavior. The simulation

provided information about the wind tunnel behavior: flow speed, temperature, and pressure, which was compared with the theorical calculations.

- The verification of all sub-systems integration (wind tunnel model, designed control and data acquisition system) was carried out through practical tests, implementing the control and data acquisition system design into real size model of the wind tunnel. Thanks to the cooperation between the Universidad Autónoma de Occidente and PUJ-Cali, it was possible to get access to a full-scale wind tunnel where the control and data acquisition system was coupled to this tunnel in order to carry out its validation.

8. Restrictions

The design constraints to be developed are presented below, which will be verifiable when the respective results are obtained.

- **Cross-sectional area in the test chamber**: It is important to determine the dimensions of the wind tunnel; in particular, it is essential to delimit the cross-sectional area of the test section, which is proposed not to exceed 50 × 50 cm. This allows for the calculation of the tunnel's overall size, airflow capacity, and required power equipment. Moreover, maintaining the area below 0.25 m^2 optimizes aerodynamic performance and aligns with the spatial and equipment constraints of an academic environment. Therefore, limiting the cross-sectional area helps ensure a uniform airflow, increases the achievable flow speed with a standard-size fan, and reduces both construction and operational costs. A larger test section would require a significantly higher flow rate to maintain the desired speed, resulting in the need for a more powerful fan and greater energy consumption.

- **Available resources:** The development of mechanical design and electronic implementation requires technological, physical and human resources. Among the technological resources are CAD design and modeling programs, such as SolidWorks; electronic design software as Proteus, and Automation Studio; fluid software simulation such as Ansys; and programming platform designed like Matlab. Physical resources include: the automation and process center (CAP), the library, the electronics laboratories, among others. Human resources include teachers, laboratorians, and experts in the different areas of interest.

- **Power supply:** Due to availability in the university laboratories, the wind tunnel implemented must operate with 110V single-phase or 220V three-phase.

- **Purpose**: The wind tunnel is for academic purposes.
- **Velocity**: The air flow inside the tunnel must be kept in subsonic velocities.

9. Results and discussion

9.1 Wind tunnel engineering specifications

Table 5 presents a summary of the main identified functional and technical attributes for the wind tunnel, as well as their description and classification. Additionally, the last column indicates the section of the document where the arguments supporting both the description and the classification are presented.

Table 5. Main identified attributes for the wind tunnel.

Attributes	Description	Classification	Section
Maximum flow speed into the test section	15 m/s	Necessary	9.1.1
Variable speed	Yes, controlled by the user	Necessary	9.1.1
Mach Number	Subsonic	Necessary	9.1.2
Test section dimensions	0.4 m x 0.27 m x 0.7 m	Necessary	9.3.1
Visibility through the test section	Transparent test section	Necessary	9.1.4
Flow straightener	Honeycomb and screen	Necessary	9.3.1.1
measurement of the airflow characteristics	Airflow speed, temperature	Necessary	9.1.1, 9.1.3
Measuring devices and instrumentation	Pitot tube, Temperature sensor	Necessary	9.1.4
Temperature control system	N/A	No	9.1.3, 9.1.4
Noise level	100 dB over 15-minute periods	Optional	9.1.5

9.1.1 Velocity

Based on documented data from similar studies at Colombian universities, as previously shown in Table 3, and considering the low-speed requirements for an institutional wind tunnel, a maximum speed of 15 m/s in the test section was chosen, as a conservative approach. This velocity is enough to achieve a considerably high Reynolds number in the test section. In addition, both the literature and the interview outcomes agree that it is crucial to be able to vary the airflow speed in the operating range to achieve different Reynold numbers. Therefore, this suggests a fan speed controller for the users.

9.1.2 Mach number

According to the selected maximum airflow speed in the test section, the Mach number (section 2.2.2) was calculated by means of Equation 22. Since $M_{TS} < 1$, the wind tunnel operates under subsonic conditions.

$$M_{TS} = \frac{15\ m/s}{343\ \mathrm{m/s}} = 0.04 \qquad \text{Equation 22}$$

9.1.3 Temperature

The literature research indicates that the temperature inside the test section remains close to room temperature [4]. Since it is desirable to work under standard environmental conditions, then, it was not necessary to implement a temperature control system in the wind tunnel. Nevertheless, the measure of the temperature is relevant to identify the airflow conditions. Therefore, a temperature sensor must be implemented.

9.1.4 Interviews

As previously mentioned, interviews with stakeholders were conducted (see Appendix 1). Based on this, some relevant insights were identified from questions 11, 12, and 13. Figure **10** summarizes the results of those questions, where it can be observed that the majority of interviewees considered highly important the visibility through the test section, and the capability of adjusting the airflow speed. Meanwhile, the temperature measurement was less important for the interviewees than the previous two capabilities.

Note: The entire interview script can be found in Appendix 1.

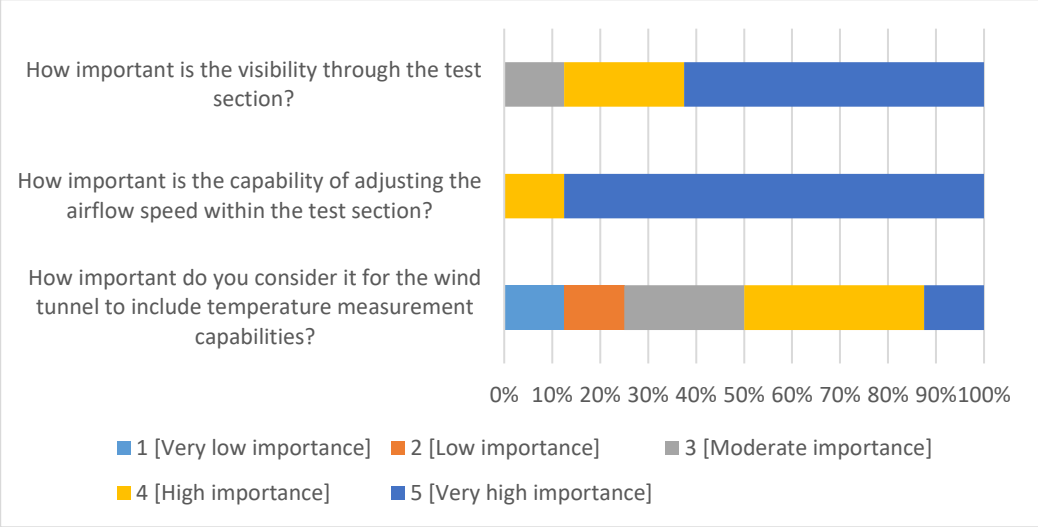

Figure 10. Results of questions 11, 12, and 13 from the interviews with stakeholders [Appendix 1].

Based on the outcomes of Figure **10**, the following attributes were defined for implementation in the wind tunnel design:

- Adjustable airflow velocity within the test section to enable different types of aerodynamic testing.
- Visualization of the internal airflow through the incorporation of a transparent material, such as acrylic, in the test section.
- Monitoring system for key variables, such as airflow velocity and temperature.

9.1.5 Noise level normative

Currently, there is no specific regulation in Colombia governing the design or implementation of wind tunnels. However, there are applicable standards related to the spatial configuration of educational environments, such as *NTC 4595:2020*, which defines the requirements for the planning and spatial design of school and laboratory facilities. Additionally, there are existing regulations concerning the maximum permissible noise levels that such equipment may emit. Specifically, *Resolution 0627 of 2006, in Chapter II – Noise Emission* [14], establishes the maximum allowable noise levels according to the classification of the surrounding environment. Table 6 summarizes the limits defined by the Ministry of Environment, Housing, and Territorial Development for areas with varying levels of acoustic sensitivity, including universities and research centers classified under Sector B: Tranquility and Moderate Noise.

Table 6. Maximum Permissible Noise Emission Levels [14].

Sector	Subsector	Maximum Permissible Noise Emission Levels in dB(A)	
		Day	Night
Sector A. Tranquility and Silence	Hospitals, libraries, daycare centers, clinics, geriatric homes.	55 dB(A)	50 dB(A)
Sector B. Tranquility and Moderate Noise	Residential areas or areas exclusively designated for housing, hotels, and lodging.	65 dB(A)	55 dB(A)
	Universities, schools, colleges, research and study centers.		
	Parks in urban zones, excluding mechanical amusement parks.		

Internationally, noise levels can be regulated by the standards and recommendations published by the World Health Organization (WHO). According to the WHO Environmental Noise Guidelines for the European Region (2009), for short-term exposures, the WHO establishes a maximum limit of 100 dB over 15-minute periods in order to protect hearing and prevent immediate damage [15].

9.2 Embodiment design

9.2.1Selection of the Wind Tunnel Type

Multiple comparable criteria between wind tunnel types and interview responses provided by faculty and laboratory staff were considered. The first column presents the name of the evaluated criterion. The second column details the technical behavior and functional justification of that criterion as it applies to the open-circuit wind tunnel configuration. The third column describes how the same criterion is addressed in a closed-circuit wind tunnel. The fourth column explains the relevance of each criterion based on the responses obtained during the interviews. Finally, the fifth column indicates the corresponding interview question number or the section of the document where the supporting arguments are presented. These criteria are consolidated, described, and justified in Table 7.

Table 7. Justification for the Selection of the Wind Tunnel Type.

Criterion	Open-Circuit Wind Tunnel	Closed-Circuit Wind Tunnel	Relevance According to Interview Responses	Interview question/ section
Flow recirculation	Air is drawn from the environment and expelled after passing through the test section.	Air is continuously recirculated in a closed loop.	Recirculation is not required; emphasis is on controlled flow with a simple structure.	Section 2.2.1
Energy efficiency	Lower efficiency due to constant loss of air in each cycle.	Higher efficiency through reuse of the same air volume.	Not a critical factor; functionality for basic academic experiments is prioritized.	Section 2.2.1
Initial cost and maintenance	Lower cost and easier to construct and maintain.	Higher cost due to structural complexity.	Low cost and easy maintenance were rated positively.	Section 4
Versatility and space requirements	Requires less space, more open configuration.	Requires more space due to the need for return ducts.	The ability to install the equipment in limited laboratory space was highlighted.	Section 2.2.1
Flow visualization	High visibility by allowing acrylic windows in the test section.	Visualization is also possible, but structure is more enclosed.	Visual observation of airflow behavior was considered essential.	Question 10
Instrumentation accessibility	Easy integration of pressure sensors, velocity sensors, Pitot tubes, etc.	May require more complex designs to access internal instrumentation.	Need for basic sensors for laboratory use was consistently emphasized.	Question 17
Automation and data acquisition	Simple access for installing external control and data systems.	Also possible, but with greater integration complexity.	Automated control and acquisition of variables such as pressure and velocity were recommended.	Question 12, Section 2.8
Design complexity	Simple, functional, and well-suited for academic environments.	More robust and complex design.	A functional, easy-to-assemble and maintain design was preferred.	Section 2.2.1
Noise during operation	Tends to generate more noise due to free-air exhaust.	Quieter due to enclosed air circulation.	Noise was considered relevant, but not a priority compared to flow speed and visibility.	Question 14, Section 9.1.5

Criterion	Open-Circuit Wind Tunnel	Closed-Circuit Wind Tunnel	Relevance According to Interview Responses	Interview question/ section
Standards and technical references	According to Resolution 0627 of 2006, Chapter II – Noise Emission, regarding the maximum permissible level of environmental noise that can be generated.	According to Resolution 0627 of 2006, Chapter II – Noise Emission, regarding the maximum permissible level of environmental noise that can be generated.	As detailed in Section 9.1.5, Resolution 0627 of 2006	

As a result of this analysis, the open-circuit wind tunnel was selected as the most suitable solution for this project, taking into account that the prioritized criteria were lower construction cost and simpler design. In addition, according to the interview results (see Appendix 1), 75% of respondents considered the open-circuit tunnel to be the most suitable for academic purposes.

9.2.2 Analysis of the layout

The selected configuration is a subsonic open-circuit wind tunnel, as shown in Figure 11. This is a wind tunnel composed of five main sections: settling chamber, contraction, test section, diffuser, and fan, each bringing a specific function to condition accelerate, test, and then diffuse the airflow before expelling it. The operation is based on controlling the airflow, the air is drawn through the wind tunnel by the ventilator to guarantee a controlled and steady flow of air.

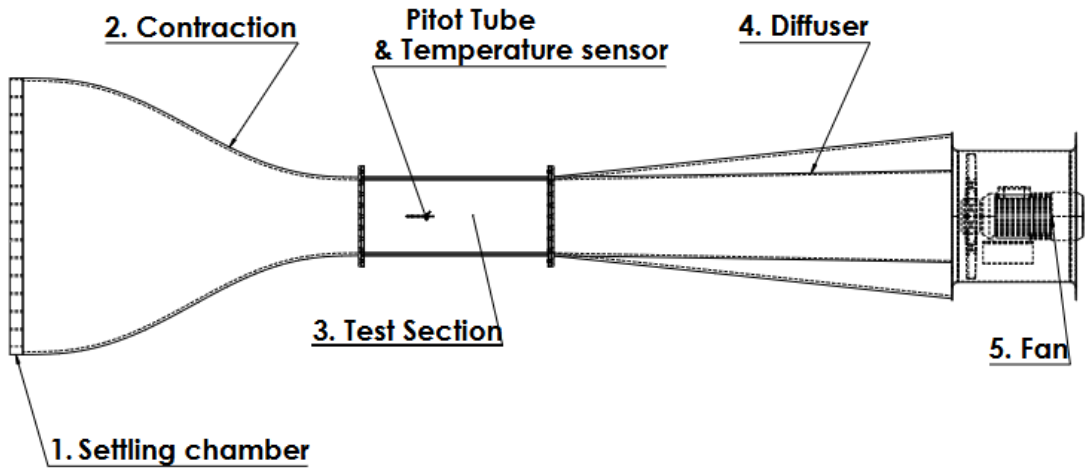

Figure 11. Open wind tunnel layout

It is important to mention the principal function of each section to understand the principle of wind tunnel operation:

- Settling chamber (section 1): Reduces turbulence
- Contraction (section 2): Accelerates the airflow
- Test section (section 3): Positions the test models and sensors.
- Diffuser (section 4): Expands the airflow
- Fan/ventilator (section 5): The driving force of the tunnel

Once the fan is on, the surrounding air is drawn into the tunnel. First, the air enters through the settling chamber, where devices such as mesh screens and honeycombs are located to reduce the turbulence and ensure a uniform velocity profile, these straighten airflow, improving flow quality for testing. After, the contraction section reduces the cross-sectional area, causing an increase in the air velocity due to the principle of mass conservation [3] .Then, the air passes through the test section, where the model under study and measuring instruments are placed, such as pitot tube and temperature sensors. The pitot tube is used to register the pressure differences and calculate the air speed using Equation 6. Finally, the air is discharged through the diffuser, gradually expanding the airflow, reducing its velocity, and increasing static pressure, preventing excessive backpressure that could reduce tunnel efficiency.

9.3 Detailed design of wind tunnel sections

For the design of a wind tunnel, it is necessary to know the characteristics of the air; this allows for calculating the conditions under which the wind tunnel operates. Since this project is carried out in Cali (~1,000 m above sea level), the standard environmental conditions are assumed to be:

- Average temperature: $\sim 25\,°C\ (298.15\ K)$
- Average atmospheric pressure: $\sim 1013\ hPa\ (101{,}300\ Pa)$
- Air density $\rho\ \approx\ 1.184\ kg/\mathrm{m}^3$
- Dynamic viscosity $\mu \approx 1.85 \times 10 - 5\ Pa$ ·s

Note that air density is considered constant. This is because the velocities reached by the wind tunnel are low, allowing the airflow to be approximated as incompressible [3].

9.3.1 Test section (TS)

Table 8 shows the score given to each of the cross-section shapes with respect to the defined features.

Table 8. Selection of the cross-sectional shape for the test section.

	Cross-sectional shape		
Features (selection criteria) [4]	Rectangular	Octagonal	Circular
Accessibility for the setup of the model	2	1	0
Visualization (transparent)	2	2	2
Manufacturing convenience	2	1	0
Recommendations from literature	2	1	0
Low cost of production	1	0	0
Low loss coefficient	2	2	2
Total	**11**	**7**	**4**

In terms of accessibility, the rectangular section offers more surface area at its base, which is convenient for the test models that must simulate contact with the ground. In the case of visualization, the three geometries can be transparent, however, rectangular geometry is much simpler to manufacture. Moreover, a review of previous work related to the construction of academic wind tunnels revealed a greater tendency for the implementation of rectangular test sections (see Table 3), since their easy manufacturability reduces production costs. Finally, Barlow [4] mentions that the differences in losses within the test section resulting from variations in cross-sectional shape are negligible. Consequently, the selection of the test section shape should be guided primarily by its utility and the aerodynamic requirements of the models to be tested.

Summarizing the information, as observed in Table 8 the rectangular cross-section is the highest-rated, therefore, the tunnel will be designed with this cross-section shape.

After consider the cross-section shape, the test section dimensions were discussed. The dimensions depend on the application and the model size. In this regard, as the tunnel has an academic purpose, and based on bibliography and interviews with stakeholders (Appendix 1), it was concluded that a common experiment to carry on into the wind tunnel is the aerodynamic measure of an airfoil geometry, this provides an environment to measure aerodynamic variables and appreciate flow behavior. Therefore, a scaled airfoil model will

be considered to design the test section. Similarly, some other academic activities can also be achieved in the same test section.

In this case, for low speed, Barlow [4] suggests a relation between the width of the test section and the model span, recommending that the aspect ratio must not be greater than 0.8 due to effects of the tunnel walls on the flow, as shown in Equation 23. R_a is the aspect ratio, ε is the model span [m], and w_{TS} is the width of the test section [m].

Another consideration by the same author is the width-to-height ratio of 1.5 in Equation 24, which is recommended for a minimum wall correction factor and big enough for a student tunnel, considering the budget and the width-to-height ratio of standard automobiles or airfoil model test. R_{wh} is the width-to-height ratio and h_{TS} is the height of the test section [m].

Finally, the wind tunnel's test section should be long enough such as the separated flow regions will be reattached or stabilized before reaching the end of the section and entering to the diffuser. For this reason, the test section typically has a length-to-width ratio of 2 or greater. However, its length should not exceed three times its own hydraulic diameter (D_h , as defined in Equation 2), in order to prevent excessive boundary-layer growth [4] [16].These restrictions are summarized in Equation 25 and Equation 26, where L_{TS} is the length [m] and $D_{h_{TS}}$ is the hydraulic diameter [m] of the test section respectively.

$$R_a = \frac{\varepsilon}{w_{TS}} = 0.8 \qquad \text{Equation 23}$$

$$R_{wh} = \frac{w_{TS}}{h_{TS}} = 1.5 \qquad \text{Equation 24}$$

$$2 \leq \frac{L_{TS}}{D_{h_{TS}}} \qquad \text{Equation 25}$$

$$L_{TS} < 3 \cdot D_{h_{TS}} \qquad \text{Equation 26}$$

Since this project aims to support academic activities at the university, it is also convenient to consider the tools available to students to develop further scaled model. In this context, one of the most common prototyping techniques is the 3D printing. PUJ Cali provides students with access to 3D printers, which are used to develop prototypes and scale models, the largest available printers are the references: Ender S1 Pro (with a maximum build volume of h: 0.23 m X w: 0.22 m X L: 0.22 m), and the Bambulab X1, (with a maximum build volume of h: 0.256 m X w: 0.256 m X L: 0.256 m).

Considering 80% of the total printable area capacity of the Bambulab X1 printer, a maximum printing area of w: 0.23 m X L: 0.23 m is obtained, with a maximum diagonal dimension of approximately 0.32 m, as shown in Figure 12. This dimension represents the maximum test model span that could be designed for 3D printing using the current 3D university´s printers. Therefore, taking into account the design suggestions from the bibliography, the typical size of the test section in wind tunnels with the same applications (see Table 3), and the available tools at PUJ Cali, a maximum model span of $\varepsilon = 0.32\ m$ is chosen. As a consequence, the width and the height of the test section were calculated with Equation 27 and Equation 28, respectively.

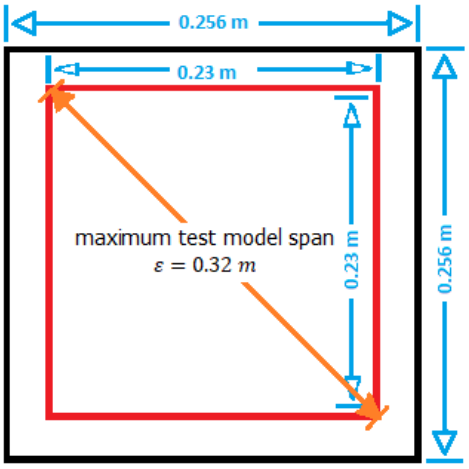

Figure 12. Printing area representation of the Bambulab X1 printer.

$$w_{TS} = \frac{\varepsilon}{0.8} = \frac{0.32\ m}{0.8} = 0.40\ m$$ Equation 27

$$h_{TS} = \frac{bF}{1.5} = 0.26\bar{6} \approx 0.27\ m$$ Equation 28

Then, for a rectangular area of w: 0.4 m X h: 0.27 m, the hydraulic diameter of the test section is $D_{h_{TS}} = 0.32\ m$ (see Equation 29). Based on this, and the restrictions from Equation 25 and Equation 26, the length of the test section should be around $0.64\ m < L_{TS} < 0.96\ m$. Thus, a test section of $L_{TS} = 0.7\ m$ length is designed for this project.

$$D_{h_{TS}} = \frac{4 \cdot A_{TS}}{p} = 0.32\ m$$ Equation 29

In summary, the desired dimensions of the test section are shown in Figure 13:

$$h_{TS} = 0.27\ m$$

$$w_{TS} = 0.4\ m$$

$$L_{TS} = 0.7\ m$$

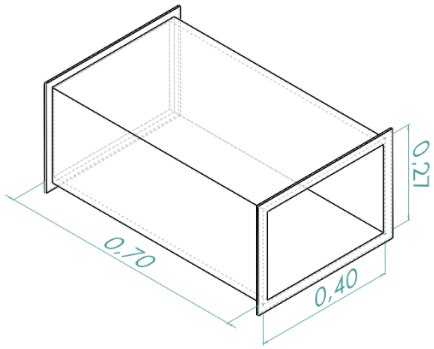

Figure 13. Representation of the test section.

9.3.1.1 Reynolds number

The Reynolds number is relevant for the calculation of the friction factor, and consequently, the loss coefficients. Using the calculated dimensions of the test section, the defined standard environmental conditions, and considering an operating speed range of 1 – 15 m/s, Equation 30 and Equation 31 present the minimum and maximum Reynolds numbers for speeds of 1 m/s and 15 m/s, respectively.

$$Re_{(1\frac{m}{s})} = \frac{\rho \cdot V \cdot D_{h_{TS}}}{\mu} = \frac{(1.184\text{kg/m}^3) \cdot (1m/s) \cdot (0.32m)}{1.85 \times 10^{-5}\ \text{Pa} \cdot \text{s}} = 20480 \qquad \text{Equation 30}$$

$$Re_{(15\frac{m}{s})} = \frac{(1.184\text{kg/m}^3) \cdot (15\ m/s) \cdot (0.32m)}{1.85 \times 10^{-5}\ \text{Pa} \cdot \text{s}} = 307200 \qquad \text{Equation 31}$$

As can be observed, the entire operating speed range corresponds to Reynolds numbers much greater than 4000, which means the airflow in the test section will have a turbulent regime. However, control excessive turbulent flow is essential for the test conditions. To reduce turbulence while maintaining the Reynolds number (Re), screens must be placed at the entrance of the settling chamber, followed by a proper design of the contraction section to preserve laminar flow, which is the desired condition for testing.

These considerations will be further addressed later in this document in sections 9.3.4 and 9.3.5.

9.3.1.2 Test section loss coefficient

There are different methods for calculating the losses in a wind tunnel's test section. In this case, the Darcy-Weisbach model is used due to its compatibility with ducts with constant cross-sectional area, including laminar of turbulent flows, as it was explained in section 2.7 (on page 17), using Equation 16 and Equation 19.

For the calculation of the friction factor, Barlow [4] suggests using the Prandtl relation (Equation 19) as an iterative solution method that converges to the solution within four to six iterations, starting with an initial guess as far off as $f = 1$. It can be seen from this equation that the friction factor f increases as the Reynolds number R_e decreases. Therefore, a low operating speed of 5 m/s is selected for estimating a representative friction factor, which corresponds to a Reynolds number around $Re = 100000$.

After five iterations, the friction factor solution converges to $f_{TS} = 0.018$ With this result, considering the test section dimensions, and using equations from section 2.7, it is possible to determine the pressure loss, the local section loss coefficient, and the head loss for the test section, presented in Equation 32, Equation 33, and Equation 34, respectively.

$$\Delta P_{L_{TS}} = f_{TS} \frac{L_{TS}}{D_{h_{TS}}} \frac{\rho V_{TS}^2}{2} = 0.018 \cdot \frac{0.7m}{0.32m} \cdot \frac{(1.184\text{kg/m}^3) \cdot (15m/s)^2}{2} = 5.24\ Pa \quad \text{Equation 32}$$

$$K_{L_{TS}} = f_{TS} \frac{L_{TS}}{D_{h_{TS}}} = 0.0301 \cdot \frac{0.7m}{0.32m} = 0.039 \quad \text{Equation 33}$$

$$h_{L_{TS}} = \frac{\Delta P_L}{\rho g} = f_{TS} \frac{L_{TS}}{D_{h_{TS}}} \frac{V_{TS}^2}{2g} = 0.018 \cdot \frac{0.7m}{0.32m} \cdot \frac{(15m/s)^2}{2 \cdot 9.81m/s^2} = 0.45\ m \quad \text{Equation 34}$$

9.3.2 Mass and volumetric flow rate

The mass flow rate refers to the mass of fluid that moves per unit of time. It is calculated using the air density and the volumetric flow rate of the airflow. Based on this value, it is possible to determine the airflow velocity in each section, as well as other variables such as pressure and head losses.

Likewise, the volumetric flow rate is the volume of fluid that moves per unit of time. It is a key parameter in wind tunnel design, as this represents the volume of air that the fan must displace inside the wind tunnel sections.

Based on the rectangular area of the test section ($A_{TS} = 0.4\text{m X } 0.27\text{ m}$) and a maximum speed V of 15 m/s, the volumetric and mass flow rate are calculated in Equation 35 and Equation 36, respectively.

$$Q = V \cdot A = 15\frac{m}{s} \cdot (0.4\,m \cdot 0.27\,m) = 1.62\,\frac{m^3}{s} \quad \text{Equation 35}$$

$$\dot{m} = \rho \cdot Q = 1.184\frac{kg}{\text{m}^3} \cdot \left(1.62\,\frac{m^3}{s}\right) = 1.91\,\frac{kg}{s} \quad \text{Equation 36}$$

It is known that the mass flow in a duct is theoretically the same across all sections. Therefore, the continuity equation must be satisfied, as shown in Equation 37 [3], where $\dot{m}_{TS}$ is the mass flow rate of the test section, $\dot{m}_D$ the mass flow rate of the diffuser, $\dot{m}_C$ the mass flow rate of the contraction, and $\dot{m}_{SC}$ the mass flow rate of the settling chamber.

$$\dot{m} = \dot{m}_{TS} = \dot{m}_D = \dot{m}_C = \dot{m}_{SC} \quad \text{Equation 37}$$

Additionally, since the tunnel operates at low speeds, the air density remains constant along the sections. Based on this, the airflow is considered incompressible [3], which allows the density to be removed from the expression, resulting in the volumetric flow rate being the same throughout all sections of the tunnel, as shown in Equation 38, where Q_{TS} is the volumetric flow rate of the test section, Q_D the volumetric flow rate of the diffuser, Q_C the volumetric flow rate of the contraction, and Q_{SC} the volumetric flow rate of the settling chamber.

$$Q = Q_{TS} = Q_D = Q_C = Q_{SC} \quad \text{Equation 38}$$

9.3.3 Diffuser (D)

This section is attached to the outlet of the test section. Thus, its inlet cross-sectional area is the same of the test section cross-section. From the inlet the area gradually increases along its length at an angle of approximately 5° relative to the horizontal axis, forming a conical geometry that culminates in a circular cross-sectional area at the outlet to ensure a suitable connection with the fan. This shape is designed to reduce airflow velocity and increase static pressure. The diffuser aims to minimize energy losses and maintain an almost uniform total pressure profile at the exit, preserving flow uniformity and preventing boundary layer separation. Figure 14 below shows a schematic representation of the diffuser, where $A1_D$ is the entrance square area and $A2_D$ is the exit circular area.

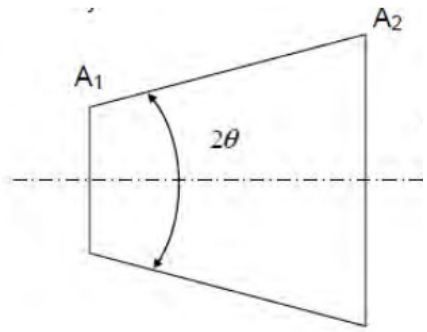

Figure 14. Schematic of the diffuser [5].

Based on this geometry representation, the length of the diffuser can be calculated using Equation 39, where R_{h2D} is the hydraulic radius of the diffuser outlet, R_{h1D} is the hydraulic radius of the diffuser inlet, and θ is an angle of 5°. The value of R_{h1D} is known, since the test section dimensions are fixed. Considering the inlet area of $A1_D = 0.108\, m^2$ for the diffuser, the corresponding hydraulic radius is $R_{h1D} = 0.16\, m$. On the other hand, the R_{h2D} depends on the area of the fan, however, it is recommended that the area ratio between the outlet and inlet of the diffuser does not exceed 2.5 [17].

$$L_D = \frac{R_{h2D} - R_{h1D}}{\tan\theta} \qquad \text{Equation 39}$$

Given these restrictions and using an area ratio of $A_{R_D} = 2.5$, the outlet area of the diffuser is $A2_D = 0.27\, m^2$ (circular), and its corresponding hydraulic radius is $R_{h2D} = 0.29\, m$. As a consequence, the length of the diffuser is $L_D = 1.48\, m$, as is shown in Equation 40.

$$L_D = \frac{0.29m - 0.16m}{\tan 5} = 1.48\, m \qquad \text{Equation 40}$$

In summary, the desired dimensions of the diffuser section are shown in Figure 15:

$$A1_D = 0.108\, m^2\ (Square\colon 0.4\, m\ X\ 0.27\, m)$$

$$A2_D = 0.27\, m^2\ (circular)$$

$$L_D = 1.48\, m$$

$$\theta = 5°\ (\text{ relative to the horizontal axis})$$

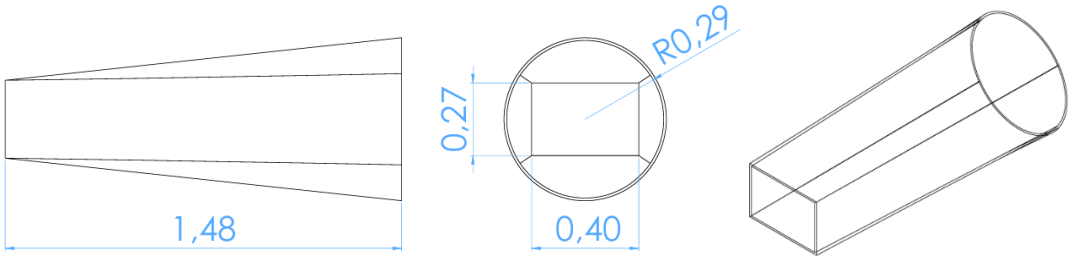

Figure 15. Representation of the diffuser.

9.3.3.1 Diffuser loss coefficient

The fluid mechanics is more complex in the diffuser than in the test section, since the cross-sectional area is not constant along the duct. In this case, the exit area is greater than the entrance area, thus, the fluid gets expanded. In order to consider this expansion, the loss coefficient K_{L_D} can be decomposed as a sum of a friction loss coefficient K_{f_D} and an expansion loss coefficient K_{EX_D}, as indicated by Equation 41 [4].

$$K_{L_D} = K_{f_D} + K_{EX_D} \qquad \text{Equation 41}$$

Barlow [4] presents experimental correlations for both terms. K_{f_D} depends on the friction loss coefficient f and the diffuser area ratio A_{R_D} (see Equation 42). On the other hand, K_{EX_D} is a product of two factors (see Equation 43), one factor is a function of the diffuser area ratio A_{R_D} and the other is a function of the equivalent conical angle $K_e(\theta)$.

$$K_{f_D} = \left(1 - \frac{1}{{A_{R_D}}^2}\right)\frac{f}{8 \cdot \sin\theta} \qquad \text{Equation 42}$$

$$K_{EX_D} = K_e(\theta) \cdot \left(\frac{A_{R_D} - 1}{A_{R_D}}\right)^2 \qquad \text{Equation 43}$$

As Barlow [4] discusses from experimental data, the factor $K_e(\theta)$ is estimated according to Equation 44, since this expression is used for square cross-sectional diffusers.

$$K_e(\theta)_{Square} = \begin{cases} 0.09623 - 0.004152\theta & for \quad 0 < \theta < 1.5° \\ 0.1222 - 0.04590\theta + 0.02203\theta^2 + 0.003269\theta^3 \\ -0.0006145\theta^4 - 0.00002800\theta^5 + 0.00002337\theta^6 & for \quad 1.5° \leq \theta \leq 5° \\ -0.01322 + 0.05866\theta & for \quad 5° < \theta \end{cases}$$

Equation 44

Applying the correlations above, Equation 45, Equation 46, Equation 47, and Equation 48 are used to calculate the loss coefficient of the diffuser.

$$K_e(5°)_{Square} = 0.845 \quad \text{Equation 45}$$

$$K_{EX_D} = 0.845 \cdot \left(\frac{2.5-1}{2.5}\right)^2 = 0.304 \quad \text{Equation 46}$$

$$K_{f_D} = \left(1 - \frac{1}{2.5^2}\right) \cdot \frac{0.018}{8 \cdot \sin 5°} = 0.022 \quad \text{Equation 47}$$

$$K_{L_D} = 0.304 + 0.022 = 0.326 \quad \text{Equation 48}$$

Since K_{L_D} is obtained, the correlations from Equation 14 and Equation 15 are considered to calculate the pressure loss and the head loss for the diffuser, using Equation 49 and Equation 50, respectively. Note that the diffuser mean velocity $V_D = 15\ m/s$ is equal to the test section velocity, this is calculated by dividing the volumetric flow rate Q by the inlet area $A1_D$ of the diffuser.

$$\Delta P_{L_D} = K_{L_D} \cdot \frac{1}{2} \cdot \rho \cdot V_D^2 = 0.326 \cdot \frac{1}{2} \cdot 1.184\ \frac{kg}{\mathrm{m}^3} \left(15 \frac{m}{s}\right)^2 = 43.42\ Pa \quad \text{Equation 49}$$

$$h_{L_D} = K_{L_D} \cdot \frac{V_D^2}{2g} = 0.326 \cdot \frac{\left(15 \frac{m}{s}\right)^2}{2 \cdot 9.81} = 3.73\ m \quad \text{Equation 50}$$

9.3.4 Contraction (C)

The contraction has two main purposes: it increases the airflow speed and enhances flow uniformity to provide a maximum speed for the test section, while also aiming to minimize the boundary layer separation. The design of the cross-sectional area is large at the inlet, but decreases progressively along its length, causing the air to accelerate due to the conservation of mass. In this sense, the contraction is the geometric opposite of the diffuser, with a significantly smaller exit area compared to the entrance.

A long contraction avoids disturbances; however, this results in an increase of tunnel length, cost and exit boundary layer thickness. Technical notes from experts declare: "A design satisfying all criteria will be such that separation is just avoided and the exit non-uniformity is equal to the maximum tolerable level for a given application" [16]. Therefore, typical area ratios are in the range of 6-9 for the smaller tunnels and it is suggested a length-width ratio of 1.25 [5].

The exit of the contraction is connected to the entrance of the test section, therefore, both cross-sectional geometries are the same. Since the exit of the contraction

will be a rectangular area of $A2_C = A_{TS} = 0.108\, m^2$ (0.4m X 0.27 m) and consider an area ratio of 9, then, its entrance area should be a square area of $A1_C = 0.97\, m^2 \approx 1\, m^2$. As a consequence, the length of the contraction will be $L_C = 1.25\, m$.

On the other hand, another important design consideration for contraction sections is the wall shape, this is in addition to the common criteria of wanting to avoid boundary layer separation. After extensive researches, Bell and Mehta purposed the following polynomial shapes (see Equation 51, Equation 52, and Equation 53) to obtain a reasonable mean flow uniformity at the contraction outlet [18]:

I. $$Y(X) = H_i - (H_i - H_e)(-2(X')^3 + 3(X')^2)$$ Equation 51

II. $$Y(X) = H_i - (H_i - H_e)(6(X')^5 - 15(X')^4 + 10(X')^3)$$ Equation 52

III. $$Y(X) = H_i - (H_i - H_e)(-20(X')^7 + 70(X')^6 - 84(X')^5 + 35(X')^4)$$ Equation 53

Where $H_i = 0.5\, m$ is the contraction mid-height at inlet, $H_e = \frac{0.27}{2} m$ is the contraction mid-height at exit, and $X' = x/L_C$ is the non-dimensional streamwise distance. These polynomials represent the wall contour shapes, illustrated in Figure 16.

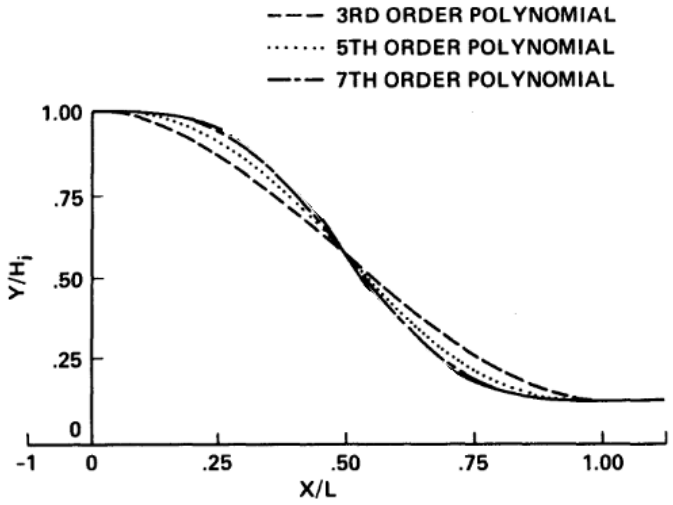

Figure 16. Wall contour shape [18].

By computing the designed contraction section parameters into Equation 51, Equation 52, Equation 53, previously described, the graphs of the three different contraction section profiles (3rd, 5th, and 7th order polynomials) were generated, as shown in Figure 17.

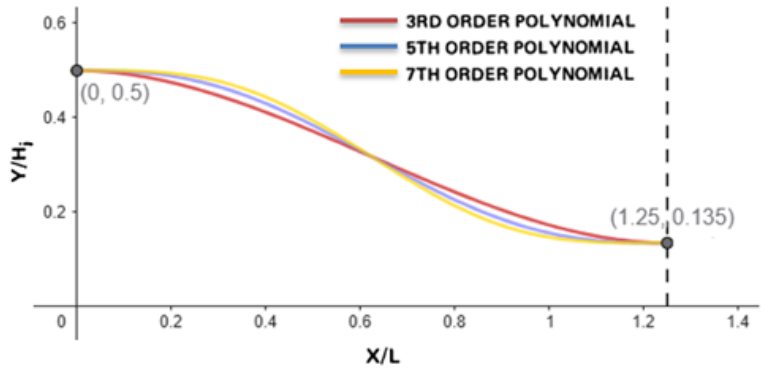

Figure 17. Contraction section profiles generated with 3rd, 5th, and 7th order polynomials.

In Bell and Mehta investigation's, each polynomial wall shape was compared under the same operating conditions, nevertheless, it was concluded that the 5th order polynomial performs optimally for low-speed tunnels in terms of giving minimum R_e and avoiding separation [18]. For this reason, the 5th order polynomial is chosen for the design of the wall contour shape (blue line in Figure 17). As a result, the selected contraction section contour is descripted by Equation 54.

$$Y(X) = 0.5 - (73/200)(6(X/1.25)^5 - 15(X/1.25)^4 + 10(X/1.25)^3) \qquad \text{Equation 54}$$

In summary, the desired dimensions of the contraction section are shown in Figure 18:

$$A1_C = 1\ m^2$$

$$A2_C = 0.108\ m^2\ (Square: 0.4\ m\ X\ 0.27\ m)$$

$$L_C = 1.25\ m$$

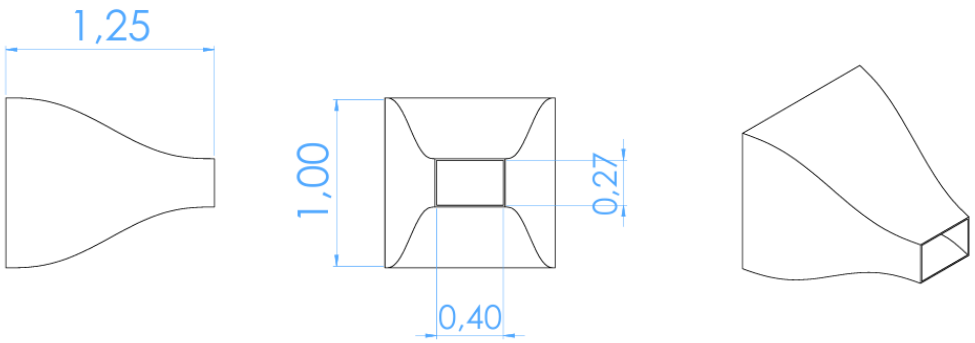

Figure 18. Representation of the contraction.

9.3.4.1 Contraction loss coefficient

Typically, the contraction loss is of the order of 3% of the total wind tunnel loss. Therefore, errors in estimating the contraction loss coefficient are much less important than errors in estimating losses in the high-speed part of the circuit. The losses in the contraction section are assumed to result solely from friction. This analysis is sufficient for energy considerations as this section consumes a small proportion of the drive power. In this context, the pressure drop is obtained by integrating the standard pipe friction law in Equation 55:

$$\Delta p_f = \int_0^{L_C} f \frac{\rho}{2} \frac{{V_C}^2}{D_{h_C}} dx \qquad \text{Equation 55}$$

where L_C is the length of the contraction, $D_{h_C} = D_{h_C}(x)$ the local contraction hydraulic diameter, and V_C the local section mean speed. Continuity gives ${V_C}^2 = {V_{SC}}^2 \left(\frac{D_{h_{SC}}}{D_{h_C}}\right)^4$, where V_{Sc} corresponds to the speed in the settling chamber and therefore at the entrance to the contraction section. By combining Equation 56 and Equation 14, the expression in Equation 56 is obtained.

$$K_{L_C} = f_{av}\left(\frac{L_C}{D_{h_{SC}}}\right)\int_0^1 \frac{{D_{h_{SC}}}^5}{{D_{h_C}}^5}\, d\left(\frac{x}{L_C}\right) \qquad \text{Equation 56}$$

As discussed by Barlow [4], these losses coefficient are referred to the test-section dynamic pressure. As a result, Equation 47 illustrates the total loss coefficient $K_{L_{lt}}$ based on test-section dynamic pressure. Where K_L is the loss coefficient, $q_l = \frac{1}{2}\rho_l {V_l}^2$ the dynamic pressure at the entrance and q_{TS} the dynamic pressure of the test section.

$$K_{L_{lt}} = K_L\left(\frac{q_l}{q_{TS}}\right) \qquad \text{Equation 57}$$

Therefore, according to Equation 57 and the contraction loss coefficient K_{L_C}, the total loss coefficient $K_{L_{Ct}}$ for the contraction section is shown in Equation 58.

$$K_{L_{Ct}} = K_{L_C}\left(\frac{q_{SC}}{q_{TS}}\right) = K_{L_C}\left(\frac{{V_{SC}}^2}{{V_{TS}}^2}\right) \qquad \text{Equation 58}$$

Where K_{L_C} is the contraction loss coefficient, q_{SC} the dynamic pressure at the settling chamber and q_{TS} the dynamic pressure of the test section. Consequently, using Equation 56 and the principle of continuity $\frac{{V_{SC}}^2}{{V_{TS}}^2} = \left(\frac{D_{h_{TS}}}{D_{h_{SC}}}\right)^4$, Equation 58 can be rewritten as Equation

$$K_{L_{Ct}} = f_{av}\left(\frac{L_C}{D_{h_{TS}}}\right)\int_0^1 \frac{{D_{h_{TS}}}^5}{{D_{h_C}}^5}\, d\left(\frac{x}{L_C}\right) \qquad \text{Equation 59}$$

For a common contraction shape, the integral of Equation 59 has been found to be approximately 0.32, and the friction factor is the average of the values for contraction entrance and exit Reynolds numbers [4]. In this sense, an acceptable approximation for the total loss coefficient of the contraction is given by Equation 60.

$$K_{L_C} = 0.32\, f_{av}\left(\frac{L_C}{D_{h_{TS}}}\right) \qquad \text{Equation 60}$$

Considering a Reynolds number average $Re_{av} = 205440$, then $f_{av} = 0.0128$. Finally, the contraction loss coefficient is calculate using Equation 61.

$$K_{L_C} = 0.32\, f_{av}\left(\frac{L_C}{D_{h_{TS}}}\right) = 0.32 \cdot 0.0128 \cdot \left(\frac{1.25\, m}{0.32\, m}\right) = 0.016 \qquad \text{Equation 61}$$

Since K_{L_C} is obtained, the correlations from Equation 14 and Equation 15 are considered to calculate the pressure loss and the head loss for the contraction, using Equation 62 and Equation 63, respectively. Note that the contraction mean velocity is $V_C = 15\ m/s$, this is calculated by dividing the volumetric flow rate Q by the inlet area $A2_C = 0.108\, m^2$ of the contraction.

$$\Delta P_{L_C} = K_{L_C} \cdot \frac{1}{2} \cdot\ \rho \cdot {V_C}^2 = 0.016 \cdot \frac{1}{2} \cdot 1.184\ \frac{kg}{\mathrm{m}^3}\left(15\frac{m}{s}\right)^2 = 2.13\ Pa \qquad \text{Equation 62}$$

$$h_{L_C} = K_{L_C} \cdot \frac{{V_C}^2}{2g} = 0.016 \cdot \frac{\left(15\frac{m}{s}\right)^2}{2 \cdot 9.81} = 0.18\, m \qquad \text{Equation 63}$$

9.3.5 Settling chamber (SC): honeycomb (H) and screen (S)

The settling chamber is a key part of airflow stabilization placed at the wind tunnel inlet. This section contains turbulence control screens and straighteners; the latter are commonly called honeycombs. The usual arrangement consists of a honeycomb followed by screens. These devices help to control the boundary layer: screens bring the different parts of the flow closer to a constant speed and the honeycombs force the flow to all go in essentially the same direction [4]. On the authority of Prandtl [19], "a honeycomb is a guiding device through which the individual air filaments are rendered parallel".

An important note was made at the end of the section 9.3.1.1, where the Reynolds number range was calculated according to the wind tunnel operating speed range. As a result of that range, high Reynolds number were identified, which means a considerable turbulent regimen characterized by a disordered movement of the airflow. However, researchers have evidenced that honeycomb and screen techniques improve the airflow quality at high Reynolds numbers [19], [7], [12]. Therefore, the settling chamber represents the solution in order to reduce those turbulences, aiming to stabilize and keep airflow uniformity.

9.3.5.1 Honeycomb (H)

The design criteria for honeycomb are the ratio of streamwise length L_H to single-cell hydraulic diameter D_{h_H}, and the porosity. This ratio enables an appropriate correlation among ease of construction, panel rigidity, and aerodynamic performance. According to Barlow [4], the length-to-cell-diameter ratio typically ranges from 6 to 8, and porosity β_H is usually about 0.8.

In practice, there are some common implementations of honeycomb with different cross-sectional shapes, as illustrated in Figure 19. After studying and analyzing its performance in a wind tunnel, Göv [20] reports a comparison among of hexagonal, square, and circular cells: Honeycombs with square cells produce a more favorable flow pattern than circular ones, and hexagonal-cell honeycombs deliver an even better flow regime than the other two. On the other hand, Mehta and Bradshaw [17] suggest about 150 honeycomb cells "across" the settling chamber diameter.

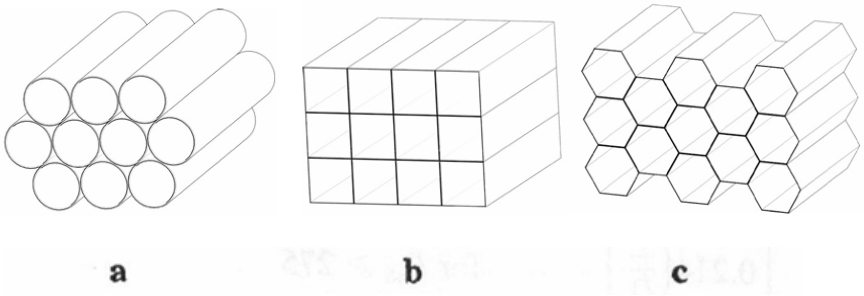

Figure 19. Schematic of several honeycomb cross-sections including: **(a)** circular cell, **(b)** square cell, and **(c)** regular hexagonal cell.

Based on the design recommendations, the following parameters were chosen:

I. A Length-to-cell-diameter ratio of 8, corresponding to a cell hydraulic diameter of $D_{h_H} = 6\,mm$ and cell length $L_H = 48\,mm$, since larger ratios provide better performance for airflow straighteners.
II. A typical porosity of $\beta_H = 0.8$.
III. 22500 square cells arrange in a matrix of 150 x 150, since square honeycombs produce a more favorable flow pattern than circular ones but are easier manufactured, compared to the hexagonal ones. This matrix covers the same cross section area of the contraction $A1_H = A1_C$.

9.3.5.2 Honeycomb loss coefficient

The losses in the honeycomb typically do not exceed 5% of the total pressure losses in the wind tunnel [4], therefore, the losses in this section are not considered significant. In order to determine the value of $K_{L_H} = honeycomb\ loss$, Barlow proposes Equation 64 [4], where λ_H is the friction coefficient for the honeycomb, defined in Equation 65.

$$K_{L_H} = \lambda_H \left(\frac{L_H}{D_{h_H}} + 3\right)\left(\frac{1}{\beta_H}\right)^2 + \left(\frac{1}{\beta_H} - 1\right)^2 \qquad \text{Equation 64}$$

$$\lambda_h = \begin{cases} 0.375\left(\dfrac{\Delta}{D_{h_H}}\right)^{0,4} {R_{e_\Delta}}^{-0,1}, & para\ R_{e_\Delta} \leq 275 \\ 0.214\left(\dfrac{\Delta}{D_{h_H}}\right)^{0,4}, & para\ R_{e_\Delta} > 275 \end{cases} \qquad \text{Equation 65}$$

First, the hydraulic diameter D_{h_H} is determined in order to calculate the ratio L_H/D_{h_H} (see Equation 66) and the Reynolds number in the honeycomb. This relationship is needed to determine the friction coefficient of the honeycomb.

$$\frac{L_{h_H}}{D_{h_H}} = 8 \qquad \text{Equation 66}$$

The Reynolds number in the honeycomb, Re_H (Equation 68)calculated based on the general Reynolds formulation presented in section 2.3.1 (Equation 1), taking into account the standard environment conditions described in 9.3 and the mean velocity of the honeycomb, according to the relationship shown in Equation 67. Note that the honeycomb mean velocity V_H considers the porosity of the honeycomb $A1_H = \beta_H \cdot A1_H = 0.8\,m^2$.

$$V_H = \frac{Q}{A1_H} = \frac{1.62\ \frac{m^3}{s}}{0.8\ m^2} = 2.02\ m/s \qquad \text{Equation 67}$$

$$Re_H = \frac{(1.184 Kg/m) \cdot (2.02\ m/s) \cdot (0.006m)}{1.85 \times 10^{-5}\ pa.s} = 775.68 \qquad \text{Equation 68}$$

To determine the term Re_Δ (roughness-based Reynolds number) is used the correlation of Equation 69.

$$Re_\Delta = Re_H \frac{\Delta}{D_{h_H}} \sqrt{\frac{f}{8}} \qquad \text{Equation 69}$$

The friction factor f is derived from the Colebrook equation [3], which is defined in Equation 70. This is used for pipes or ducts operating under turbulent flow conditions.

$$f = \frac{1}{\left\{1.8 \log 10 \left[\frac{6.9}{Re_H} + \left(\frac{\Delta/D_{h_H}}{3.7}\right)^{1,11}\right]\right\}^2} \qquad \text{Equation 70}$$

The roughness value (Δ) is essential for determining the friction factor f. White [7] provides recommended roughness values for various types of materials, as shown in Table 9. For the calculations, stainless-steel material is selected.

Table 9. Roughness of Selected Materials.

Duct Material	Absolute Roughness ε\varepsilon [m]
Stainless steel	$\Delta_{SSN} = 0.000002$
Smooth drawn plastic pipe (PVC)	$\Delta_P = 0.0000015$
Wood	$\Delta_w = 0.0005$

After, the honeycomb loss coefficient is calculated by Equation 71, Equation 72, Equation 73, and Equation 74:

$$f = \frac{1}{\left\{1.8 \log 10 \left[\frac{6.9}{775.68} + \left(\frac{2 \times 10^{-6} m/0{,}006m}{3.7}\right)^{1,11}\right]\right\}^2} = 0.0734 \qquad \text{Equation 71}$$

$$Re_\Delta = 775.68 \frac{2 \times 10^{-6} m}{0{,}006m} \sqrt{\frac{0.0734}{8}} = 0{,}0247 \qquad \text{Equation 72}$$

$$\lambda_H = 0{,}375\left(\frac{\Delta}{D_{h_H}}\right)^{0,4} {R_{e_\Delta}}^{-0,1} = 0.022$$ Equation 73

$$K_{L_H} = 0.022\left(\frac{48\,mm}{6\,mm}+3\right)\left(\frac{1}{0{,}8}\right)^2 + \left(\frac{1}{0{,}8}-1\right)^2 = 0.441$$ Equation 74

Since K_{L_H} is obtained, the correlations from Equation 14 and Equation 15 are considered to calculate the pressure loss and the head loss for the contraction, using Equation 75 and Equation 76, respectively.

$$\Delta P_{L_H} = K_{L_H} \cdot \frac{1}{2} \cdot \rho \cdot {V_H}^2 = 0.441 \cdot \frac{1}{2} \cdot 1.184\ \frac{kg}{\mathrm{m}^3}\left(2.02\,\frac{m}{s}\right)^2 = 1.06\ Pa$$ Equation 75

$$h_{L_H} = K_{L_H} \cdot \frac{{V_H}^2}{2g} = 0.441 \cdot \frac{\left(2.02\,\frac{m}{s}\right)^2}{2 \cdot 9.81} = 0.09\ m$$ Equation 76

9.3.5.3 Screen (S)

Mehta and Bradshaw recommend installing one screen upstream of the honeycomb [17]. This is normally made from metal wires that are woven together to form a square or rectangular mesh. The crucial design parameters of screens are: the mesh size M, the wire diameter d, as depicted Figure 20, and the solidity σ_S defined in Equation 77. Likewise, β_S is porosity for a square mesh screen, as illustrated in Equation 78. The solidity is typically between 0.3 and 0.4.

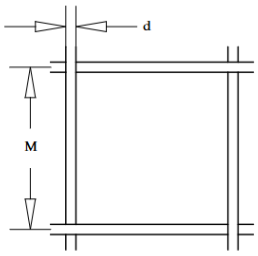

Figure 20. Definition of mesh width M , and wire diameter d [21].

$$\sigma_S = 1 - \beta_S$$ Equation 77

$$\beta_S = \left(1 - \frac{d}{M}\right)^2$$ Equation 78

Given these considerations, the screen parameters used in this wind tunnel are presented in Table 10. This screen covers the same cross section area of the contraction $A1_S = A1_C$.

Table 10. Data for the screens used in the wind tunnel.

	$\boldsymbol{M}[mm]$	$\boldsymbol{d}[mm]$	$\boldsymbol{\beta_S}$	$\boldsymbol{\sigma_S}$
$\boldsymbol{Screen}$	3.6	0.6	0.7	0.3

9.3.5.4 Screen loss coefficient

Barlow [4] presents an approximation for the loss coefficient K_{L_S} for a screen, as shown in Equation 79. Where K_{mesh} is the mesh factor, K_{Rn} the wire Reynolds number factor (Equation 80), and Re_w the wire Reynolds number (Equation 81).

$$K_{L_S} = K_{mesh} \cdot K_{Rn} \cdot \sigma_S + \frac{{\sigma_S}^2}{{\beta_S}^2} \quad \text{Equation 79}$$

$$K_{Rn} = \begin{cases} 0.785\left(\frac{Re_w}{241} + 1.0\right)^{-4} + 1.01, & 0 < Re_w < 400 \\ 1, & Re_w \geq 400 \end{cases} \quad \text{Equation 80}$$

$$Re_w = \frac{\rho \cdot V_S \cdot d}{\mu} \quad \text{Equation 81}$$

Considering $d = 0.0006\,m$ and $K_{mesh} = 1.3$. Equation 82, Equation 83, and Equation 84 are used to find the loss coefficient. Note that the screen mean velocity is $V_S = 2.31\,m/s$, this is calculated by dividing the volumetric flow rate Q by the inlet area $A1_S = \beta_S \cdot A1_S = 0.7\,m^2$ (taking into account the porosity of the screen).

$$Re_w = \frac{\left(\frac{1.184\text{kg}}{\text{m}^3}\right) \cdot \left(\frac{2.31m}{s}\right) \cdot (0.0006m)}{1.85 \times 10^{-5}\ \text{Pa} \cdot \text{s}} = 88.70 \quad \text{Equation 82}$$

$$Since\ \ 400 \geq Re_w, then:$$
$$K_{Rn} = 0.785\left(\frac{Re_w}{241} + 1.0\right)^{-4} + 1.01 = 1.23 \quad \text{Equation 83}$$

$$K_{L_S} = 1.3 \cdot 1.23 \cdot 0.3 + \frac{0.3^2}{0.7^2} = 0.663$$ Equation 84

Since K_{L_S} is obtained, the correlations from Equation 14 and Equation 15 are considered to calculate the pressure loss and the head loss for the contraction, using Equation 85 and Equation 86, respectively.

$$\Delta P_{L_S} = K_{L_S} \cdot \frac{1}{2} \cdot \rho \cdot {V_S}^2 = 0.66 \cdot \frac{1}{2} \cdot 1.184 \ \frac{kg}{\mathrm{m}^3} \left(2.31 \frac{m}{s}\right)^2 = 2.08 \ Pa$$ Equation 85

$$h_{L_S} = K_{L_S} \cdot \frac{{V_S}^2}{2g} = 0.66 \cdot \frac{\left(2.31 \frac{m}{s}\right)^2}{2 \cdot 9.81} = 0.18 \ m$$ Equation 86

9.3.6 Total losses

Table 11 summarizes the airflow condition in each win tunnel section, including the volumetric flow rate, the mean velocity, the loss coefficient, the pressure loss, and the head loss.

Table 11. Total losses

Section	$\boldsymbol{Q[m^3/s]}$	$\boldsymbol{V\ [m/s]}$	$\boldsymbol{K_L}$	$\boldsymbol{\Delta P_L[pa]}$	$\boldsymbol{h_L[m]}$
Test section (TS)	1.62	15	0.039	5.24	0.45
Diffuser (D)		15	0.326	43.42	3.73
Contraction (C)		15	0.016	2.13	0.18
Honeycomb (H)		2.02	0.441	1.06	0.09
Screen (S)		2.31	0.663	2.08	0.18
Total loss	-	-	-	**53.93**	**4.63**

9.3.7 Fan selection

As a result of the geometric characteristics of the tunnel and the total pressure losses, a required flow rate of 1.62 $\left[{m^3}/{s}\right]$ and a total minor loss of 53.93 $[Pa]$ were estimated. Once the minor losses have been determined, Bernoulli's equation (Equation 3) is used to calculate the static pressure (Equation 87) and with this, select the appropriate fan.

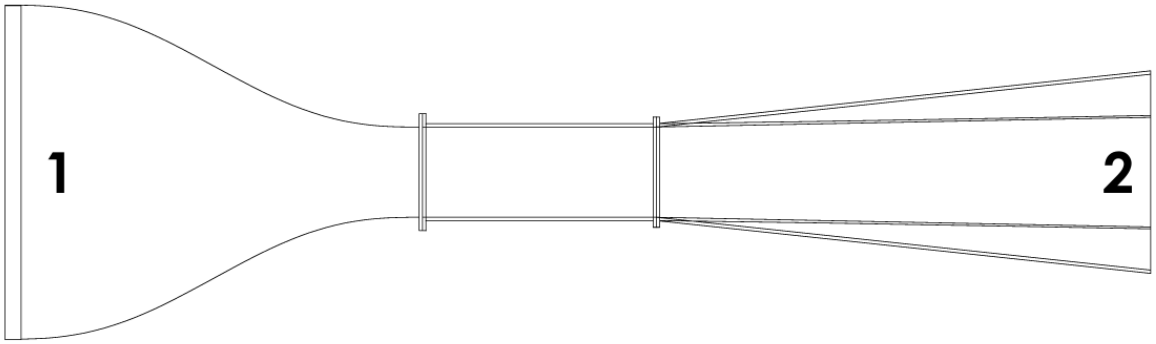

Figure 21. Basic outline of Bernoulli's equation.

The Bernoulli equation, applied between the inlet (1) and outlet (2) of the tunnel, is expressed as:

$$\frac{P_1}{\rho} + \frac{V^2{}_1}{2} + gz_1 + \frac{P_v}{\rho} = \frac{P_2}{\rho} + \frac{V^2{}_2}{2} + gz_2 + \frac{\Delta P_{1-2}}{\rho} \qquad \text{Equation 87}$$

Were:

P_1 → Pressure at the inlet (1)
$V^2{}_1$ → Wind velocity at the inlet (1)
z_1 → Height in the direction of gravity
P_2 → Pressure at the outlet (2)
$V^2{}_2$ → Wind velocity at the outlet (2)
z_2 → Height in the direction of gravity
P_v → Fan pressure (added to the system)
ΔP_{1-2} → Pressure losses due to friction or minor losses in the system
ρ → Fluid density
g → Gravity

Since the pressure at points 1 and 2 is equal to atmospheric pressure, and the height Z is constant between both points, these terms cancel each other out. Also, inlet speed V_1 is considered zero to assume the worst case where the airflow starts from repose. As a result, the equation is simplified, allowing the term corresponding to the fan pressure to be isolated. The sum of all minor losses in the system (total losses) is represented by the term $\frac{\Delta P_{1-2}}{\rho}$ which groups the losses in each section of the tunnel. Based on this, the static pressure (Equation 88) is determined, which provides the required fan pressure value. As a consequence, the entire values necessary for fan selection are shown in Table 12.

$$\frac{P_v}{\rho} = \frac{V^2{}_2}{2g} + \frac{\Delta P_{1-2}}{\rho} = 56.199\ Pa \qquad \text{Equation 88}$$

Table 12. Fan requirements for wind tunnel.

Parameter	Unit	Value
Volumetric Flow rate	$\left[m^3/_s\right]$	1.62
Mass Flow rate	$\left[Kg/_s\right]$	1.91
Head loss	$[m]$	4.83
Static Pressure	$[Pa]$	56.19

A comparative methodology was employed for fan selection, based on the technical requirements established in Section 9.3.6, which included an approximate flow rate of 1.62 m³/s and a total pressure loss of 53.93 Pa. Four commercial axial fan models were identified that met these operational conditions, taking into account additional factors such as local market availability, energy efficiency, noise level, and compatibility with variable frequency drive (VFD) systems. Each option was evaluated based on its technical datasheets and performance curves. Ultimately, the TGT/4-560-6 fan was selected for offering the best balance between flow capacity, pressure generation, efficiency, and physical integration feasibility, meeting all the established criteria.

Based on these criteria, a technical comparison was made between several commercial fans, giving priority to compliance with the required flow rate. Table 13 below compares the models evaluated, which are described in the first column, the flow rate in the second column $\left[m^3/_s\right]$: maximum volumetric flow rate provided by the fan; pressure $[Pa]$ described in the third column: maximum static pressure that the fan can exceed; and finally, columns 4, 5, and 6 describe whether it complies with the flow rate/pressure/size: direct evaluation of each key criterion.

Table 13. Comparative Evaluation of Commercial Fan Models.

Model	Flow Rate [m³/s]	Static Pressure [Pa]	Fan Diameter [mm]	Fulfills Flow rate	Fulfills Pressure	Fulfills Diameter
Siemens 2CC2 504-5YB6	2.93	78	500	YES	YES	NO
S&P TCBB/4-500	2.36	70–80	500	YES	YES	NO
Ziehl-Abegg FN063-VDK.6N. V7P1	1.39	80	720	NO	YES	NO
TGT/4-560-6	2.36	210	560	YES	YES	YES

Considering the results, the TGT/4-560-6 model proves to be the most efficient and optimal choice for the tunnel conditions. This fan not only meets the required flow rate and

pressure, but also complies with the size restriction and is available on the Colombian market, which facilitates its acquisition and integration.

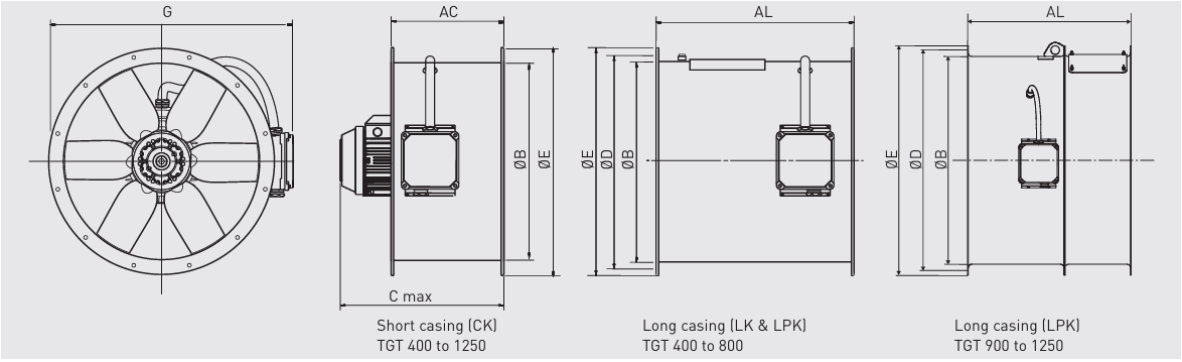

Figure 22. TGT Axial Fan Configurations with External Motor Mounting

The dimensions of the fan are provided by the manufacturer. For a better understanding, Figure 22 shows the fan plans with the values in letters, Table 14 shows the dimensions in millimeters of the different references, and the size of the selected model are indicated in the red box.

Table 14. Dimensions of the selected motor (TGT/4-560-6)

Model	AC	AL	B	C	D	E	F	G	GL	H	N
400	250	380	400	402	450	487	12	558	-	-	8
450	250	480	450	457	500	537	12	613	-	-	8
500	250	480	500	467	560	595	12	662	-	-	12
560	280	600	560	564	620	655	12	726	-	-	12
630	280	700	630	564	690	725	12	795	-	-	12
710	380	600	710	564	770	806	12	849	-	-	16
800	380	600	800	564	860	896	12	940	-	-	16
900	450	750	900	737	970	1005	15	1045	-	-	16
1000	450	780	1000	767	1070	1105	15	1145	-	-	16
1120	500	1150	1120	950	1190	1225	15	1268	-	-	20
1250	500	1150	1250	950	1320	1355	15	1421	-	-	20
1250 - IEC 250	625	1175	1250	830	1320	1358	15	1505	-	-	20
1409	625	1175	1400	1130	1470	1512	15	1659	1663	781	20
1609	625	1275	1600	1250	1680	1772	20	1900	1910	910	24

Table 15 shows the technical specifications of a series of 4-pole axial fans operating at 1450 rpm, including the TGT/4-560-6/-0.75 model, which was selected for the wind tunnel design presented in this study. This fan was chosen based on its ability to meet the required flow rate of $1.62\ {}^{m^3}/_{s}$ ($5{,}832\ {}^{m^3}/_{h}$), as calculated in Section 9.3.3, and for offering an adequate balance between power consumption and physical size. This model features a 560 mm inlet diameter, a rated power of 0.55 *kW*, and a maximum airflow capacity of $8{,}510\ {}^{m^3}/_{h}$, providing a safe operational margin. It draws 2.2 *A* at 230 V, and weighs 51 kg (short casing), which facilitates installation and integration with the tunnel's structural frame.

Table 15. Technical specifications of model TGT/4-560-6[9]

Model	Inlet Ø (mm)	Motor Power (kW)	Rated Motor Current		Max Flow Rate (m³/h)	Weight (kg)	
			230 V	400 V		short casing	long casing
TGT/4-400-6/-0.25	400	0.25	1.4	0.8	4,670	32	38
TGT/4-450-6/-0.37	450	0.37	1.8	1.1	6,150	41	49
TGT/4-450-6/-0.55	450	0.55	2.2	1.3	7,970	44	52
TGT/4-500-6/-0.75	500	0.75	2.8	1.6	9,760	46	55
TGT/4-500-6/-1.1	500	1.1	4.2	2.4	10,970	51	60
TGT/4-560-6/-0.55	560	0.55	2.2	1.3	8,510	51	68

The pressure-flow curves are shown in Figure 23. which relates the flow (X-axis) and pressure (Y-axis) to the angle of inclination of the fan blades represented by the black curves. In this figure, an operating point is identified at a flow rate of 1.62 m³/s and a static pressure of 56.199 Pa (intersection of green lines). Under these conditions, the system crosses the characteristic curve of 10° blade angle and registers a dynamic pressure of approximately 28 Pa, which is shown in the red curve intersecting 5832 m³/h.

[9] Soler & Palau Sistemas de Ventilación SLU, "Ventiladores Helicoidales Tubulares Serie TGT," Versión de revisión EasyVent v11 (Mayo de 2020), 5, PDF, www.solerpalau.es.

crosses the characteristic curve of 10° blade angle and registers a dynamic pressure of approximately 28 Pa, which is shown in the red curve intersecting 5832 m³/h.

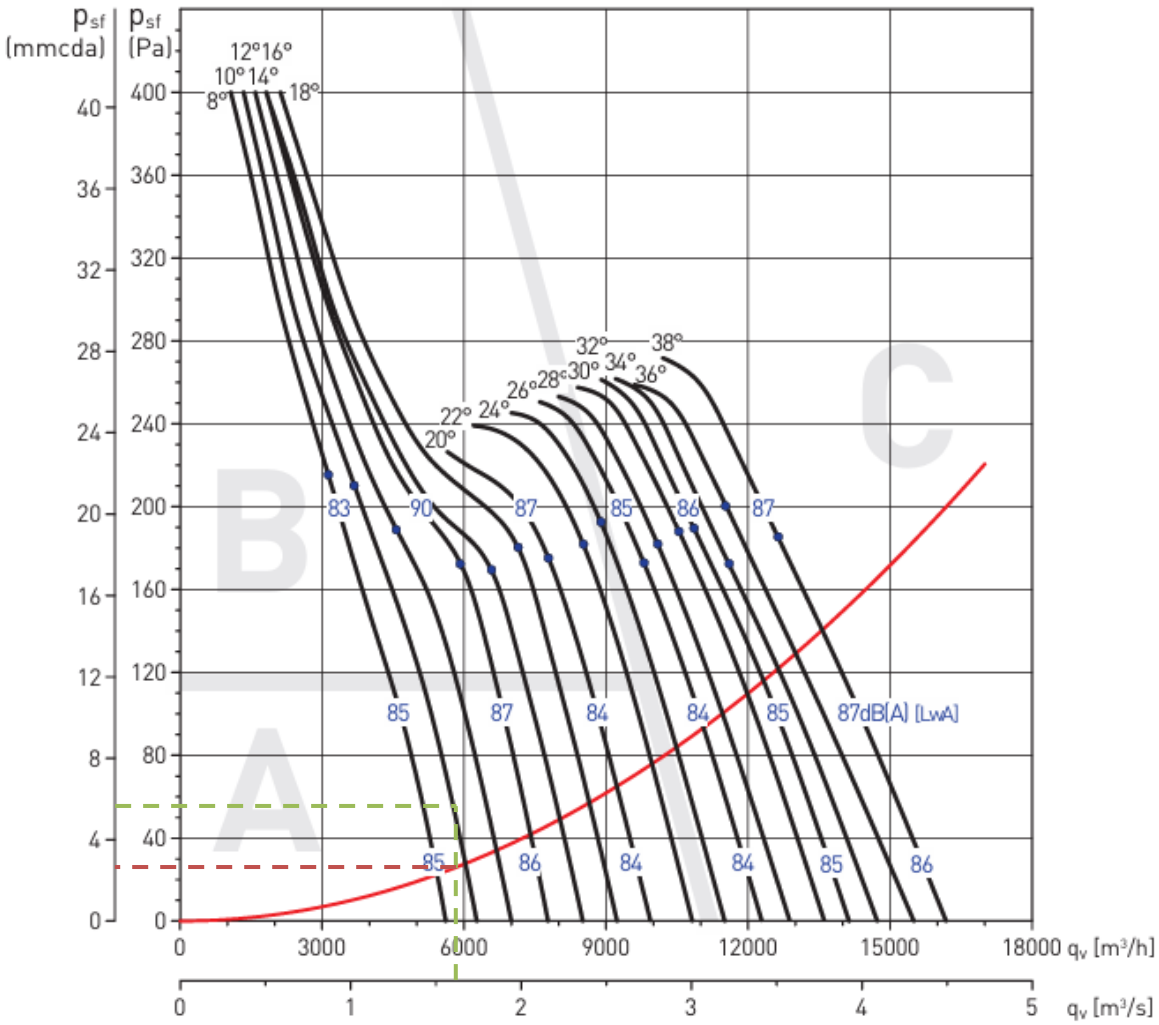

Figure 23. Fan Performance: Airflow vs. static Pressure of model TGT/4-560-6.[9]

In addition, Figure 24 shows that, for an inclination of 10°, the power absorbed rises to approximately 450 W.

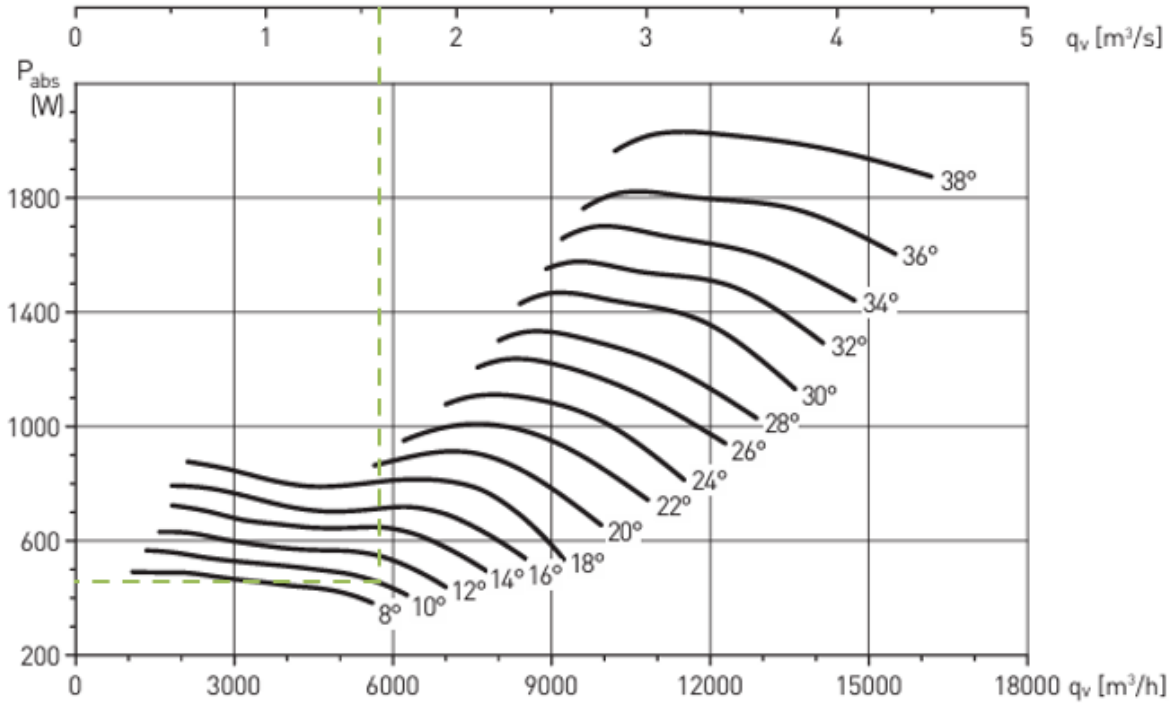

Figure 24. Fan Performance: Absorbed Power (W) vs. Airflow of model TGT/4-560-6.[9]

9.3.8 Build of material (BOM)

In order to select the appropriate materials for the construction of the wind tunnel, a comparative technical analysis was carried out for each of its main sections: the settling chamber, the contraction, the test section, the diffuser, and the structure holding up the tunnel. The selection criteria included structural strength, roughness, corrosion resistance, total weight, and estimated component cost.

Table **16** presents a technical comparison between several viable materials for each section of the wind tunnel, considering factors such as surface roughness, corrosion resistance, density, and estimated cost. However, as part of the design process, a single material must be selected for each component, based on functional, manufacturing, and economic criteria.

Table 16. List of materials for the wind tunnel.

Section	Suggested Material	Technical Reason / Observation	Roughness (mm)	Corrosion Resistance	Weight (kg)	Cost Per KG (USD)
Contraction section	Galvanized steel	• High stiffness; can be shaped into smooth 1:5 profiles; durable and easy to maintain. • Very good corrosion resistance	≈ 0.15	Good (coating)	7.065	0.55
	Aluminum		≈ 0.0015	Very good	2.432	2.50
Test section	Acrylic (PMMA)	• Transparent material. • Allows flow visualization • Good structural behavior if reinforced. • Compatible with sensors	≈ 0.00001–0.0001	High	1.062	2.30
	Polycarbonate		≈ 0.00001–0.0001	High	1.080	2.30
Diffuser section	Stainless steel	• Structural resistance to flow expansion. • Good noise dissipation • Low visual inspection demand. • Lower cost. • Less corrosion resistance	≈ 0.000015	Excellent	7.200	1.00
	Carbon structural steel		≈ 0.015 - 0.03	Poor (requires coating)	≈ 7.020	0.70–0.85

Section	Suggested Material	Technical Reason / Observation	Roughness (mm)	Corrosion Resistance	Weight (kg)	Cost Per KG (USD)
Settling chamber	Aluminum	Very good corrosion resistance	≈ 0.0015	Very good	2.432	2.50
	Galvanized steel	Suitable for holding screens and honeycomb	≈ 0.15	Good (coating)	~6.000	0.55
Structure	Galvanized steel	• Suitable for holding screens and honeycomb • High rigidity and corrosion protection with coating	≈ 0.15	Good (coating)	~6.000	0.55
	Carbon structural steel	High mechanical strength; widely used in structural frames. Excellent weldability and availability.	≈ 0.015 - 0.03	Poor (requires coating)	≈ 7.020	0.70–0.85

Following the comparative analysis presented in the table, the most suitable material was selected for each component of the wind tunnel. This selection is based on the established design criteria and is detailed below for each section of the system.

- Contraction and diffuser: Aluminum 6061-T6 was selected due to its high specific strength, good corrosion resistance, low weight, excellent machinability, and wide commercial availability. While carbon steel is more affordable, aluminum offers a better strength-to-weight ratio, which benefits the tunnel's structural stability and handling.
- Test section: Acrylic (PMMA) was chosen as the primary material because it enables clear visualization of internal airflow, which is essential for academic purposes. Its light weight and good chemical resistance also make it suitable for laboratory environments. The final selection decision was since PMMA is widely available in commercial sheet formats, making it a cost-effective and accessible solution for manufacturing.
- Settling chamber: Aluminum 6061-T6 was selected for its excellent corrosion resistance, light weight, and sufficient structural rigidity. This material also facilitates

machining and assembly processes, making it suitable for the fabrication of aerodynamic components. Its natural oxide layer offers long-term protection without the need for additional coatings, making it a durable and low-maintenance option.

- Support structure: Carbon structural steel was chosen for its high stiffness, excellent weldability, and low cost. Although its corrosion resistance is poor, this limitation can be mitigated by applying a protective coating (e.g., paint or hot-dip galvanizing).

9.4 Control and data acquisition system design

9.4.1 Characterization of variables

9.4.1.1 Temperature

Since open wind tunnels work under standard environmental conditions, the operating temperature range of the tunnel must be defined by the environmental condition changes where it is located. Therefore, due to the wind tunnel is designed for PUJ Cali, the historic record temperatures of Santiago de Cali, Colombia have been considered for this. Figure 25 presents the historical temperature data for Cali 2024, which illustrates an average temperature range from 16°C to 32°C. However, to ensure measurement in extreme conditions, a measurement range of 10-50°C is proposed for the wind tunnel.

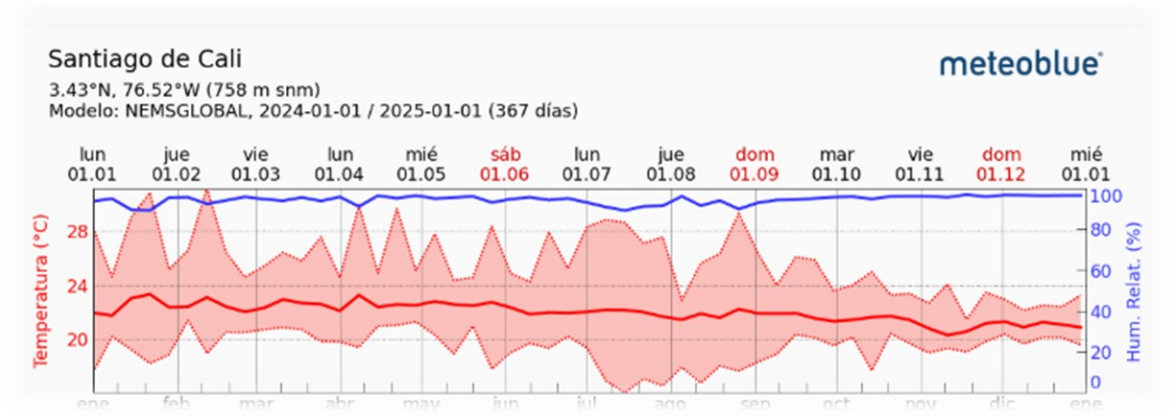

Figure 25. Historical temperature data for Cali 2024 [10].

[10] Obtained from " Santiago de Cali Meteorological Archive - meteoblue", Meteoblue, Historical temperature data for Cali 2024.

9.4.1.2 Airflow speed

The airflow speed is perhaps the most important parameter of an experiment inside of a wind tunnel. This term is present in important parameters for model similarity and dimensionless numbers, such as the Reynolds number, Mach number, and Froude number (see Equation 11, Equation 12, and Equation 13), therefore its measurement and control is key for the wind tunnel usage. This wind tunnel is designed to achieve a maximum speed of 15 m/s in the test section, in which the air velocity can be adjusted from 1m/s up to the maximum air velocity.

Airflow speed measurement

The airflow speed must be measured in the test section since the test models are placed here. The measurement must be within the range 1-15 m/s, with the ability to measure variations of 0.3 m/s within the measuring range. However, in practice, the instantaneous values of the velocity fluctuate about an average value due to turbulence, which suggests that the velocity can be expressed as the sum of an average value $\bar{u}$ and a fluctuating component u', as shown in Figure 26. For this reason, a tolerance range of +/- 0.2 m/s is established.

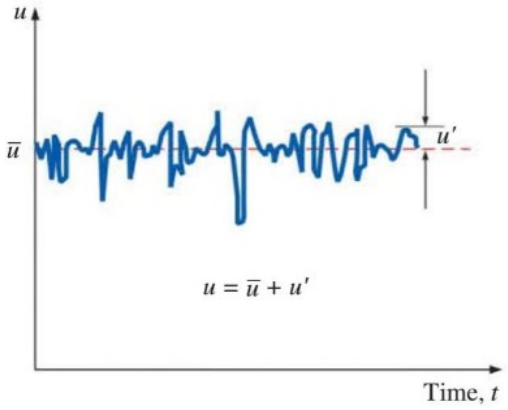

Figure 26. Fluctuations of the velocity component u with time at a specified location in turbulent flow [3].

Airflow speed control

The airflow speed is determined by the fan's revolutions per minute (fan RPM). Therefore, controlling the fan RPM is analogous to controlling the air speed. In this case, with a three-phase motor fan, it was advisable to use a variable frequency driver (VFD) to modulate the RPM, adjusting the three-phase power frequency provided by the local power grid. This grid operates at 60 Hz, so the 0-60 Hz range was used to achieve speeds of 1-15 m/s.

Although this project contemplates the use of test models of different sizes, the control system is not designed to compensate for large disturbances caused by

external factors, such as obstructions in the ducts at the entrance to the wind tunnel. Thus, the control system took into account the flow dynamics due to the total geometry of the tunnel, assuming that this geometry does not change, that environmental conditions do not present significant changes, and that fan dynamics do not change due to malfunction. Therefore, the system for regulating airflow speed works as an open-loop control. The decision of this implementation was primarily based on the simplicity of the application, the predictable behavior of the system under known load conditions, and the acceptable level of accuracy required for educational purposes. This approach is particularly advantageous when the process dynamics are well understood, the disturbances are minimal, and the response is repeatable.

9.4.2 CDAQ system operation description

The wind tunnel control and data acquisition system integrate multiple components working together to regulate airflow, by an open-loop control, and monitor environmental variables within the test section, such as, dynamic pressure, airflow speed, and temperature. The system consists of a Programmable Logic Controller (PLC), a Human-Machine Interface (HMI), a Variable Frequency Drive (VFD), sensors, an Arduino-based data acquisition module, communication interfaces, and a power supply. Figure 27 shows the system block diagram, this integrates the CDAQ system process.

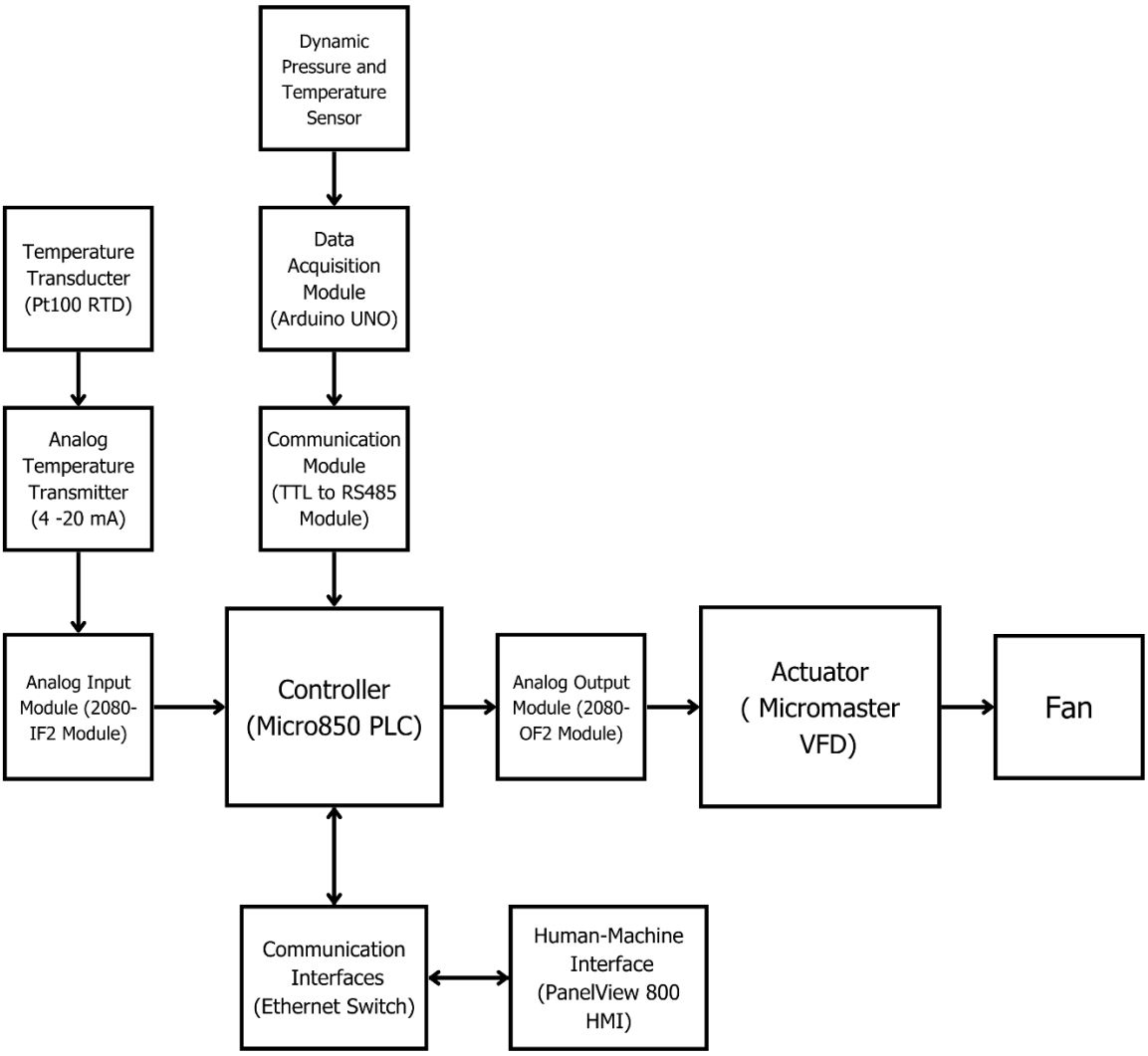

Figure 27. CDAQ system block diagram.

Open-loop Control System Workflow

1. **User Control via HMI:**

   The Allen-Bradley PanelView 800 HMI serves as the user interface, allowing the operator to input setpoints for the desired airflow speed. The HMI communicates directly with the PLC through an Ethernet industrial network, sending commands and displaying real-time process data, including airflow speed, dynamic pressure, and temperature.

2. **PLC Main Control Logic:**

   The Allen-Bradley Micro850 PLC is the core controller. It receives the command of airflow speed setpoint from the HMI, then sends a 0–10V analog output

signal through the 2080-OF2 analog output module to the VFD, regulating the fan motor's RPM to control airflow.

The control has to allow the operator to input target speed from 1-15 m/s, and to turn the fan on or off. In addition, the system must contain increment and decrement buttons to manually adjusts the airflow speed. With each tap, the system must variate the motor operating frequency in 0.1 Hz, without exceeding the operating speed range (1-15 m/s). From this workflow, a GRAFSET was designed for the PLC control program logic, as shown in Figure 28.

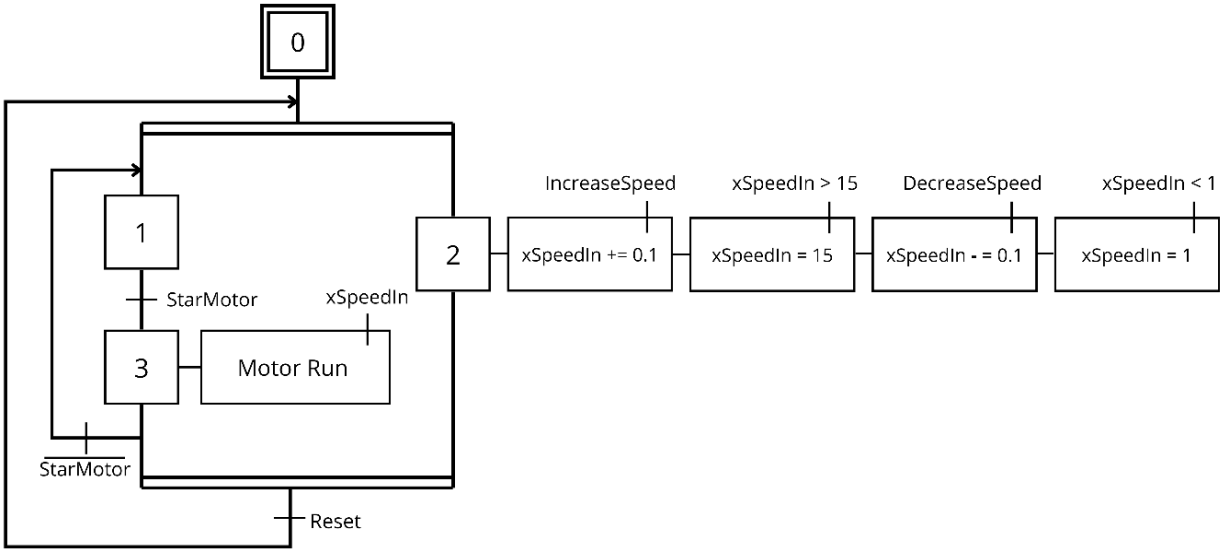

Figure 28. Control system GRAFCET.

3. **Fan Speed Control with VFD:**

The Siemens Micromaster VFD adjusts the fan motor's speed based on the analog signal from the analog output module connected to the PLC. When the module outputs 0V, the motor runs at 0 Hz (stopped); when it outputs 10V, the motor runs at 60 Hz, delivering maximum airflow. The VFD regulates the output frequency and voltage to the three-phase motor, ensuring smooth and efficient control.

Data Acquisition Process (Monitoring Only)

1. **Pressure and Temperature Sensing:**

The DLVR differential pressure sensor, mounted in the test section, communicates with the PLC through the protocol gateway, which converts I2C to Modbus RTU. The gateway was implemented using an Arduino UNO. The sensor provides accurate readings of dynamic pressure and air temperature. On the other

hand, the PLC also receives a 4-20 mA analog signal from the Pt100 temperature transmitter, which it reads using the 2080-IF2 analog input module. This means, the system has two temperature sensors for more versatility in measurements.

2. **Arduino Data Processing:**

   The Arduino reads the data from the DLVR sensor and applies a moving average filter with a configurable window size to stabilize the signal. Then, it calculates the airspeed using Bernoulli's principle, based on the measured dynamic pressure. Finally, the Arduino processes the variables: average pressure (Pa), airspeed (m/s), and temperature (°C).

3. **Communication to PLC:**

   These processed variables are transmitted to the PLC via Modbus RTU over RS485.

4. **Monitoring**

   Dynamic pressure (Pa), airspeed (m/s), and temperature (°C) can be monitored in the HMI. The current values and historical graphics are plotted through the screen for the user visualization.

Component Connections:

In order to illustrate the CDAQ system connections, a wiring diagram of the system was developed, as shown in Figure 29.

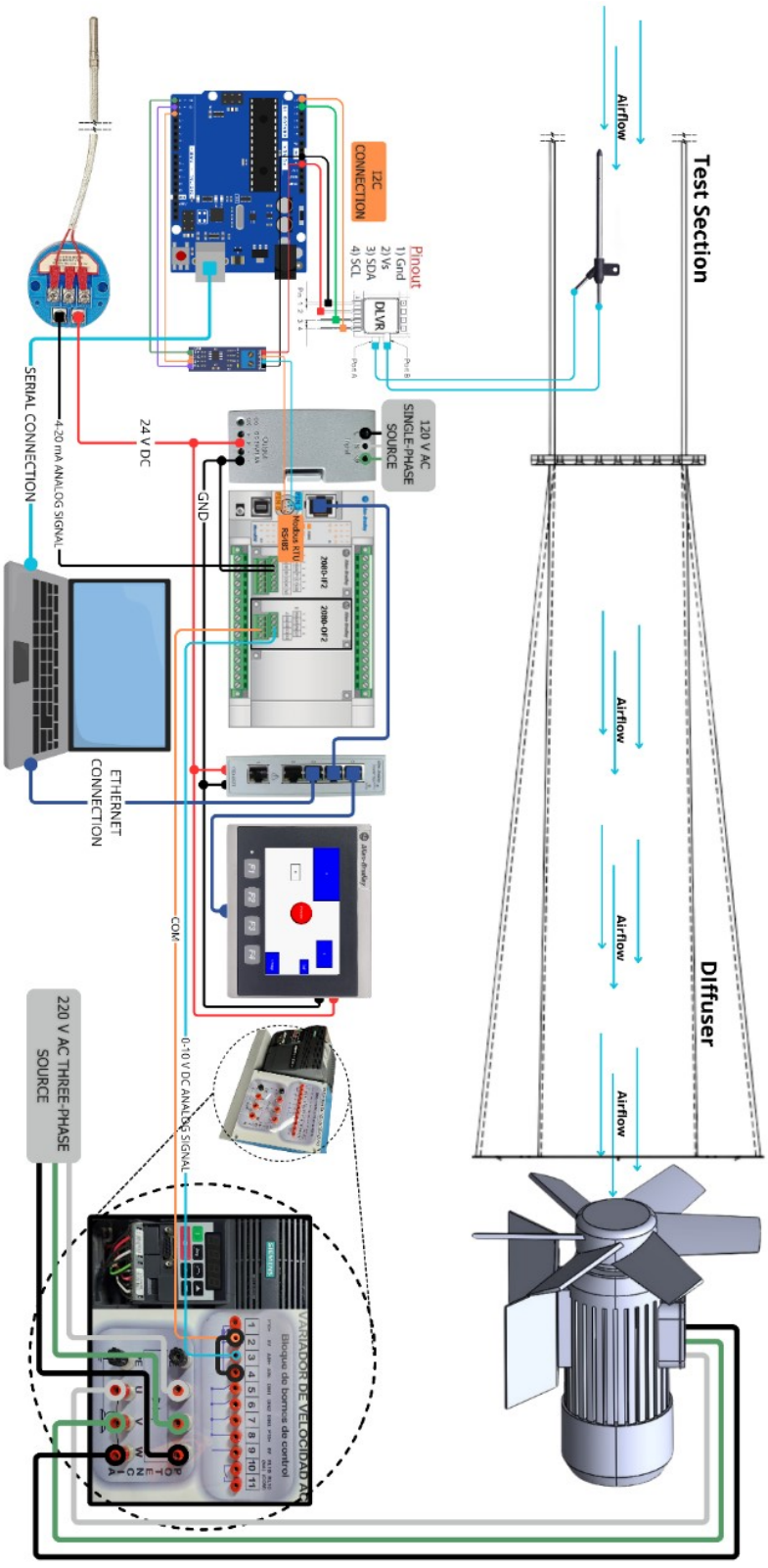

Figure 29. Wiring diagram of the CDAQ system.

9.4.3 CDAQ system components

Table 17. Proposed components for the CDAQ system.

Component	Device	Function	Details in Section
Controller	Allen-Bradley Micro850 PLC + 2080- IF2 Module + 2080- OF2 Module	Executes the control logic of the system. This receives and sends analog signals through input/output modules.	9.4.3.1
Human-Machine Interface	Allen-Bradley PanelView 800 HMI	Enables monitoring and interaction with the user.	9.4.3.2
Sensors	Pt100 temperature transmitter	Measures the air temperature.	9.4.3.3
	DLVR Series Low Voltage Digital Pressure Sensors (DLVR-L01D-E1NS-C-NI5F) + Pitot Tube	Measure temperature and dynamic pressure, the latter determines the airspeed inside the test section,	9.4.3.3
Data Acquisition and Communication Module	Arduino UNO + TTL to RS485 Module	Reads, saves, converts, and transmits data interfaces between the digital pressure sensors (DLVR-L01D-E1NS-C-N5F) and the Allen-Bradley Micro850 PLC.	9.4.3.4
Actuator	Siemens Micromaster 6SE9 221-8CC13 VFD	Controls the fan's rotational speed and thus regulate airflow.	9.4.3.5
Communication Interfaces	Allen-Bradley Stratix 2000 Ethernet Switch	Enable communicates among PLC, HMI and computer (for downloading programs) by Ethernet connection.	9.4.3.6
Power Supply	Allen-Bradley Micro800 24 V DC Power Supply	Provides electrical power to the components	9.4.3.7

9.4.3.1 Controller: Allen-Bradley Micro850 PLC

The Allen-Bradley Micro850 PLC serves as the central control unit of the system. It is equipped with an analog input module (2080-IF2) and an analog output module (2080-OF2), which expand its capabilities (see Figure 30). These plug-in modules add extra embedded non-isolated unipolar (0...10V, 0...20 mA) analog I/O and offer 12-bit resolution[11].

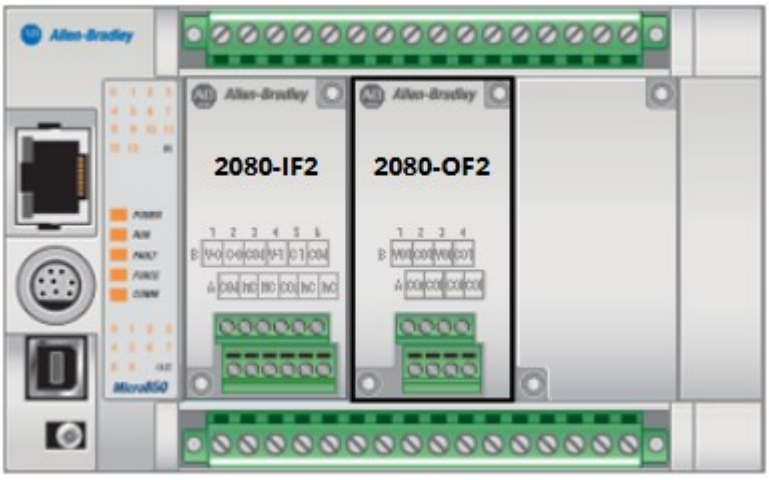

Figure 30. Allen-Bradley Micro850 PLC.

The Allen-Bradley Micro850 PLC is powered at 24V DC by the Allen-Bradley Micro800 24 V DC power supply. Using the compatible software "Connected Components Workbench" (CCW), the programming of the controller was developed. The main program was built with ladder diagram, while, the sensor and actuator programs were implemented by structured text. The complete transcription of these codes can be found in Appendix 3: PLC Codes.

This project implemented the Ethernet Port for local network communication with the HMI and the computer (for downloading programs). It also used RS-485 Port for Modbus communication to send data from the Data Acquisition Module (Arduino UNO) to holding registers created in the PLC memory.

The analog input module (2080-IF2) allows the PLC to read the signal from the Pt100 temperature transmitter, which converts the resistance of the Pt100 into a standard analog current signal (typically 4–20 mA). As shown in Figure 31, the Channel 0 was enabled to operate with current as input type at 60 Hz, while, Channel 1 was completely disabled.

[11] Obtained from analog I/O plug-in module user manual.

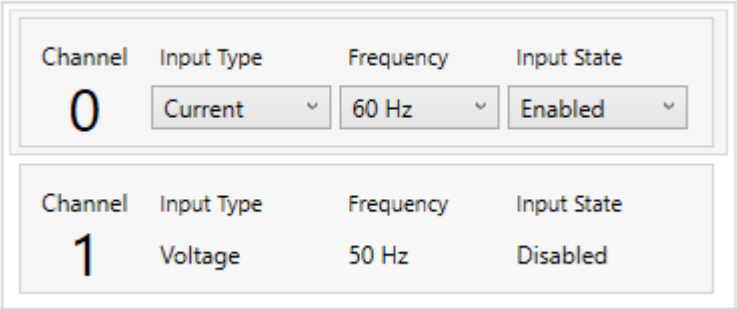

Figure 31. 2080-IF2 Configuration.

The analog output module (2080-OF2) is used to generate a continuous analog control signal (0–10 V) that is sent to the Variable Frequency Drive (VFD). This signal directly regulates the motor speed by adjusting the fan frequency, allowing for precise control of the airflow inside the wind tunnel. As shown in Figure 32, the Channel 0 was enabled to operate with voltage as output type, while, Channel 1 was completely disabled.

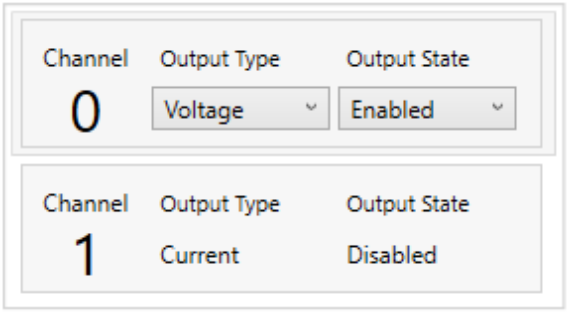

Figure 32. 2080-OF2 Configuration.

9.4.3.2 Human-Machine Interface: Allen-Bradley PanelView 800

The Allen-Bradley PanelView 800 HMI serves as the primary user interface for the wind tunnel control system. This monitor allows the user to control the airflow speed by writing the desired target airspeed in the panel. Additionally, it provides real-time monitoring of critical variables such as pressure, temperature, and airflow velocity within the tunnel.

HMI Interface functions

The Figure 33 shows the user interface main screen which contains the principal functions of the CDAQ system.

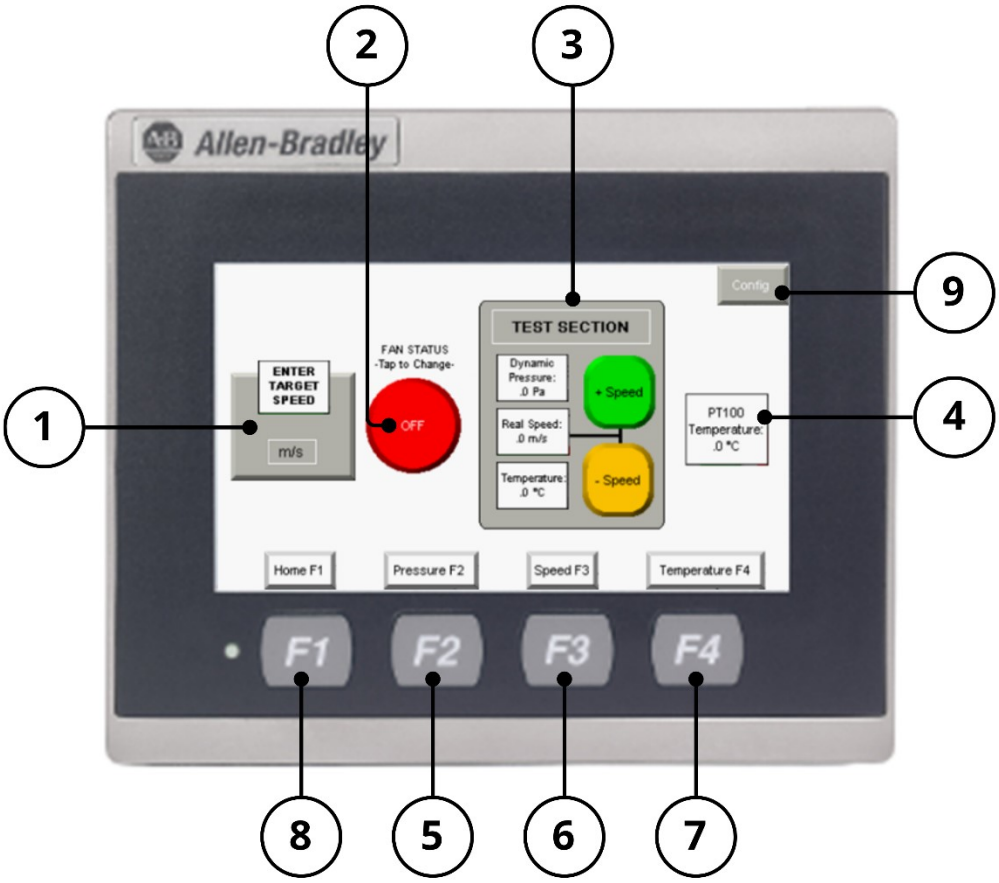

Figure 33. User interface main screen

From the main screen the user can:

- **[1] Target Speed Input**

  This numeric input field allows the operator to enter the desired airflow speed in meters per second from 1 to 15 m/s. This value is used to generate the analog output (0–10 V) that controls the fan speed via the VFD.

- **[2] Fan Status Button (ON/OFF Toggle)**

  Toggle button used for the fan start/stop command. This sends an output digital signal to the VFD which turn ON/OFF the fan.

- **[3] Test Section Display**

  This panel shows live sensor readings from the test section: dynamic pressure [Pa], airspeed [m/s], and Temperature [°C]. In addition, manual speed increase/decrease buttons are included, each tap changes the fan frequency by 0.1 Hz.

- **[4] Pt100 Temperature Display**

  Shows the ambient air temperature measured by the Pt100 temperature transmitter, processed through a 4–20 mA transducer connected to the PLC.

- **[5] Navigation Button – Pressure (F2)**

  Directs the operator to a dedicated screen focused on the dynamic pressure graph over time (see Figure 34).

Figure 34. Graph of dynamic pressure inside the test section

- **[6] Navigation Button – Speed (F3)**

  Directs the operator to a dedicated screen focused on the airflow speed graph over time (see Figure 35).

Figure 35. Graph of airflow speed inside the test section

- **[7] Navigation Button – Temperature (F4)**

  Directs the operator to a dedicated screen focused on the temperature graph over time (Figure 36).

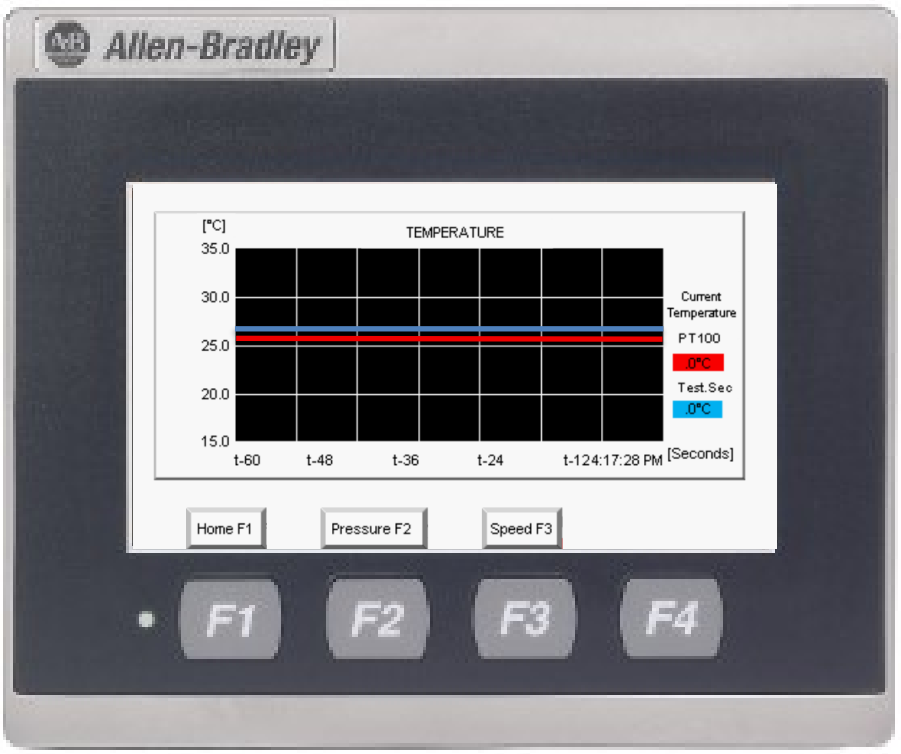

Figure 36. Graph of temperature inside the test section

- **[8] Home Button (F1)**
  Returns to the main overview screen.

- **[9] Configuration Access**
  Opens the HMI admin menu. For PLC program downloading

9.4.3.3 Sensors:

Pt100 RTD Transmitter

The objective of this device is to allow the user with the flexibility to measure the temperature at different points of the test section, or even outside the tunnel, depending on the need of the tests to be performed. This transducer has a 1-meter cable, which allows to achieve different points. The Pt100 RTD transducer works by changing its resistance as the temperature changes. It is connected to a transmitter that converts this change in resistance into a 4-20 mA current signal for temperature measurements from 0 to 200 °C respectively. This transmitter is powered by the Allen-Bradley Micro800 24 V DC power supply, and then sends the current signal (4-20 mA) to the analog input module 2080-IF2 (See Figure 37). The current signal is read by the module which converts the analog signal to UNIT type Raw Data (from 0 to 2^{16}) stored in the global variables of the PLC.

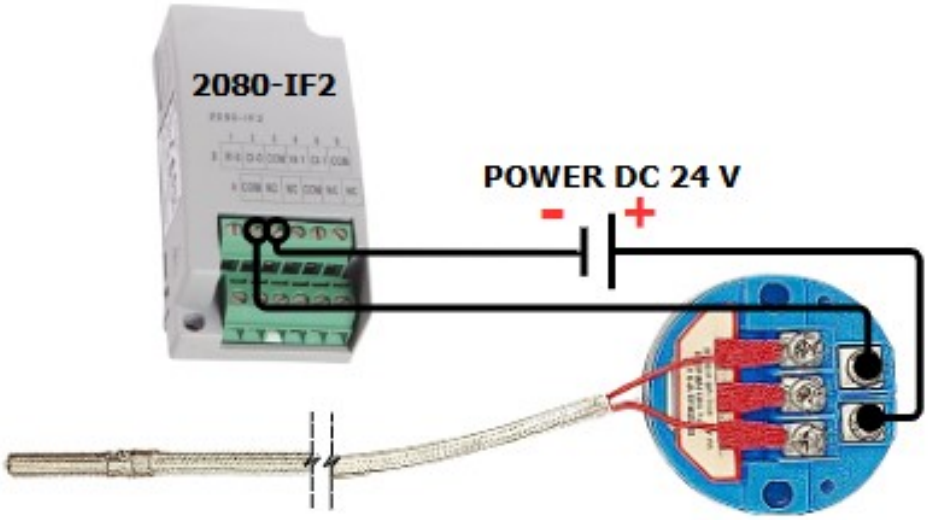

Figure 37. Pt100 connection to 2080-IF2 Module.

The following system reference points were considered to obtain the output transfer function, as shown in Equation 89:

1. Transmitter:
   4 - 20 mA = 0 – 200 °C, respectively.

2. 2080-IF2 Module:
   4 - 20 mA = 13107 – 65525 Raw data, respectively (effective reading range of the module).

$$Temperature\ (\ ^{\circ}C\ ) = \left(Raw\ Data\ \cdot \frac{200}{52428} \right) - 50 \qquad \text{Equation 89}$$

As it was mentioned in section 9.4.1.1, a measurement range of 10-50°C is proposed for the wind tunnel. For this, the sensor measurement had to be calibrated. For this purpose, a calibrated "Checktemp" laboratory thermometer was used as a reference sensor. This has an operating range of -50ºC a 150ºC with an accuracy of ± 0,3ºC.

Figure 38. "Checktemp" laboratory thermometer [12].

Initially, both sensors were used to take 5 temperature samples: 2 samples relative to ambient temperature and 3 samples relative to the boiling point of water in the city of Cali. For the second experiment, the water was heated until reaching its boiling point, where its temperature remains constant during the phase change from liquid to gas. The temperature results were consolidated in columns A and C of Table 18, while the Pt100 transmitter raw data was recorded in column B.

Based on the differences between the reference sensor and the temperature recorded by the P1100 transmitter (column A–C), it was decided to adjust the transfer function shown in Equation 89 to improve the measurement. Two changes were proposed:

1. First, multiply the "Raw Data" variable by a scaling factor to adjust the slope of the Pt100 transmitter's transfer function. For this, the slope of the data in columns A and C were taken as a reference. Based on this, the correction scaling factor was proposed as $F = \frac{21.52}{21.42}$ as shown in Equation 90. The results were recorded in column D.

$$Temperature\ (\ ^{\circ}C\ ) = \left(\frac{21.52}{21.42} \cdot Raw\ Data\ \cdot \frac{200}{52428}\right) - 50 \qquad \text{Equation 90}$$

2. Second, adjust the independent term of the sensor's linear transfer function to calibrate its offset. For this, the difference between the temperature from the reference sensor (column A) and the data obtained in column D is calculated. These results were consolidated in column 7 (column A–D). Based on this, it is observed that there is an average offset of **0.62** from the Pt100 transmitter above the reference sensor, therefore, this value is subtracted from the independent term of the transfer function, as shown in Equation 91. The results were recorded in column E.

[12] Image obtained from "Termómetro de laboratorio - Checktemp® - HANNA Instruments - digital / de sonda" HANNA instruments. "Checktemp" laboratory thermometer.

$$Temperature\ (°C) = \left(\frac{21.52}{21.42} \cdot Raw\ Data\ \cdot \frac{200}{52428}\right) - 50.62 \qquad \text{Equation 91}$$

Table 18. Experimental samples and calibration of the Pt100 transmitter.

Column / Test #	Real Temperature (Reference sensor) [°C]	PT100 to PLC Raw Data [UINT]	Temp. from PT100 Raw Data Based on **Equation 90** [°C]	Reference Vs PT100 Sensor Temp. Dif. [°C]	Temp. from PT100 Raw Data after Slope Ajustment [°C]	Dif. Temp. after Slope Adjustment Based on **Equation 91** [°C]	Temp. from PT100 Raw Data after Offset Adjustment [°C]	Dif. Temp. after Offset Adjustment Based on **Equation 92** [°C]
	A	B	C	A-C	D	A-D	E	A-E
1	24.8	19687	25.1	-0.3	25.4	-0.6	24.8	0.0
2	24.9	19686	25.1	-0.2	25.4	-0.5	24.8	0.1
3	96.4	38382	96.4	0.0	97.1	-0.7	96.5	-0.1
4	96.5	38392	96.5	0.0	97.1	-0.6	96.5	0.0
5	96.6	38411	96.5	0.1	97.2	-0.6	96.6	0.0
	SLOPE 21.52		**SLOPE** 21.42			**AVERAGE** -0.62		**AVERAGE** 0.00

Finally, thanks to the transfer function stated in Equation 91, a measurement from the Pt100 transmitter is obtained with greater accuracy. This can be observed in the last column (column A–E) of Table 18, where the difference between the temperature measured by the reference sensor and the Pt100 transmitter is close to zero.

After the calibration, test measurements were performed within the operating range of **10–50 °C**, with increments of **5 °C**. In Figure 39, the measurements of the Pt100 transmitter versus the reference sensor within the operating range can be compared. Small differences are observed, on the order of **±0.2 °C** on average, however, these are considered acceptable for academic wind tunnel applications.

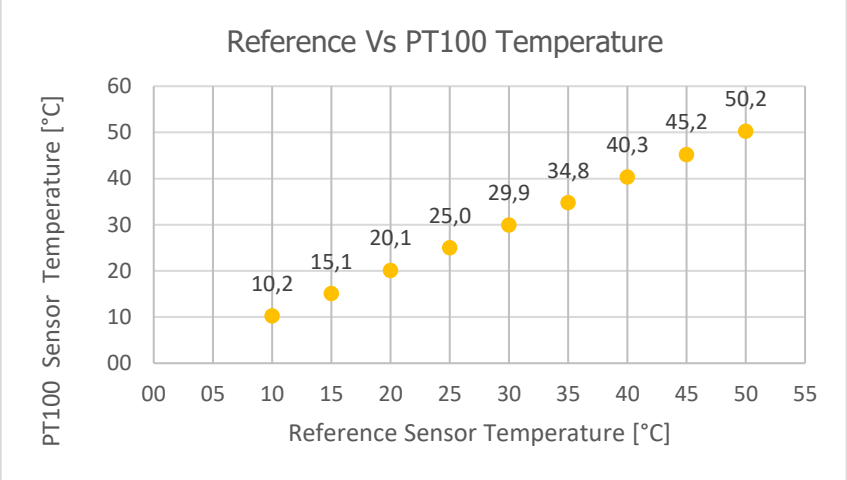

Figure 39. Test measurements: the PT100 transmitter Vs the reference sensor.

DLVR Series Low Voltage Digital Pressure Sensors (DLVR-L01D-E1NS-C-NI5F) + Pitot Tube

The DLVR sensor measures the temperature and dynamic pressure inside the tunnel. They communicate via the I²C protocol and deliver precise digital signals, which are read by the data acquisition module. The DLVR-L01D sensor package actually combines **two pneumatic ports** with **four electrical pins** as shown in Figure 40.

The pneumatic Port A is used to connect with static pressure source, while Port B is used to connect with stagnation pressure source. This is possible because of the pitot tube, which is located in the test section and separates the static pressure from the stagnation pressure in two different pipes.

On the other hand, the electrical pins are connected to the data acquisition module (Arduino UNO). Pin 1 (Gnd) is used to connect the sensor ground reference, Pin 2 (Vs) is used to connect the 5V supply voltage, Pin 3 (SDA) is used to connect the Serial Data line of the I²C bus, and Pin 4 (SCL) is used to connect the Serial Clock line of the I²C bus.

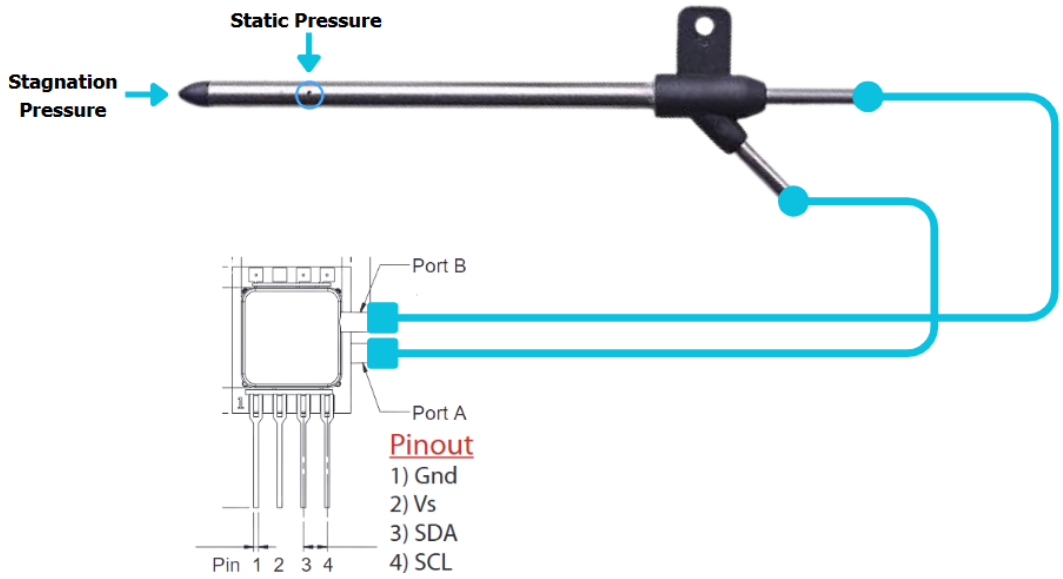

Figure 40. DLVR-L01D-E1NS-C-NI5F sensor package and Pitot Tube[13]

[13] Obtained from DLVR-L01D-E1NS-C-NI5F datasheet

Digital Interface Data Format

The first 16 bits consist of the 2 Status bits followed by the 14-bit the pressure value. The third byte provides the 8 most significant bits of the measured temperature; the fourth byte provides the 3 least significant bits of temperature, followed by 5 bits of undefined filler data. Table 19 shows the overall data format of the sensor.

Table 19. Output Data Format[13]

D[31:30]	D[29:24]	D[23:16]	D[15:8]	D[7:5]	D[4:0]
S[1:0]	P[13:8]	P[7:0]	T[10:3]	T[2:0]	X[4:0]
Status	Pressure MSB	Pressure LSB	Temperature MSB	Temperature LSB	Filler bits (Undefined]

Bit Definitions:
Status (S): Normal/ command/ bussy/ diagnostic
Pressure (P): Digital pressure reading
Temperature (T): Temperature reading

Based on the sensor characteristics and the data format, The Pressure Output Transfer Function Structure is shown in

Equation 92. From this structure, The Output Transfer Function for this application is defined in Equation 93. Then, to convert inH_2O to pascals, multiply Equation 93 by the conversion factor 249 and subtract the result by 0.982 to calibrate the DLVR sensor offset close to zero, as shown in Equation 94 .

$$Pressure(inH_2O) = 1.25 \cdot \left(\frac{Pout_{dig} - OS_{dig}}{2^{14}}\right) \cdot FSS(inH_2O) \quad \text{Equation 92}$$

$$Pressure(inH_2O) = 1.25 \cdot \left(\frac{Pout_{dig} - 8192}{2^{14}}\right) \cdot 2 = \frac{Pout_{dig} - 8192}{6553} \quad \text{Equation 93}$$

$$Pressure(Pa) = (Pressure(inH_2O) \cdot 249) - 0.982 \quad \text{Equation 94}$$

Where,

$Pout_{dig}$	Is the sensor pressure 14 bit digital output.
OS_{dig}	Is the specified digital offset (differential = 8192).
$FSS(inH_2O)$	Is the sensor Full Scale Span in inH2O (differential = 2).

On the other hand, The Temperature Output Transfer Function is shown in Equation 95.

$$Temperature\ (°C) = Tout_{dig} \cdot \left(\frac{200}{2^{11} - 1}\right) - 50$$ Equation 95

Where,

$Tout_{dig}$ Is the sensor temperature 11 bit digital output.

9.4.3.4 Data Acquisition and Communication Module: Arduino UNO +TTL to RS485 Module

The Arduino functions as the data acquisition module, reading signals from the DLVR sensor through the I²C protocol. This sensor measures two direct variables: temperature and dynamic pressure. Both require calibration. In the case of temperature, the reading quickly stabilizes at the ambient temperature. However, the dynamic pressure measurement is very small and is therefore affected by fluctuations caused by noise, air turbulence and instantaneous changes in local pressure. Thus, this measurement was processed using a moving average filter with a configurable window size signal to stabilize the measurement. Then, the Arduino map these values to Modbus holding registers, and after send this data through a TTL to RS485 Module which converts the TTL communication to Modbus RTU. Finally, they are interpreted by the PLC. A wiring diagram of this implementation is shown in Figure 41.

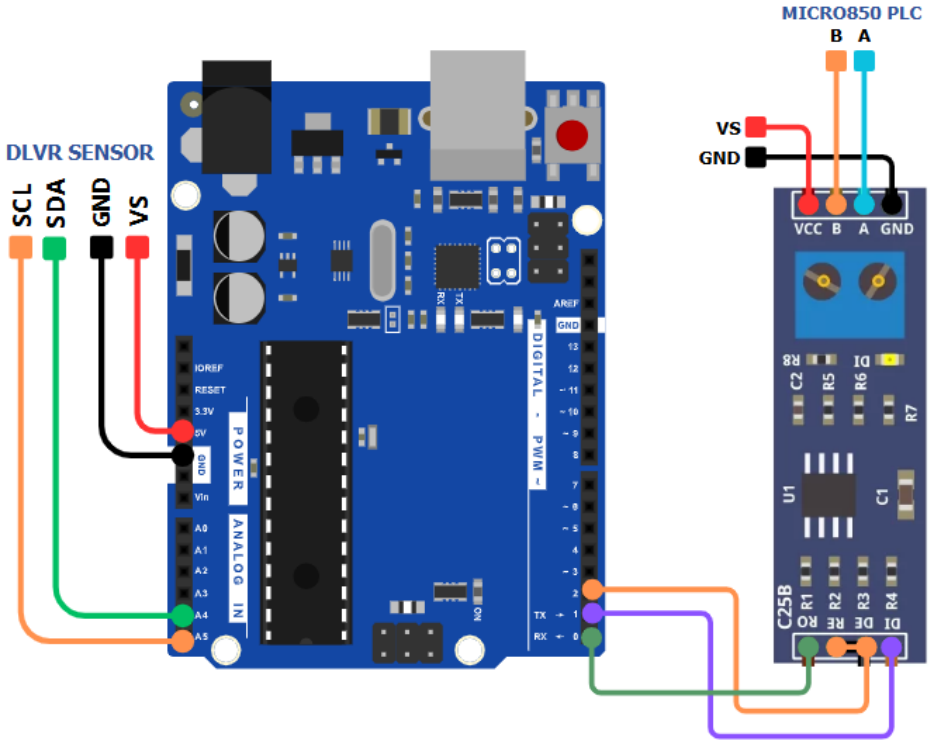

Figure 41. Arduino UNO and TTL to RS485 Module wiring diagram.

Code Functionality Description

> **Note:** The complete code transcription of the data acquisition module can be found in Appendix 4: Data Acquisition Module Code

a. I²C Sensor Interface:

The Arduino communicates with the DLVR sensor using the I²C protocol. Each reading retrieves four bytes: two bytes corresponding to the differential pressure and two bytes for temperature. The raw data from the pressure sensor is decoded and converted into engineering units (inH_2O and Pascals), applying a linear transformation based on the manufacturer's datasheet. The temperature bytes are decoded from the 11-bit format used by the DLVR sensor and converted to degrees Celsius.

b. Digital Signal Processing (DSP):

A moving average filter with a configurable window size (100 samples) is applied to the pressure data. This filtering reduces noise, stabilizes the signal, and improves the reliability of the pressure and derived airspeed values.

c. Airspeed Calculation:

The Arduino computes the average airspeed using Equation 6, assuming an air density of 1.184 kg/m³.

d. Modbus RTU Communication:

The processed data—average pressure (Pa), average airspeed (m/s), and temperature (°C)—are sent to Modbus holding registers in the PLC by the Arduino. Communication with the PLC is implemented via an RS485 transceiver module, with the DE/RE control handled through digital pin 2.

9.4.3.5 Actuator: Siemens Micromaster 6SE9 221 - 8CC13 Variable Frequency Drive (VFD)

For the selection of the VFD, the availability of equipment within the university community of the city of Cali was consulted. The Micromaster VFD (see Figure 42) was provided by the Universidad Autónoma de Occidente, who contributed to this project by providing equipment and laboratory facilities for the development of this design.

Figure 42. Siemens Micromaster 6SE9 221-8CC13 Variable Frequency Drive.

The VFD controls the rotational speed of the fan. As the motor RPM increases, the airflow speed also increases, thereby regulating the airflow inside the wind tunnel. This VFD receives 0 to 10-volt analog signal from the 2080-OF2 PLC module and modifies the output frequency (see Figure 43), when the module sends 0 volts, the motor runs at 0 Hz (stopped), and when it sends 10 volts, the motor runs at 60 Hz, which translates into precise control of airflow velocity in the tunnel. The VFD not only controls the speed but also protects the motor from overloads and provides smooth start and stop functions.

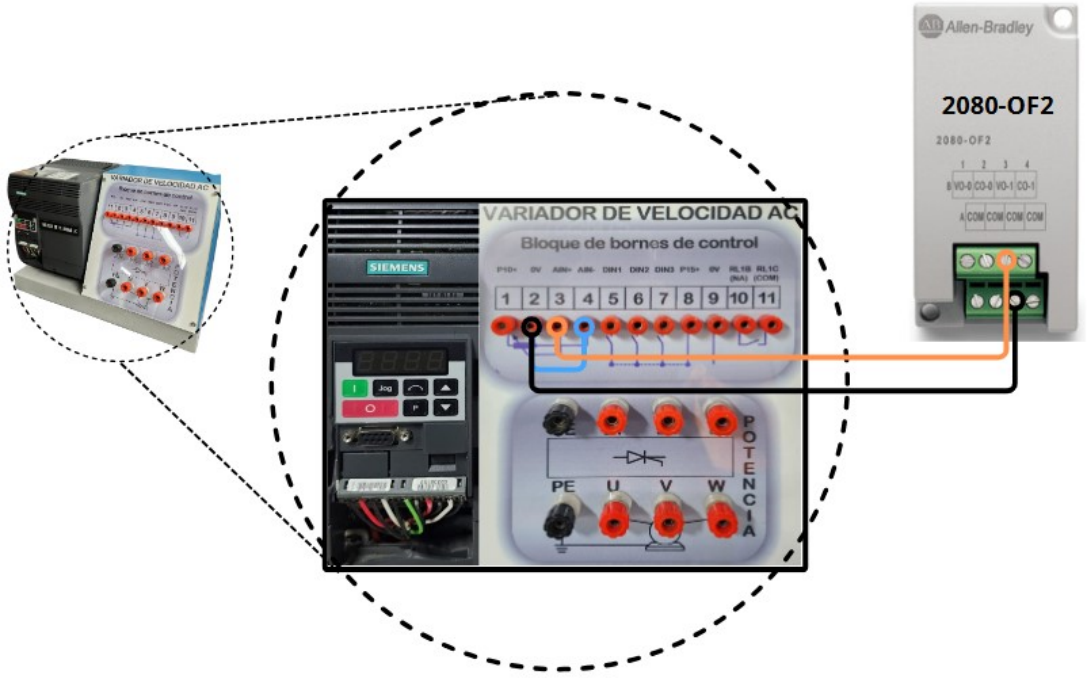

Figure 43. Micromaster VFD and 2080-OF2 Module wiring diagram.

The Micromaster VFD is powered by a three-phase AC input, typically at 220 volts. It can supply enough power to handle three-phase motors of various horsepower ratings (2.4, 3, and 5 HP). which makes it very versatile to control different motors with power requirements under 5 HP. For this control, it is important to configure the VFD and input the motor parameters. The most relevant parameters are show in Table 20:

Table 20. Micromaster VFD Parameters.

Parameter	**Function**	**VFD Configuration**	**Description/ Observations**
P002	Acceleration time (seconds)	10	Time it takes the motor to accelerate from standstill to maximum frequency
P003	Deceleration time (seconds)	4	Time it takes the motor to decelerate from max frequency to standstill.
P004	Acceleration/deceleration ramp rounding (seconds)	4	Used to smooth the acceleration/deceleration ramp. Effective only if ramp time exceeds 0.3s.
P006	Frequency setpoint source	1	1 = Analog (0-10V input)
P007	Keypad control	1	1 = Keypad buttons enabled (start, stop, etc.)
P081	Sets the motor's nominal frequency (Hz).	These parameters must be adjusted according to the engine used	
P082	Sets the nominal RPM of the motor according to its nameplate (RPM).		
P083	Sets the motor's nominal current based on the motor nameplate (A).		
P084	Sets the nominal motor voltage according to the motor nameplate (V).		
P085	Sets the nominal power of the motor (kW)		

9.4.3.6 Communication Interfaces: Allen-Bradley Stratix 2000 Ethernet Switch.

It establishes communication between the PLC, the HMI, and potentially an external computer for data monitoring or storage. Its function is to maintain a reliable Ethernet industrial network, facilitating data exchange between the different devices. Figure 44 illustrates the ethernet switch.

Figure 44. Allen-Bradley Stratix 2000 Ethernet Switch.

A static IP address was settled for this communication protocol based on the following configuration:

- Micro850 PLC
  - IP Address: 192.168.1.10
  - Mask: 255.255.255.0
- HMI
  - IP Address: 192.168.1.20
  - Mask: 255.255.255.0
- Computer
  - IP Address: 192.168.1.30
  - Mask: 255.255.255.0

9.4.3.7 Power Supply: Allen-Bradley Micro800 24V DC Power Supply

The Allen-Bradley Micro800 24V DC power supply is responsible for delivering stable and reliable electrical power to the entire control and data acquisition system. It converts standard AC mains voltage (typically 100V-220V AC) into a 24V DC output, as shown in Figure 45. This transformation involves an internal AC-to-DC conversion process, where alternating current (AC) is rectified, filtered, and regulated to produce a clean and stable direct current (DC) output. This is used to power components of the system, including the PLC, the HMI, The Ethernet Switch, and The PT100 temperature transmitter.

Figure 45. Allen-Bradley Micro800 24V DC Power Supply.

9.5 Validation

9.5.1 Desing validation

The wind tunnel design validation was conducted through computational simulation using the integrated SolidWorks environment, based on the detailed CAD model previously developed in the same software. The three-dimensional model included the defined sections: contraction, test section, and diffuser, ensuring geometric consistency with the specifications described in Section 9.2.

The simulation was configured using input parameters consistent with standard atmospheric conditions and the initial flow properties. An ambient temperature of approximately $25\,°C$ and an atmospheric pressure of $1013\,hPa$ were established, as

described in Section 9.3. Based on these values, the air density (ρ) was estimated at $1.184\ kg/\mathrm{m}^3$, which was also used in the theoretical calculations of pressure losses and Reynolds number presented in Section 9.3.1.1. The initial velocity at the tunnel inlet was defined as 1.62 m/s, consistent with the target volumetric flow rate of $1.62\ \mathrm{m}^3/s$ detailed in Table 11. The computational mesh was resolved through 40 iterations, ensuring convergence and numerical stability of the results. These boundary conditions provided the foundation for validating the aerodynamic behavior of the tunnel and comparing it against the theoretical expectations established in the design.

- Average temperature: $\sim 25\ °C\ (298.15\ K)$
- Average atmospheric pressure: $\sim 1013\ hPa\ (101{,}300\ Pa)$
- Air density: $\rho \approx 1.184\ kg/\mathrm{m}^3$
- Initial velocity: 1.62 m/s
- Iterations: 40

Figure 46 presents the flow speed simulation in the test section. The color gradient shows a maximum velocity near 15 m/s, which matches the design objective established in section 9.3.1. This result confirms the tunnel meets the academic requirement of achieving subsonic speeds within the test chamber.

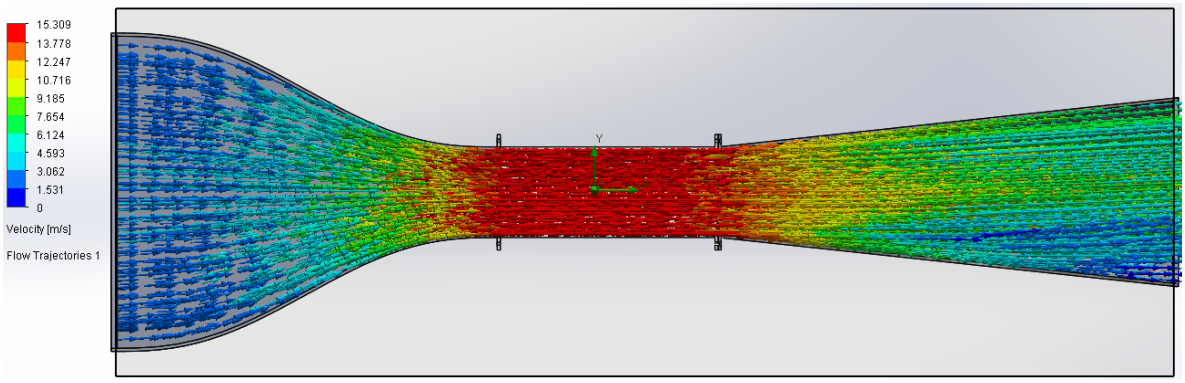

Figure 46. Airflow speed simulation.

The Figure 47 shows the dynamic pressure distribution, which increases progressively as the flow accelerates through the contraction and into the test section. This behavior aligns with Bernoulli's principle and matches the dynamic pressure values estimated from flow velocity and volumetric rate in Section 9.3.2. Based on Equation 6, for a maximum speed of 15 m/s, a dynamic pressure of 133 Pa is estimated, which coincides with the results obtained from the simulation in Figure 47.

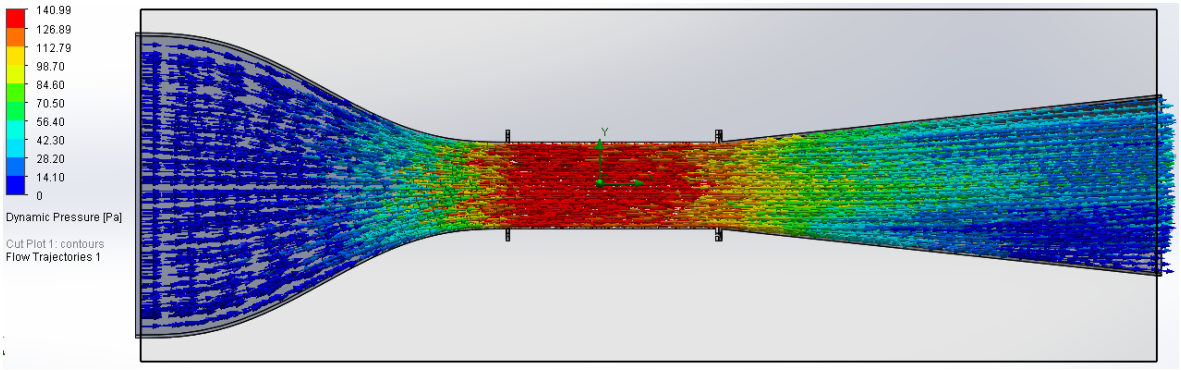

Figure 47. Dynamic pressure simulation.

Figure 48 shows the temperature distribution along the wind tunnel, represented using a color gradient. The simulation confirms an uniform ambient temperature throughout the system, which is consistent with the assumption of no internal heat generation or external heating sources. This result validates the assumption of isothermal conditions used in the theoretical analysis.

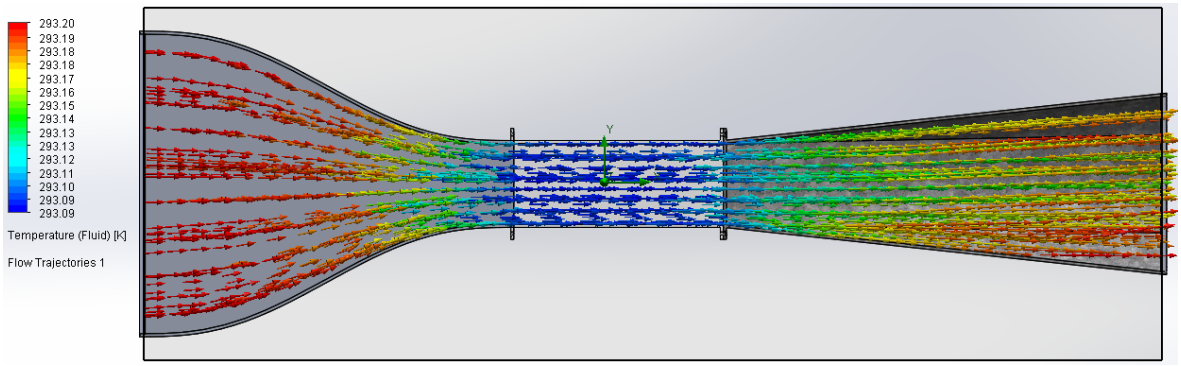

Figure 48. Temperature simulation.

9.5.2 Control and data acquisition validation

Due to time and resources constraints, it was not possible to build the designed wind tunnel. However, in the UAO there is a wind tunnel built for academic purposes in 2020 by Cesar Augusto Noguera Campo as a degree project [5] (see Figure 49). This is a low-speed open wind tunnel, with the same operating principle described in section 9.2.2. It has a 220V three-phase fan and a test section similar in size to the design proposed in section 9.3.1. Therefore, the control and data acquisition system was coupled to this tunnel in order to carry out its validation. It is worth clarifying that this tunnel does not have a control and data acquisition system.

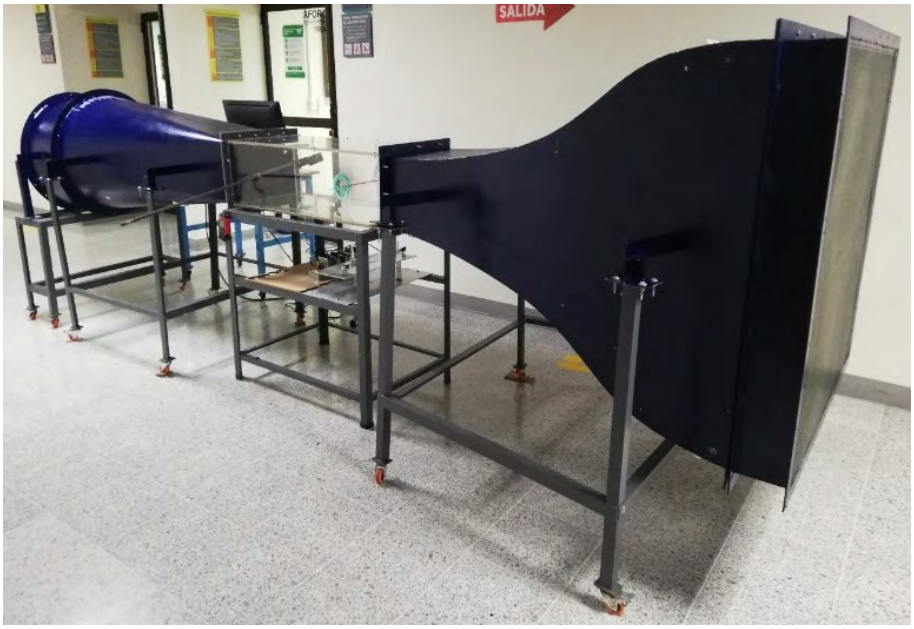

Figure 49. Universidad Autónoma de Occidente wind tunnel [5].

The control and data acquisition system was built based on the design proposed in section 9.4. Its development was carried out at the automation and process center (CAP) of PUJ-Cali. The components were mounted on a support made of aluminum profiles and an acrylic panel, as shown in Figure 50.

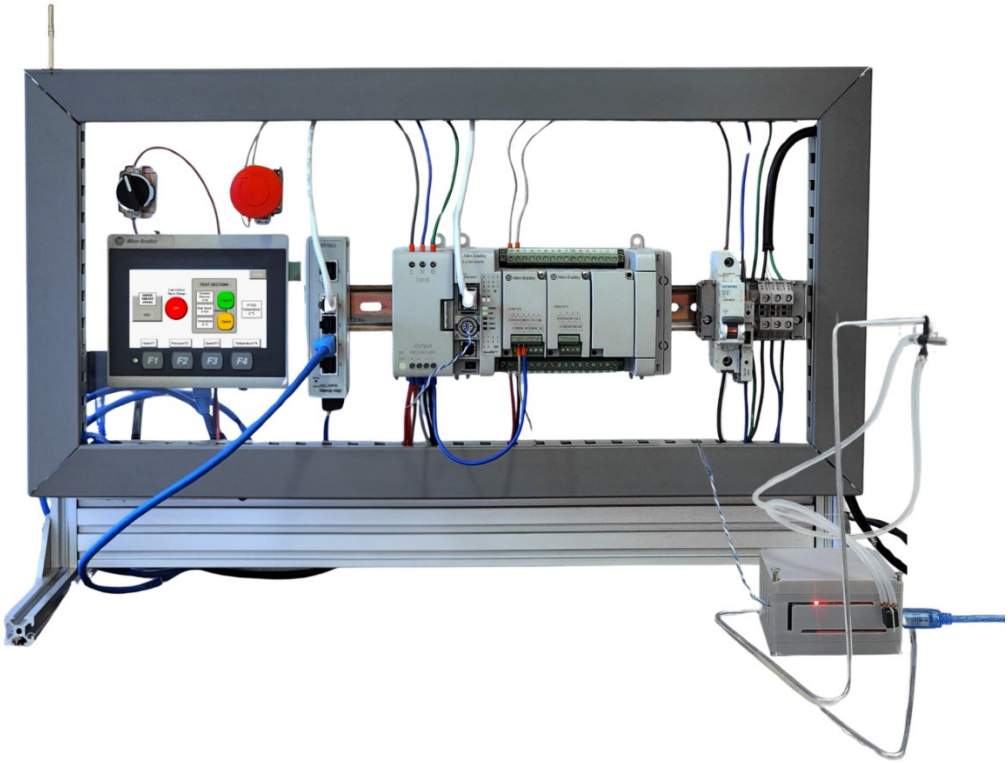

Figure 50. Implementation of the CDAQ system.

In order to perform the tests, first, the airflow velocity response in the test section was characterized, as a function of the frequency commanded by the VFD to the fan (system input parameter). For this purpose, the airflow velocity in the test section was experimentally measured at different frequency setpoints configured on the frequency drive. The frequency command is controlled from the PLC through the Raw Data; therefore, the total Raw Data range ($2^{16} = 65536$) was divided into 10 tests until reaching the maximum desired velocity of 15 m/s, as shown in Table 21.

During the tests, the electrical and mechanical behavior of the fan was observed. However, a significant increase in system vibrations was found above 41.9 Hz, which corresponds to 11 m/s (test 7 in Table 21), representing a risk for the operation of the wind tunnel in prolonged tests. Therefore, 41.9 Hz was established as the maximum fan operating frequency allowed for the validation of the control system. Based on the perceived noise coming from the vibrations of the fan motor, the operating range of the motor was color- classified. Green means low perceived noise, yellow means moderate noise and red means excessive noise. It is recommended not to reach the red range during operation for safety reasons.

Table 21. Test results of airflow speed in the test section for different VFD setpoints and PLC input signals.

Test #	PLC Raw Data	VFD Setpoint [Hz]	Real speed in the Test Section (from Reference Sensor) [m/s]
1	6553	5.8	2.1
2	13107	11.8	4.1
3	19660	17.8	6
4	26214	23.8	7.7
5	32767	29.9	9.2
6	39321	35.9	10.4
7	45874	41.9	11
8	52428	47.8	14
9	58981	53.8	14.6
10	65535	59.8	15

Based on the measured points in Table 21, a linear interpolation was performed into the intervals, as shown in Figure 51. This is the approximation that the control system uses to reach intermediate values of speed in the operating range. In other words, when the user enters a target speed, the system calculates the Raw Data value, and uses this to set

the frequency. This is done by making a linear approximation based on the minimum and maximum value of the sub-range where the target speed is located. For example, if the target speed is 6.5 m/s, the control system performs a linear interpolation between 6 and 7.7 m/s (minimum and maximum value of the sub-range) to obtain the Raw Data command equivalent to 6.5 m/s, which in this case is 21587.

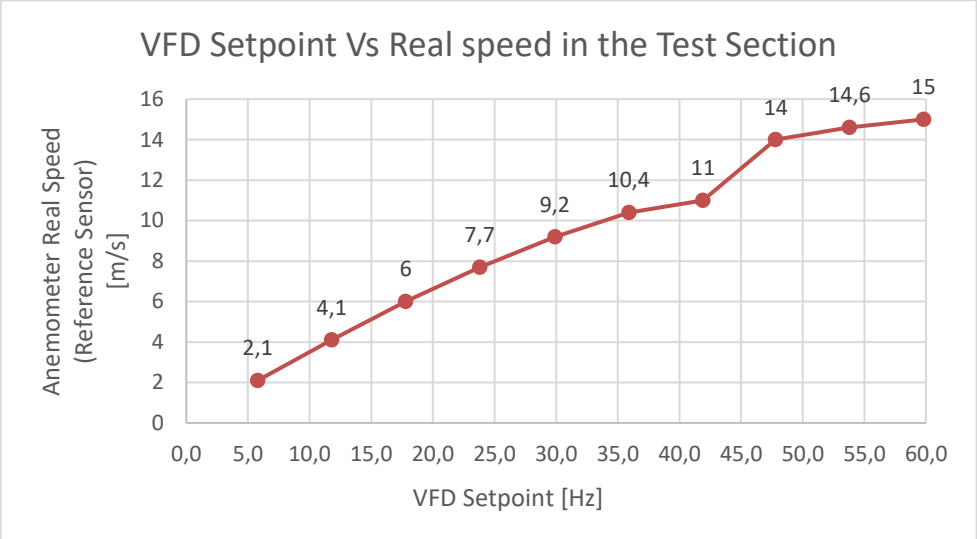

Figure 51. Relationship between VFD frequency setpoint and real airflow speed in the test section

Once the system response was characterized, the calibration of the control and data acquisition system was carried out. For this purpose, experimental tests were performed in the wind tunnel test section. Measurements were taken and compared with reference values obtained by calibrated sensors. To determine the real temperature, the calibrated "Checktemp" laboratory thermometer was again used as reference sensor. On the other hand, the UT363S Digital Anemometer (see Figure 52) with an accuracy of ±(5%+0.5m/s) was employed to measure the real airflow speed in the test section.

Figure 52. UT363S Digital Anemometer

As part of the calibration, Table 22 was generated, which consolidates the experimental results. This was developed according to the following steps:

1. The target speeds were entered through the touch screen of the HMI (column 1).
2. The Raw Data values and the VFD frequency calculated by the system, to meet the target velocity, were recorded (columns 2 and 3). Additionally, the fan RPM was recorded in column 4 to identify the fan's operating point.
3. The temperature inside the test section was measured using the reference sensor ("Checktemp" laboratory thermometer) and the DLVR temperature sensor. The latter applies the transfer function from Equation 95. The measurements were recorded in columns 5 and 6, respectively.
4. The temperature difference between the reference sensor (column 5) and the DLVR sensor (column 6) was calculated. The results were recorded in column 7. From these values, an average error of **–0.81 °C** is observed, indicating that the DLVR sensor had an offset above the reference sensor.
5. The airflow speed inside the test section was measured using the reference sensor (UT363S Digital Anemometer), as shown in Figure 53. The measurements were recorded in column 8.

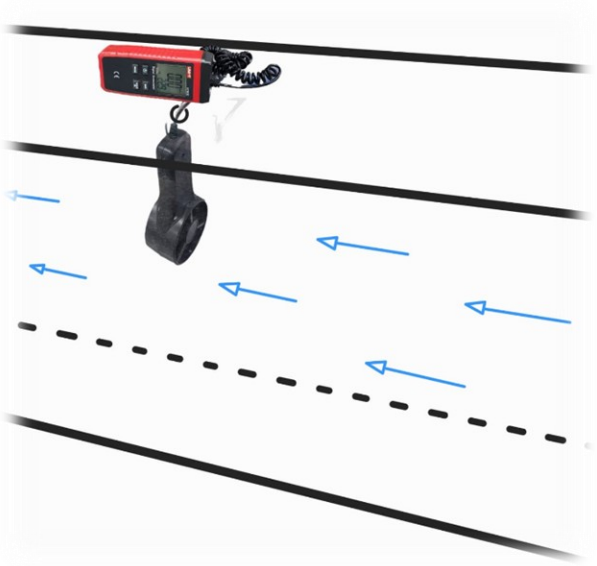

Figure 53. Representation of airflow speed measurement in the test section with the UT363S Digital Anemometer.

6. Using the Pitot Tube (see Figure 54), the dynamic pressure was measured with the DLVR sensor, and the airflow velocity was calculated based on the transfer function from Equation 94. The measurements were recorded in columns 9 and 11, respectively.

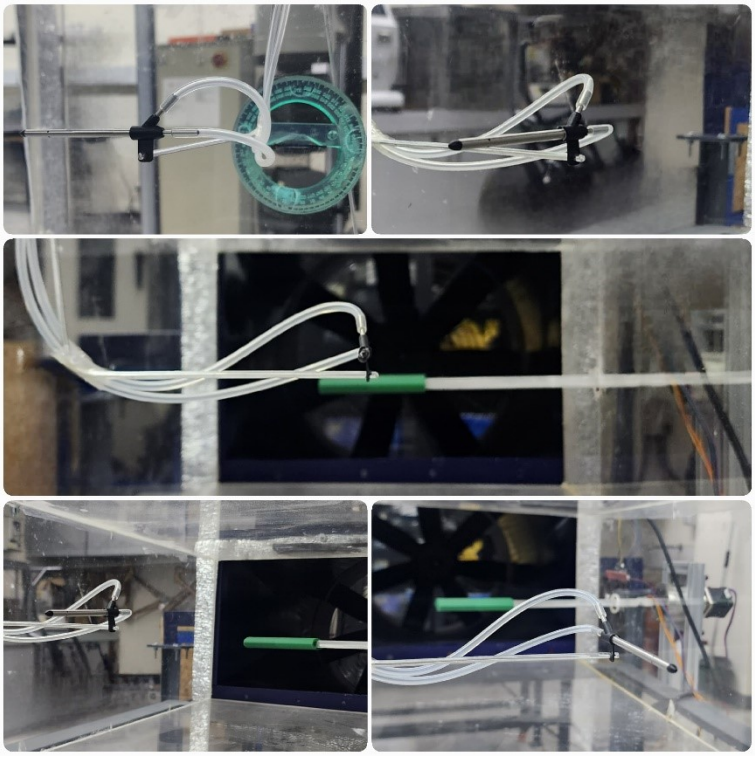

Figure 54. Photographs of the pitot tube installed inside the test section.

7. The velocity difference between the reference sensor (column 8) and the DLVR sensor (column 9) was calculated. The results were recorded in column 10. From these values, a small average error close to zero was observed, indicating that the DLVR sensor was properly calibrated with respect to the reference sensor.

Table 22. Calibration of the control and data acquisition system through airflow speed and temperature measurements.

Speed Setpoint (HMI input) [m/s]	PLC Raw Data [UINT]	VFD Setpoint [Hz]	Fan RPM	Real Temperature (Reference sensor) [°C]	DLVR Sensor Temperature Measurement [°C]	Reference Vs DLVR Sensor Temp. Dif. [°C]	Anemometer Real Speed (Reference Sensor) [m/s]	DLVR Sensor Speed Measurement [m/s]	Reference Vs DLVR Sensor Speed Dif. [m/s]	Dynamic Pressure [Pa]
2.1	6553	5.80	145	23.9	24.7	-0.80	2.1	2.04	0.06	2.40
4.1	13107	11.80	295	24.4	24.9	-0.5	4.1	4.03	0.07	24.87
6	19660	17.80	445	23.9	24.8	-0.9	6.0	5.94	0.06	20.20
7.7	26214	23.80	596	23.9	24.8	-0.9	7.7	7.68	0.02	34.90
9.2	32767	29.90	747	23.8	24.7	-0.9	9.2	9.22	-0.02	50.41
10.4	39321	35.90	897	23.8	24.7	-0.9	10.4	10.47	-0.07	65.10
11	45874	41.90	1047	23.8	24.6	-0.8	11.0	11.05	-0.05	72.35
						AVERAGE -0.81			**AVERAGE** 0.01	

Based on the results from Table 22, it is suggested to adjust Equation 96 to reduce the temperature measurement error. As mentioned in step 4, there is an average error of **–0.81**. Therefore, Equation 96 is proposed as the new transfer function to correct the

temperature measurement of the DLVR sensor. On the other hand, the transfer function for the air speed measurement remained constant.

$$Temperature\ (°C) = Tout_{dig} \cdot \left(\frac{200}{2^{11}-1}\right) - 50.8 \qquad \text{Equation 96}$$

To validate the calibration, the previous steps were repeated using different target velocities, equally spaced within the operating range, in order to validate the wind tunnel's operation. The results are consolidated in Table 23.

Table 23. Validation results of the control and data acquisition system through airflow speed and temperature measurements.

Test #	Speed Setpoint (HMI input) [m/s]	PLC Raw Data [UINT]	VFD Setpoint [Hz]	Fan RPM	Real Temperature (Reference sensor) [°C]	DLVR Sensor Temperature Measurement [°C]	Reference Vs DLVR Sensor Temp. Dif. [°C]	Anemometer Real Speed (Reference Sensor) [m/s]	DLVR Sensor Speed Measurement [m/s]	Reference Vs DLVR Sensor Speed Dif. [m/s]	Dynamic Pressure [Pa]
1	1.5	4680	4.1	102	23.8	23.9	-0.1	1.48	1.46	0.02	1.26
2	3	9502	8.5	212	24.4	24.1	0.3	3.05	2.91	0.14	5.02
3	4.5	14486	13.1	327	24.3	24.2	0.1	4.49	4.47	0.02	11.84
4	6.0	19660	17.8	445	23.9	24.1	-0.2	6.0	5.95	0.05	20.93
5	7.5	25442	23.1	578	24.7	24.4	0.3	7.56	7.49	0.07	33.18
6	9	31893	29.0	726	24.6	24.3	0.3	8.98	9.03	-0.05	48.28
7	10.5	40413	36.9	922	24.6	24.3	0.3	10.54	10.51	0.03	65.43
							AVERAGE 0.17			**AVERAGE** 0.04	

From the results obtained in Table 23, the measurements obtained from the flow velocity measured by the DLVR sensor (column 10) were graphed in relation to the dynamic pressure (column 12). These were compared with the theoretical function of Equation 6. Thus, Figure 55 shows the similarity between the experimental measurements and the theory, demonstrating that the data acquisition system is capable of correctly measuring the dynamic pressure and calculating the air flow velocity within the test section.

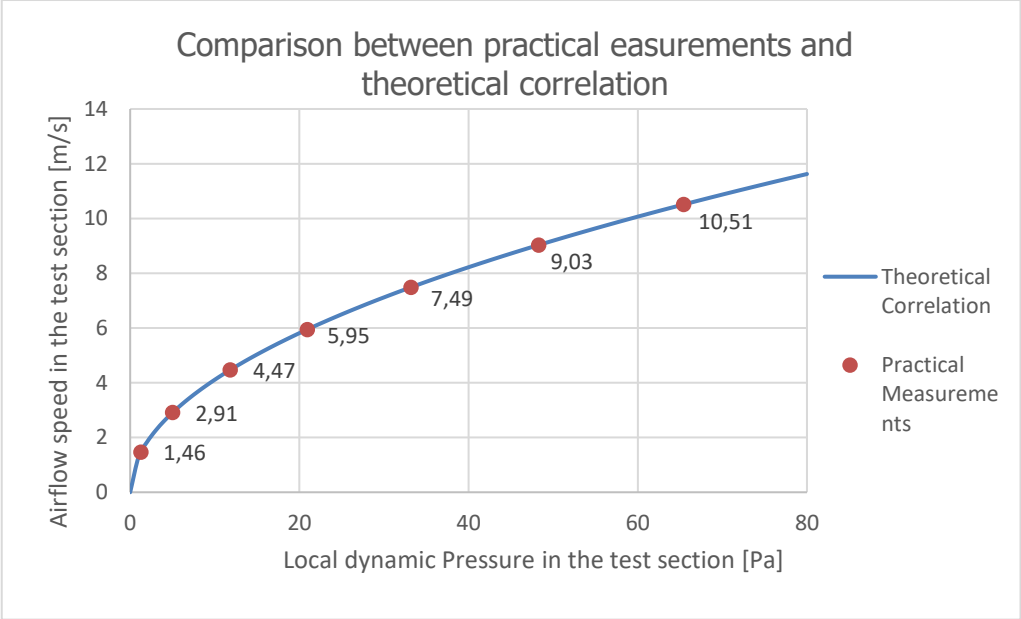

Figure 55. Validation of airflow speed measurements against theoretical dynamic pressure correlation.

To validate the control system and airflow stability, different target velocity values were inputted into the HMI terminal. For each target velocity, the fan was turned on, and after 10 seconds (fan acceleration time), the airflow velocity inside the test section was measured once per second using the calibrated DLVR sensor. The results are shown in Figure 56, these show that the control system can reach and maintain the desired airflow velocity for the different target velocities entered by the user, thus fulfilling the control system requirements.

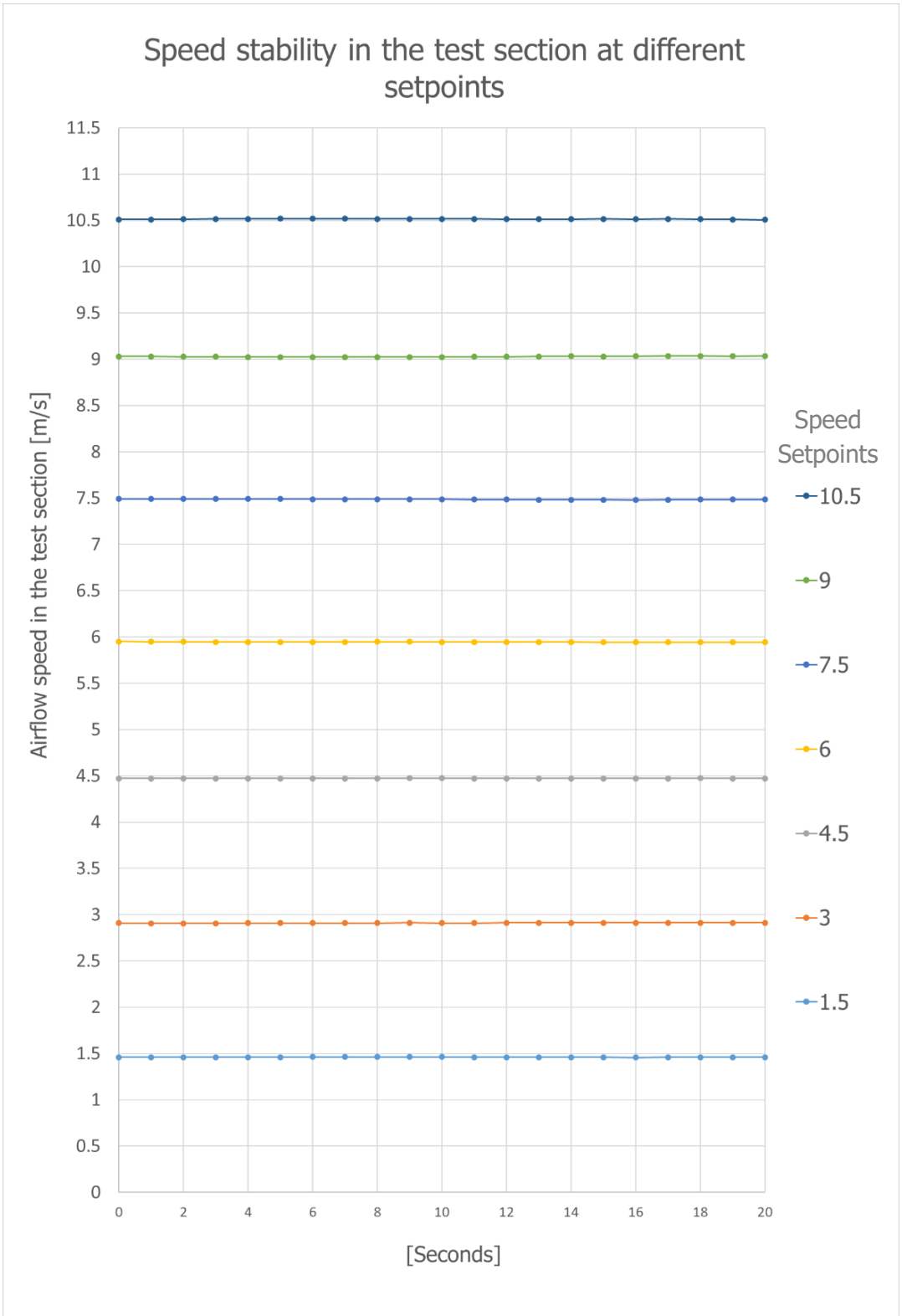

Figure 56. Airflow velocity response measured with the calibrated DLVR sensor for different target velocities set via the HMI.

10. Conclusion

- The development of the subsonic wind tunnel design for academic use allowed for the application of a structured engineering methodology, integrating tools for information gathering, technical analysis, and computational validation. Based on the analysis of functional requirements and interviews with faculty and laboratory staff, key design criteria were established that guided the selection of the tunnel type, geometric configuration, and appropriate materials for each component.
- The open-circuit wind tunnel configuration was selected due to its simplified construction, ease of integration with observation and data acquisition systems, and lower relative cost. The design was divided into functional sections—settling chamber, contraction, test section, and diffuser—allowing for a detailed analysis of the aerodynamic and structural behavior of each part.
- Through simulations carried out using SolidWorks Flow Simulation, it was confirmed that the tunnel can achieve the intended operating conditions, particularly flow velocities near 15 m/s in the test section. These simulation results showed strong similarity to the theoretical calculations of flow rate, velocity, and dynamic pressure, reinforcing the viability of the proposed design.
- The implemented CADQ system successfully fulfilled the objectives established for the subsonic wind tunnel designed for academic purposes. It allows to measure the dynamic air pressure and calculate the air velocity in the range of 1 to 15 m/s, based on Bernoulli Equation. This is possible by using a differential pressure sensor with an operating range of $\pm 250\ Pa$ and 14 bits of digital output resolution.
- The temperature sensors were calibrated with an accuracy of ±0.2°C to measure a temperature range of 10-50°C. However, experimental tests and simulations show that the temperature inside the tunnel remains close to ambient temperature.
- Under disturbance-free operating conditions, the open-loop control system with a VFD was enough to maintain a stable airflow speed within the test section, with an accuracy of ±0.1 m/s with respect to the input target speed. However, for dynamic adaptability, a Closed-loop Control is recommended to ensure real-time compensation for disturbances.

11. References

[1] C. C. Lin and C. C. Tsai, “The relationships between students’ Conceptions of Learning Engineering and their preferences for classroom and laboratory Learning environments,” *Journal of Engineering Education*, vol. 98, no. 2, pp. 193–204, 2009, doi: 10.1002/J.2168-9830.2009.TB01017.X.

[2] J. N. Libii and J. N. Libii, “Wind Tunnels in Engineering Education,” *Wind Tunnels and Experimental Fluid Dynamics Research*, Jul. 2011, doi: 10.5772/17071.

[3] Y. A. Çengel and J. M. Cimbala, *Mecánica de Fluidos. Fundamentos y aplicaciones*, vol. Primera edición. 2006.

[4] J. B. Barlow, W. H. Rae, A. Pope, and A. Pope, *Low-speed wind tunnel testing*, 3rd ed. New York: John wiley & sons, 1999.

[5] N. C. Cesar Augusto, “Diseño y Construcción de un Túnel de Viento a Escala para Estudiar la Aerodinámica en un Perfil Alar Naca 2412,” Universidad Autonoma de Occidente, Santiago de Cali, 2020.

[6] F. Acevedo Vélez, “Diseño de un Túnel de Viento para Prueba de Ventiladores y Perfiles Aerodinámicos,” Universidad EAFIT, Medellin, 2006. Accessed: Mar. 14, 2024. [Online]. Available: chrome-extension://efaidnbmnnnibpcajpcglclefindmkaj/https://core.ac.uk/download/pdf/47245284.pdf

[7] A. Arango Duque and J. M. Yepes Murillo, “Diseño, construcción y puesta en funcionamiento del túnel de viento subsónico de circuito abierto de la Universidad Nacional de Colombia sede Bogotá con implementación de sistemas de toma de datos de aire y visualización de flujo,” Fundación Universitaria Los Libertadores, Bogotá DC, 2014.

[8] W. R. Kaminski, “A Series of Heat Transfer Experiments for the Mechanical Engineering Technology Student,” Jun. 1998. doi: 10.18260/1-2--7398.

[9] R. Shiavt and A. Brodersen, “Study of instructional modes for introductory computing,” *Journal of Engineering Education*, vol. 94, no. 4, pp. 355–362, 2005, doi: 10.1002/J.2168-9830.2005.TB00863.X.

[10] E. W. Ernst, “A New Role for the Undergraduate Engineering Laboratory,” *IEEE Transactions on Education*, vol. 26, no. 2, pp. 49–51, 1983, doi: 10.1109/TE.1983.4321598.

[11] E. F. Crawley, J. Malmqvist, S. Ostlund, and D. Brodeur, *Rethinking engineering education : the CDIO approach*, no. 97. New York: Springer, 2007. Accessed: May 28, 2025. [Online]. Available: https://archive.org/details/rethinkingengine0000unse

[12] J. E. Bermeo Vallejo, D. F. Siguencia Bermeo, and P. I. Serpa Medina, “Diseño y construcción de un túnel de viento para análisis aerodinámico en vehículos a escala,” 2012, Accessed: Apr. 06, 2025. [Online]. Available: http://dspace.ups.edu.ec/handle/123456789/2001

[13] “Embodiment Design | Engineering Design - McGill University.” Accessed: May 16, 2025. [Online]. Available: https://www.mcgill.ca/engineeringdesign/step-step-design-process/design-phases-mechanical-engineering/embodiment-design

[14] V. y D. T. Ministra de Ambiente, “Resolucion 0627 De 2006,” Apr. 2006, Accessed: May 16, 2025. [Online]. Available: www.alcaldiabogota.gov.co/sisjur/normas/Norma1.jsp?i=19982

[15] WHO, “La OMS publica una nueva norma para hacer frente a la creciente amenaza de la pérdida de audición.” Accessed: May 16, 2025. [Online]. Available: https://www.who.int/es/news/item/02-03-2022-who-releases-new-standard-to-tackle-rising-threat-of-hearing-loss

[16] P. Bradshaw and R. C. Pankhurst, “The design of low-speed wind tunnels,” *Progress in Aerospace Sciences*, vol. 5, no. C, pp. 1–69, Jan. 1964, doi: 10.1016/0376-0421(64)90003-X.

[17] R. D. Mehta and P. Bradshaw, “Design Rules for Small Low Speed Wind Tunnels,” *Aeronautical Journal*, vol. 83, no. 827, pp. 443–449, 1979, doi: 10.1017/s0001924000031985.

[18] J. H. Bell and R. D. Mehta, “Contraction design for small low-speed wind tunnels,” Stanford, Sep. 1988.

[19] L. Prandtl, “Attaining a steady air stream in wind tunnels,” 726, Oct. 01, 1933

[20] İ. Göv, “Comparison of hexagonal, square, and circular sectioned honeycomb performance in a wind tunnel,” *The International Journal of Energy & Engineering Sciences*, vol. 6, no. 2, pp. 38–49, 2021.

[21] B. Lindgren and A. V Johansson, “Design and Evaluation of a Low-Speed Wind-Tunnel with Expanding Corners,” 2002.

12. Appendices

12.1 Appendix 1: Interviews

Re Wind Tunnel Requirements

Dear professor, collaborator and/or expert of the Faculty of Engineering of the Pontificia Universidad Javeriana Cali.

We are María Nicolle Gómez and Jaime Iriarte Martínez, 8th semester students, and we are developing our degree work.
In order to gather relevant information for our thesis, entitled ***Design of a subsonic wind tunnel for academic activities***, we ask you to answer the following survey, which will allow us to establish the most pertinent criteria for the design of such a tunnel.

Below, you will find questions related to the importance that you can consider in the face of certain fundamental aspects for the implementation of a wind tunnel for educational purposes.
For further context: Integrating hands-on activities into engineering education is essential to enhance learning and prepare students for real challenges. In areas such as thermodynamics and fluid sciences, guided hands-on activities help consolidate knowledge. A wind tunnel creates a controlled environment to study the behavior of objects in the airflow, simulating real atmospheric conditions. It is expected that the mechanical and electronic design of the wind tunnel will be achieved by specialized software in the different stages. **The objective is to design a wind tunnel for practical activities for engineering students.**

The thesis **contemplates the design** of a subsonic wind tunnel that will serve as an educational tool for the study and analysis of aerodynamic phenomena, providing the academic community with an adequate infrastructure for the realization of experiments and practices related to mechanical engineering and different areasof interest.

We greatly appreciate your participation and collaboration.
We invite you to answer honestly, emphasizing that this survey is for academic purposes only and will not be used for any other purpose.

Section 1: Current Use of Laboratories

In this section, we seek to understand the current use of the laboratories of the Faculty of Engineering and Sciences, specifically in relation to experiments and educational activities related to fluid dynamics and aerodynamics. Their experience and knowledge in handling these laboratories will help us identify current needs and challenges, which is critical for the design of a subsonic wind tunnel that effectively meets academic demands.

1. Names and surnames *

2. What is your role within the faculty's laboratories? *

- ◯ Teacher
- ◯ Laboratory Technician
- ◯ Coordinator
- ◯ Expert
- ◯ Other

3. What kind of experiments are currently being carried out in the laboratories under your charge? *

- ☐ Fluid Mechanics
- ☐ Mechanics of solids
- ☐ Thermodynamics
- ☐ Structure Analysis
- ☐ Other

4. How often are laboratories used for fluid dynamics-related experiments? *

- ◯ Often
- ◯ Occasionally
- ◯ Rarely
- ◯ Never

5. What specialized equipment is currently used for fluid dynamics teaching? *

6. What are the main limitations you face in conducting experiments related to aerodynamics? *

Section 2: Design Requirements for a Wind Tunnel for Academic Purposes

In this section, we focus on the specific requirements for the design of a subsonic wind tunnel intended for academic activities. Their knowledge and experience will be crucial to define the characteristics and functionalities that this equipment should have.

7. What types of experiments do you think should be carried out in the wind tunnel? *

- [ ] Vehicle aerodynamics
- [ ] Study of aerodynamic profiles
- [ ] Heat Transfer Laboratories
- [ ] Adidimensional numbers
- [ ] Other

8. What type of wind tunnel do you consider most suitable for academic purposes? *

- ◯ Open Circuit Wind Tunnel
- ◯ Closed-loop wind tunnel
- ◯ Suction wind tunnel
- ◯ Pressurized wind tunnel

9. What dimensions do you consider appropriate for the test section of the wind tunnel? Taking into accountthe purposeand constraints of the wind tunnel,knowing that it can be supported by models adimencionales *

- ◯ Less than 10x10x100 cm
- ◯ Between 10x10x100 cm and 20x20x100 cm
- ◯ Between 20x20x100 cm and 30x30x100 cm
- ◯ More than 30x30x100 cm

10. What doyou consider appropriate for the wind tunnel test section? *

- [ ] Visible Test Section
- [ ] Measurement sensors in the test section
- [ ] Flow visualization
- [ ] Other

11. How important is it to you that the wind tunnel has temperature measurements? In aschoolfrom1 to 5, where 5 is "Very important" and 1 is "Not importantbefore"

1	2	3	4	5

12. How important is it that the speed in the test section is variable? *

1	2	3	4	5

13. How important is the visualization of the flow and the test section for you? *

1	2	3	4	5

14. How important is the noise level generated by the wind tunnel to you? *

1	2	3	4	5

15. What norms and standards do you think should be followed in wind tunnel design? *

- ◯ ISO 5801 (wind tunnel fans)
- ◯ ASME PTC 19.5 (Fluid Pressure Measurement)
- ◯ Other

16. Whatare the supply voltage ranges oftheequipment you are normallyusing? *

- ◯ Less than 110V
- ◯ Between 110V and 220V
- ◯ More than 220V

17. What measuring and instrumentation devices do you consider essential for the wind tunnel? *

- ☐ Anemometers
- ☐ Pressure gauges
- ☐ Pressure Sensors
- ☐ Pitot Tube
- ☐ Hot Wire Anemometer
- ☐ Other

18. What additional aspects or general feedback would you like to provide about wind tunnel design? *

Section 3: Experience with Wind Tunnels (Only for those who have worked with them)

In this section, we seek to gather information about your previous experience working with wind tunnels. Their knowledge and experiences will allow us to better understand the characteristics and challenges associated with the use of this equipment in an academic environment. We ask that you answer the following questions based on your personal experience.

19. Have you worked with wind tunnels before? *

- ◯ Yes
- ◯ No

20. If you have worked with wind tunnels, did you perform the instrumentation and control of the circuit or did you not have a control loop? *

- ◯ Yes, he performed instrumentation and control
- ◯ No, it had no control loop

21. Were the speeds handled by the wind tunnel variable? *

- ◯ Yes
- ◯ No

22. What type of data acquisition system did you use for the wind tunnel? *

23. In case you handled the instrumentation and control, what hardware or software did you use? *

24. How did you implement the instrumentation and control of the wind tunnel? *

12.2 Appendix 2: Drawing

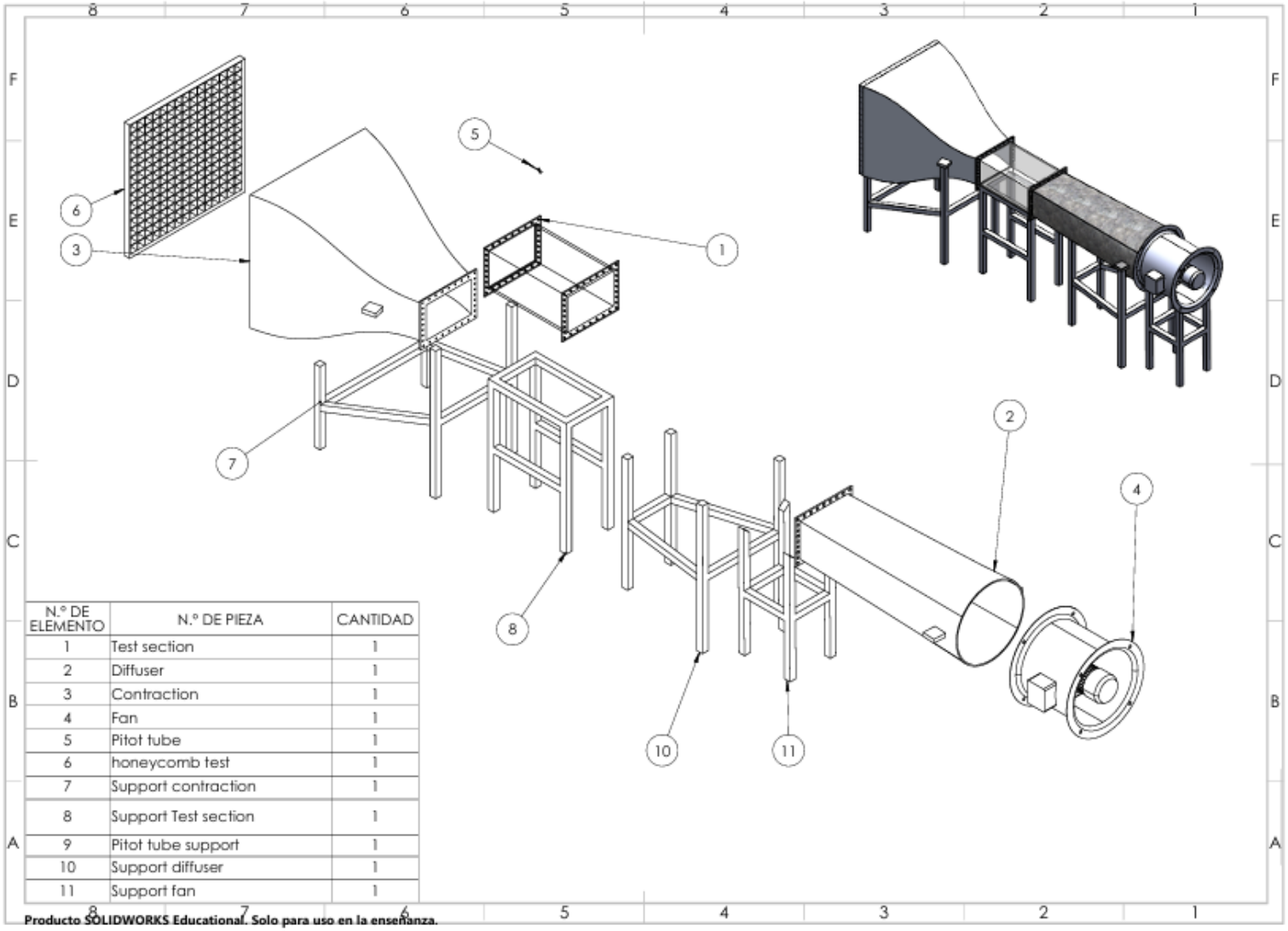

N.º DE ELEMENTO	N.º DE PIEZA	CANTIDAD
1	Test section	1
2	Diffuser	1
3	Contraction	1
4	Fan	1
5	Pitot tube	1
6	honeycomb test	1
7	Support contraction	1
8	Support Test section	1
9	Pitot tube support	1
10	Support diffuser	1
11	Support fan	1

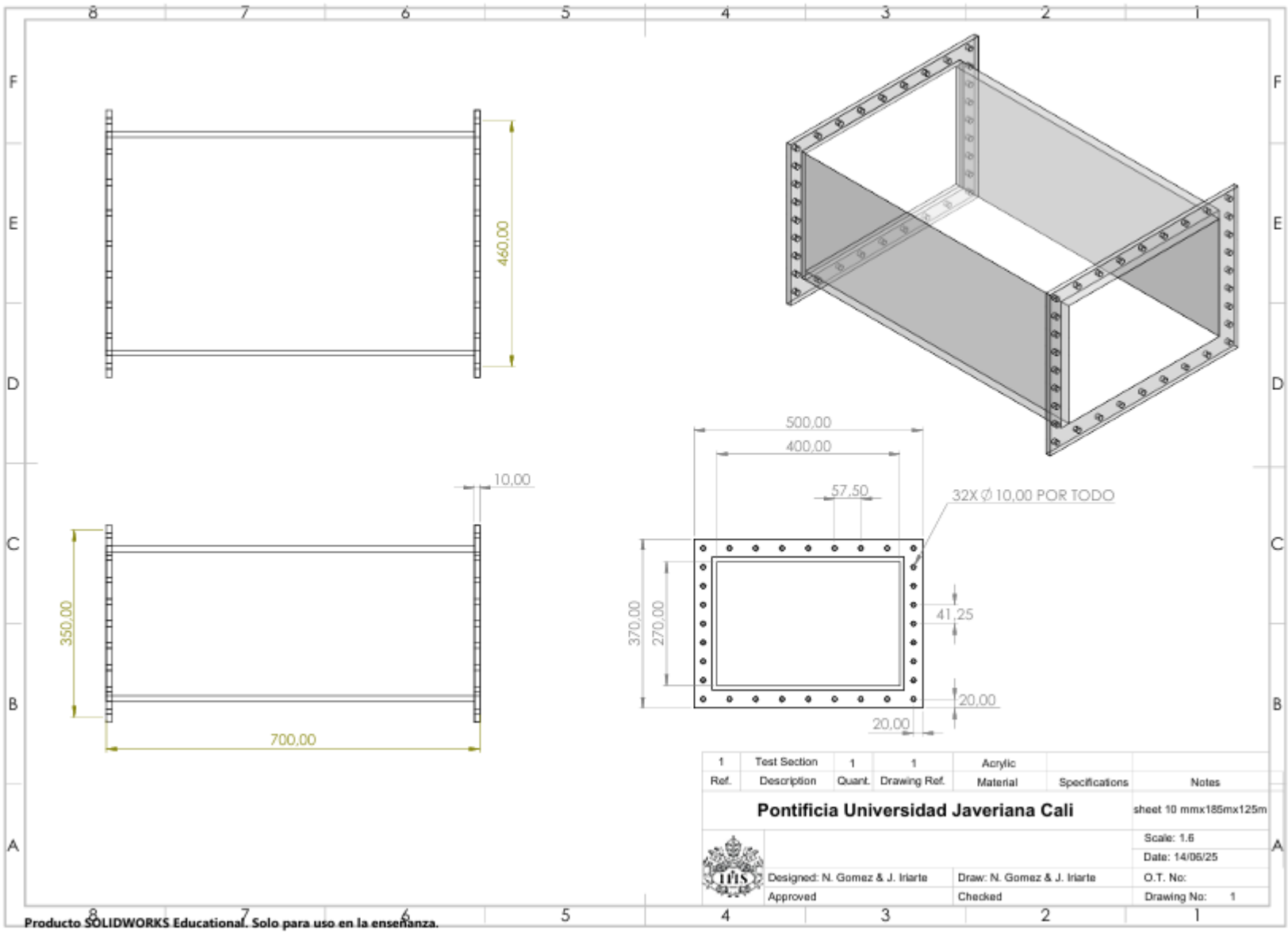
460,00
10,00
350,00
700,00
500,00
400,00
57,50
32X ∅ 10,00 POR TODO
370,00
270,00
41,25
20,00
20,00
1 Test Section 1 1 Acrylic
Ref. Description Quant. Drawing Ref. Material Specifications Notes
Pontificia Universidad Javeriana Cali
sheet 10 mmx185mx125m
Scale: 1.6
Date: 14/05/25
Designed: N. Gomez & J. Iriarte
Draw: N. Gomez & J. Iriarte
O.T. No:
Approved
Checked
Drawing No: 1
Producto SOLIDWORKS Educational. Solo para uso en la enseñanza.

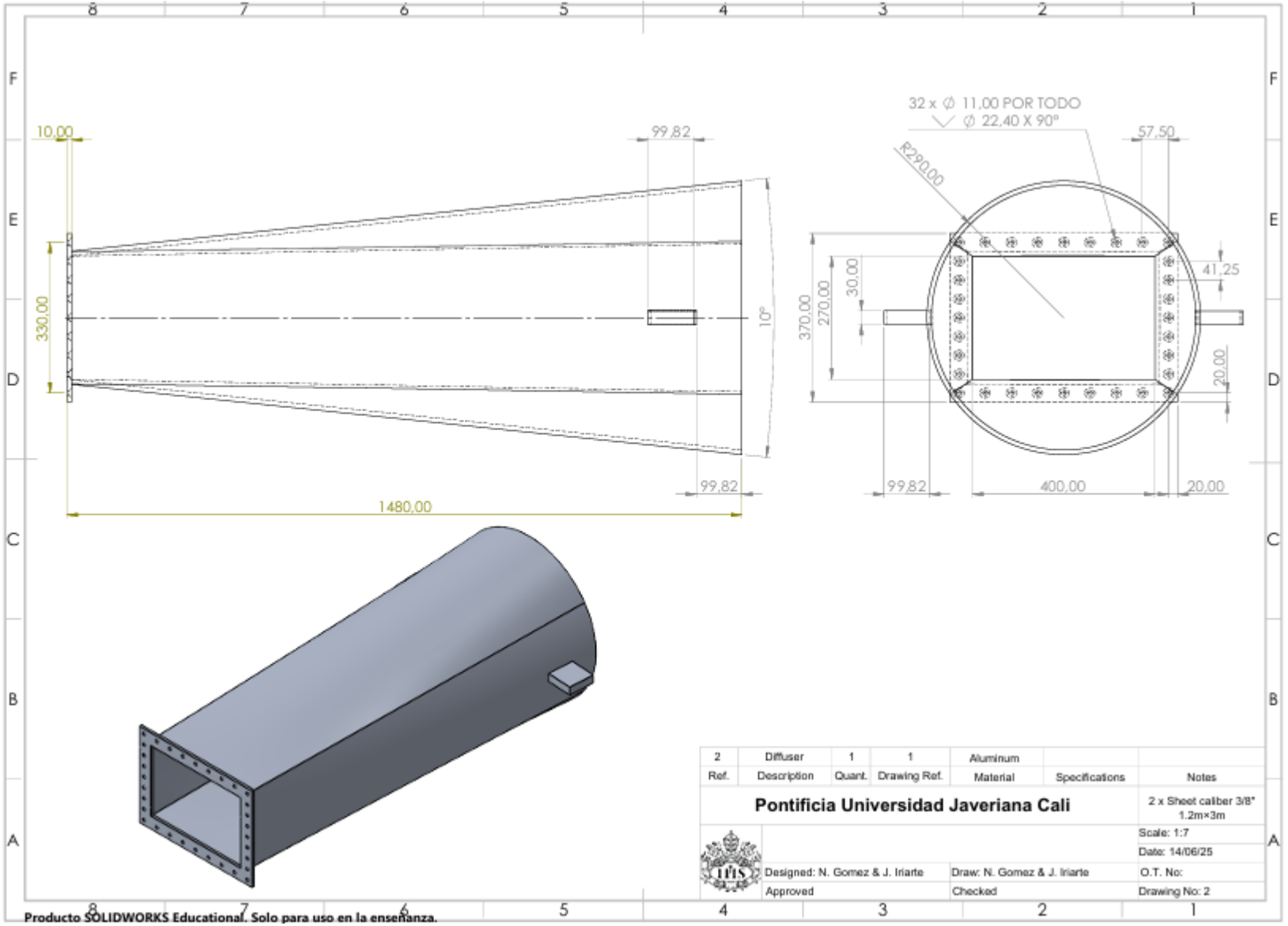
10,00
99,82
330,00
10°
99,82
1480,00
32 x ∅ 11,00 POR TODO
∅ 22,40 X 90°
57,50
R290,00
41,25
370,00
270,00
30,00
20,00
99,82
400,00
20,00
2 | Diffuser | 1 | 1 | Aluminum
Ref. | Description | Quant. | Drawing Ref. | Material | Specifications | Notes
Pontificia Universidad Javeriana Cali
2 x Sheet caliber 3/8" 1.2m×3m
Scale: 1:7
Date: 14/06/25
Designed: N. Gomez & J. Iriarte
Draw: N. Gomez & J. Iriarte
O.T. No:
Approved
Checked
Drawing No: 2
Producto SOLIDWORKS Educational. Solo para uso en la enseñanza.

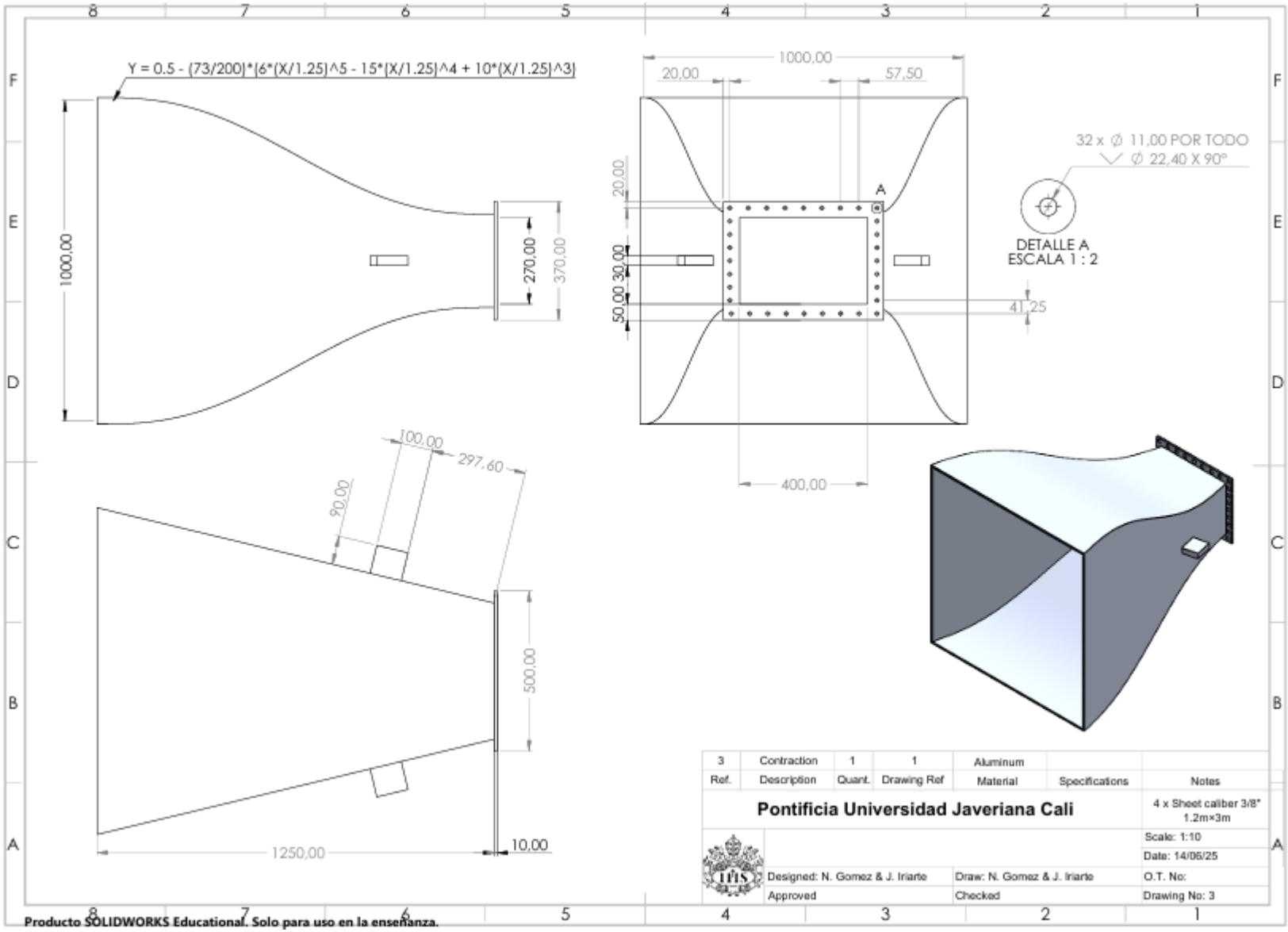
Y = 0.5 - (73/200)*(6*(X/1.25)^5 - 15*(X/1.25)^4 + 10*(X/1.25)^3)
1000,00
270,00
370,00
1000,00
20,00
57,50
20,00
30,00
50,00
A
32 x ∅ 11,00 POR TODO
∅ 22,40 X 90°
DETALLE A
ESCALA 1 : 2
41,25
400,00
100,00
297,60
90,00
500,00
1250,00
10,00
3 Contraction 1 1 Aluminum
Ref. Description Quant. Drawing Ref Material Specifications Notes
Pontificia Universidad Javeriana Cali
4 x Sheet caliber 3/8" 1.2m×3m
Scale: 1:10
Date: 14/05/25
Designed: N. Gomez & J. Iriarte
Draw: N. Gomez & J. Iriarte
O.T. No:
Approved
Checked
Drawing No: 3
Producto SOLIDWORKS Educational. Solo para uso en la enseñanza.

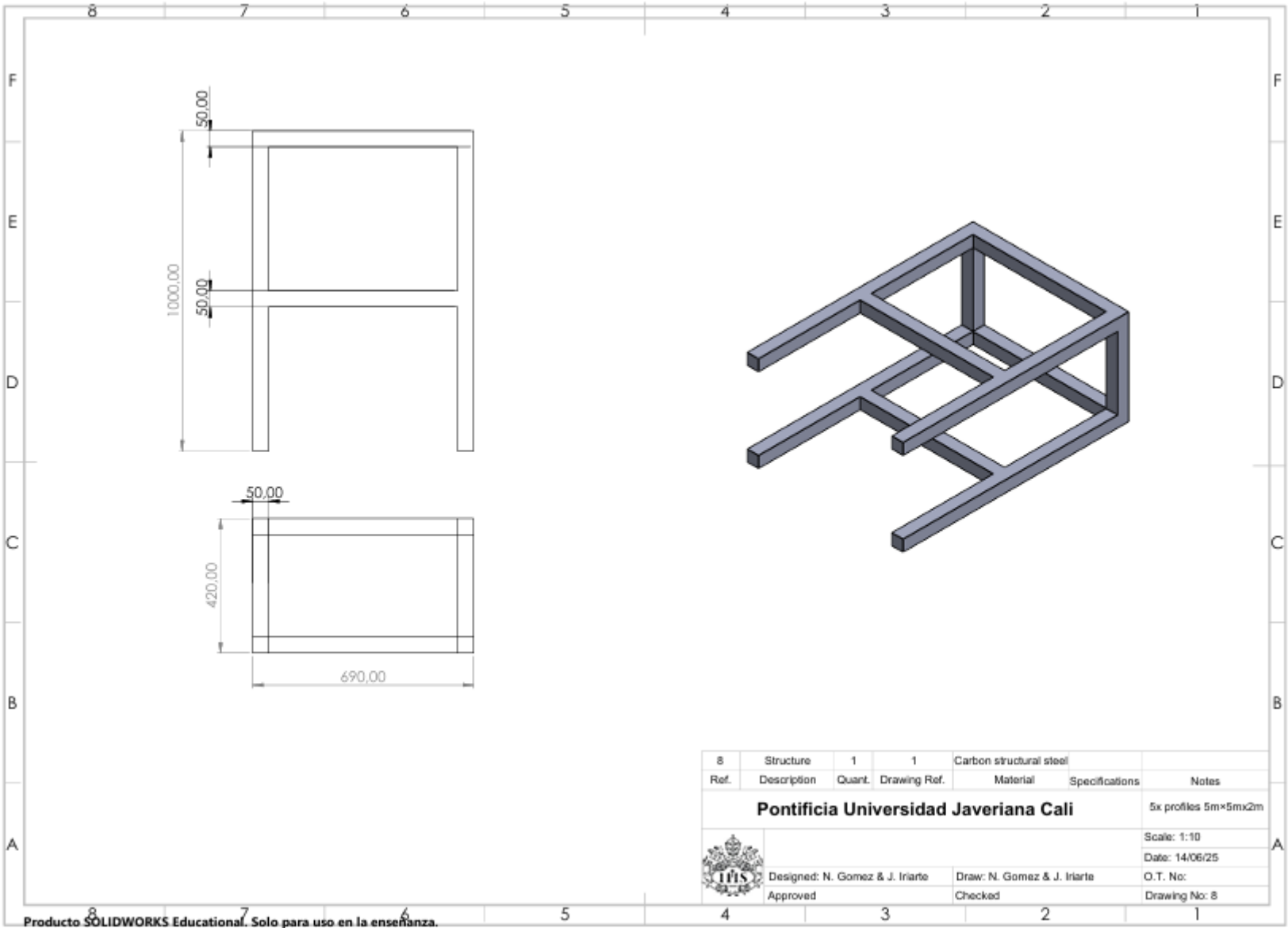
50,00
1000,00
50,00
50,00
420,00
690,00
8 Structure 1 1 Carbon structural steel
Ref. Description Quant. Drawing Ref. Material Specifications Notes
Pontificia Universidad Javeriana Cali
5x profiles 5m×5mx2m
Scale: 1:10
Date: 14/06/25
Designed: N. Gomez & J. Iriarte
Draw: N. Gomez & J. Iriarte
O.T. No:
Approved
Checked
Drawing No: 8
Producto SOLIDWORKS Educational. Solo para uso en la enseñanza.

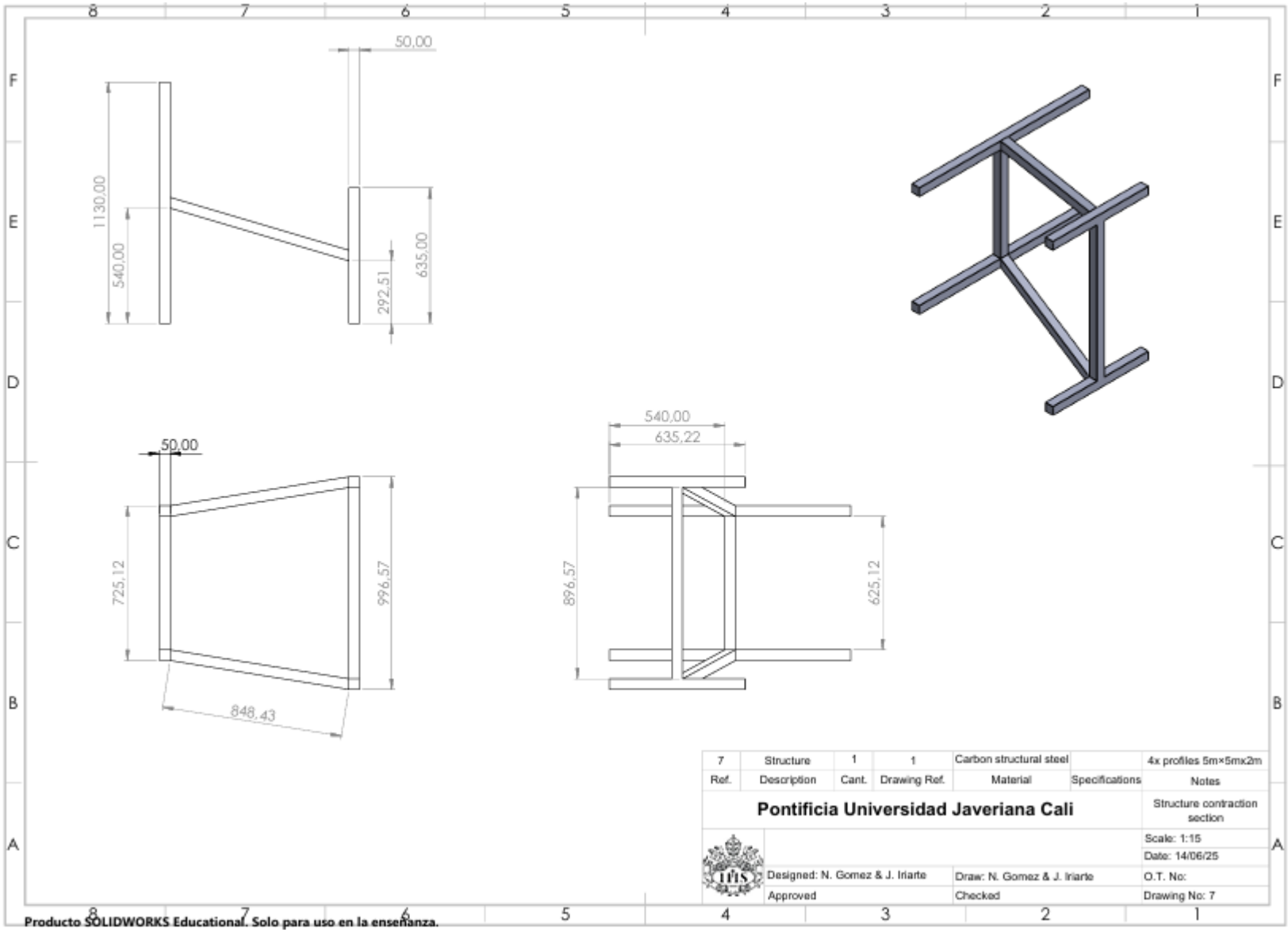
50,00
1130,00
540,00
292,51
635,00
50,00
725,12
996,57
848,43
540,00
635,22
896,57
625,12
7 Structure 1 1 Carbon structural steel 4x profiles 5m×5mx2m
Ref. Description Cant. Drawing Ref. Material Specifications Notes
Pontificia Universidad Javeriana Cali
Structure contraction section
Scale: 1:15
Date: 14/06/25
Designed: N. Gomez & J. Iriarte
Draw: N. Gomez & J. Iriarte
O.T. No:
Approved
Checked
Drawing No: 7
Producto SOLIDWORKS Educational. Solo para uso en la enseñanza.

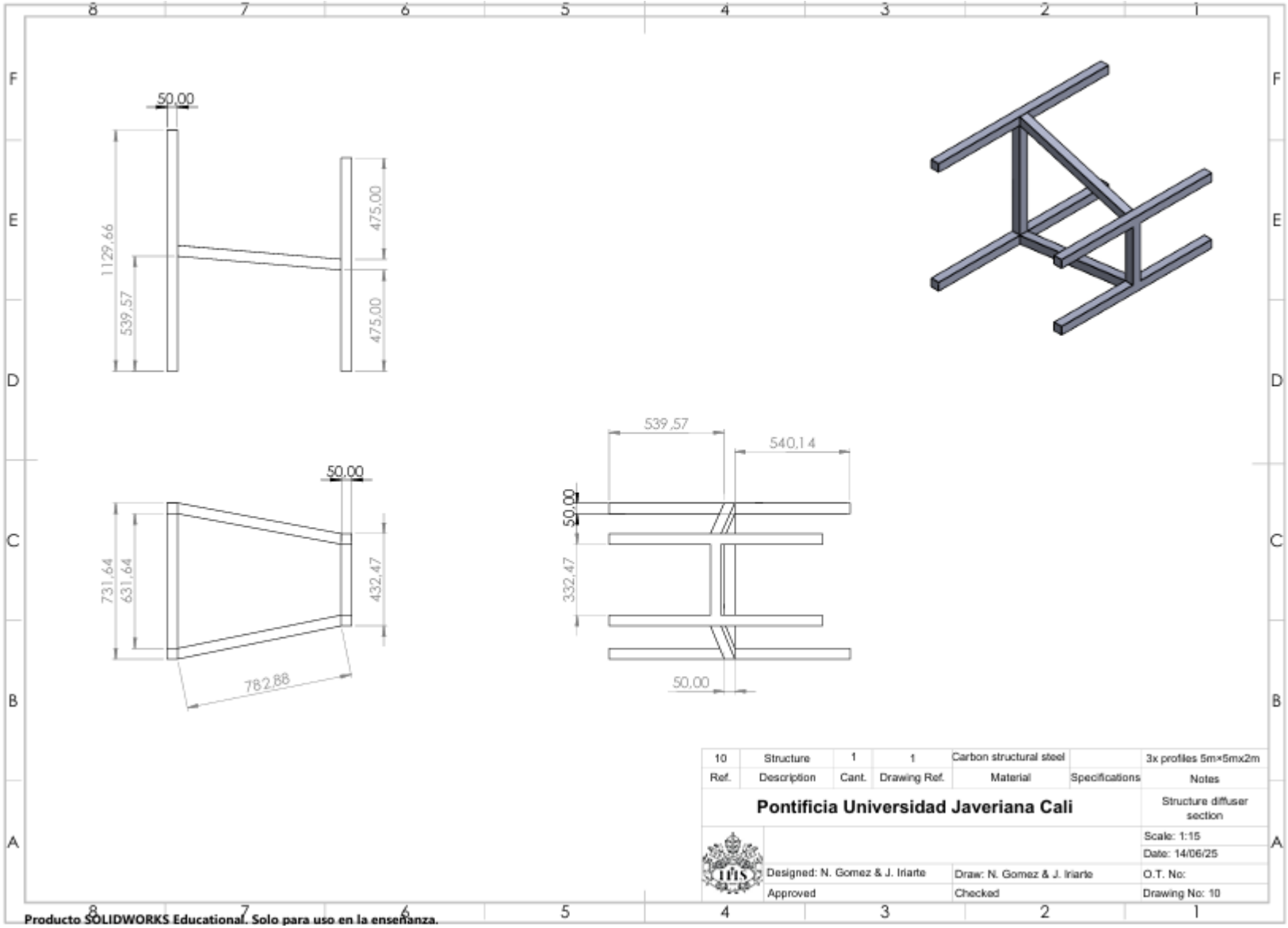
50,00
1129,66
539,57
475,00
475,00
539,57
540,14
50,00
332,47
50,00
50,00
731,64
631,64
432,47
782,88
10 | Structure | 1 | 1 | Carbon structural steel | | 3x profiles 5m×5mx2m
Ref. | Description | Cant. | Drawing Ref. | Material | Specifications | Notes
Pontificia Universidad Javeriana Cali
Structure diffuser section
Scale: 1:15
Date: 14/06/25
Designed: N. Gomez & J. Iriarte
Draw: N. Gomez & J. Iriarte
O.T. No:
Approved
Checked
Drawing No: 10
Producto SOLIDWORKS Educational. Solo para uso en la enseñanza.

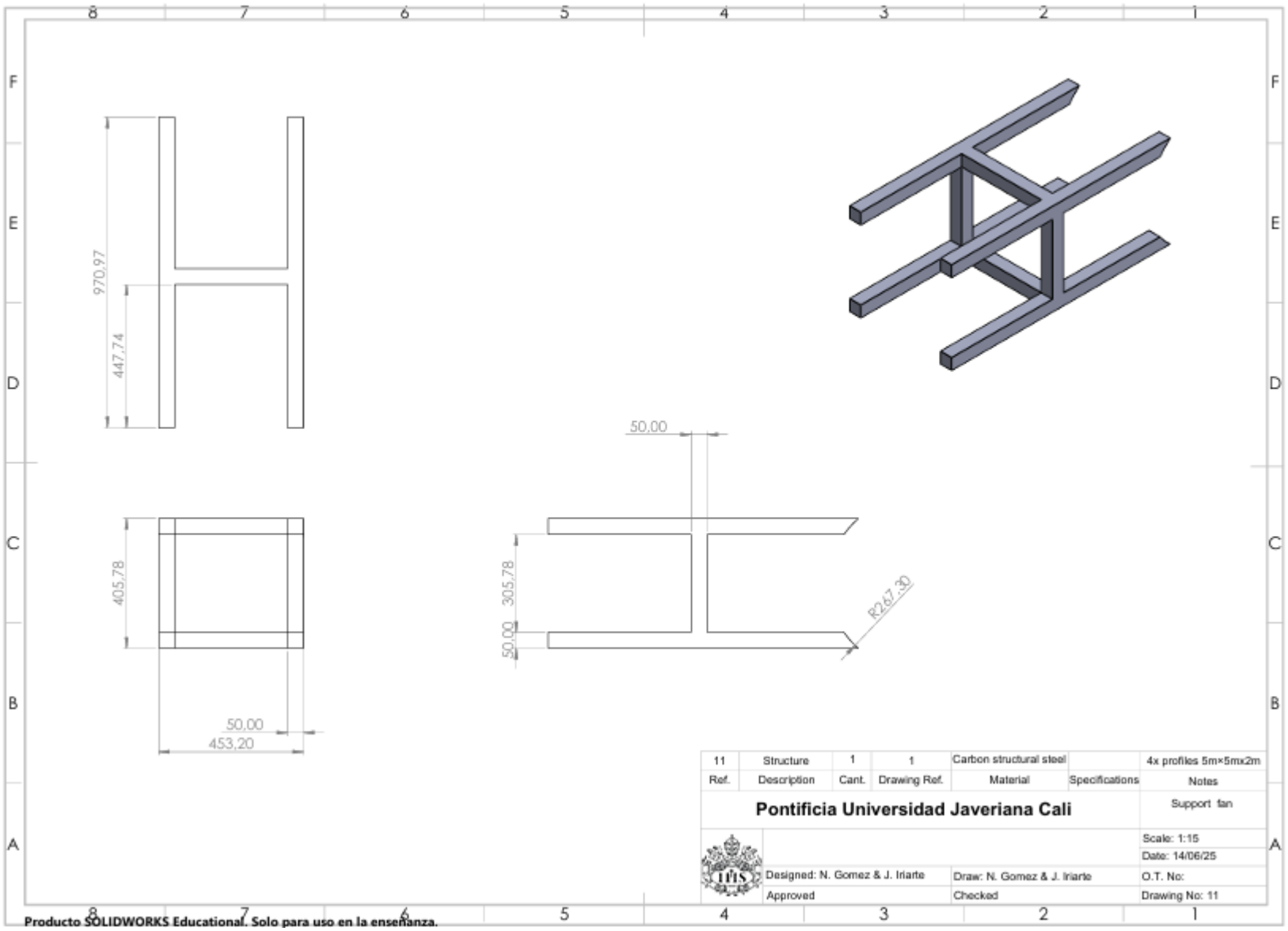

11	Structure	1	1	Carbon structural steel		4x profiles 5m×5mx2m
Ref.	Description	Cant.	Drawing Ref.	Material	Specifications	Notes
	Pontificia Universidad Javeriana Cali					Support fan
						Scale: 1:15
						Date: 14/06/25
	Designed: N. Gomez & J. Iriarte			Draw: N. Gomez & J. Iriarte		O.T. No:
	Approved			Checked		Drawing No: 11

12.3 Appendix 3: PLC Codes

Controller.Micro850.Micro850.MAIN_CONTROL

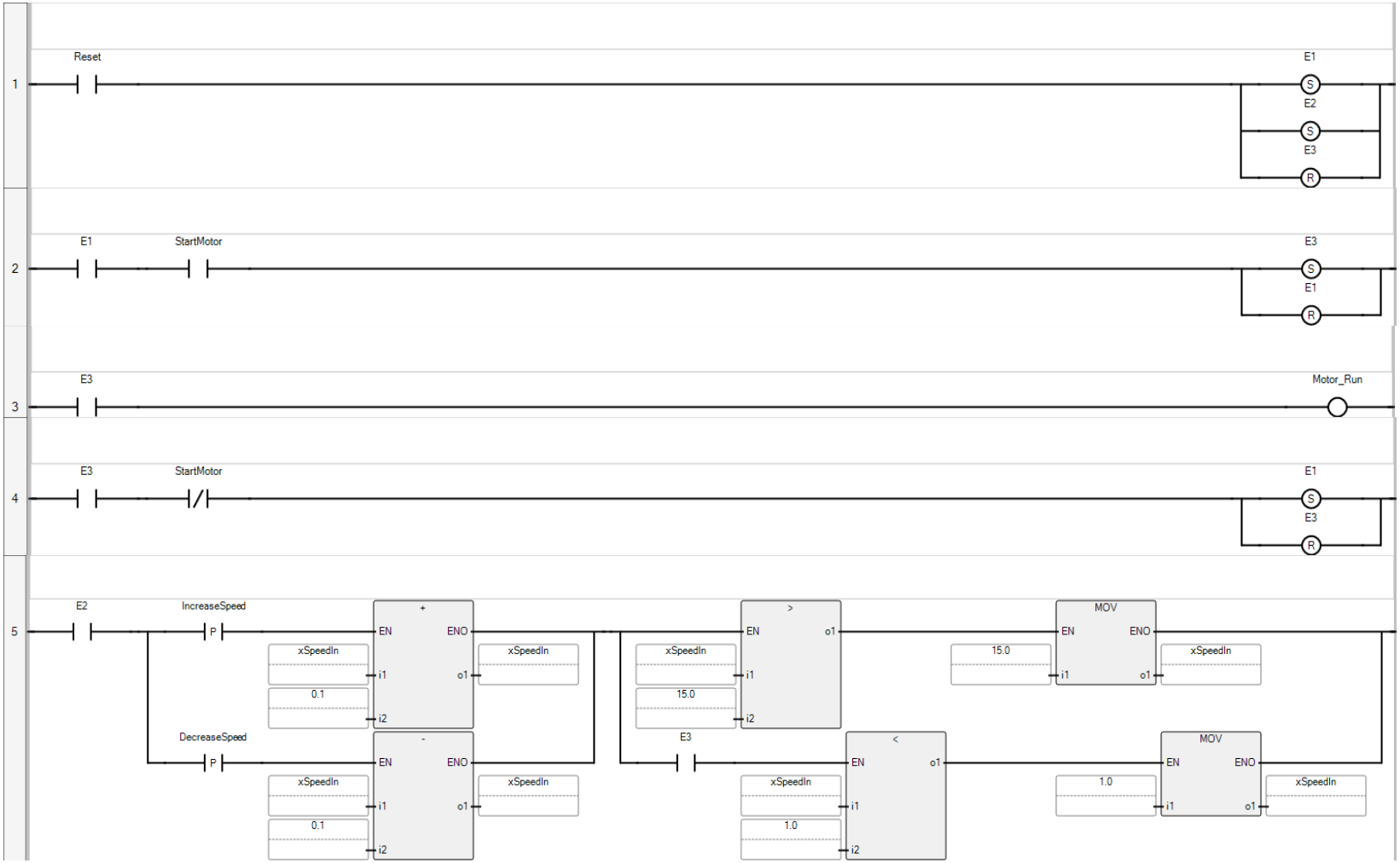

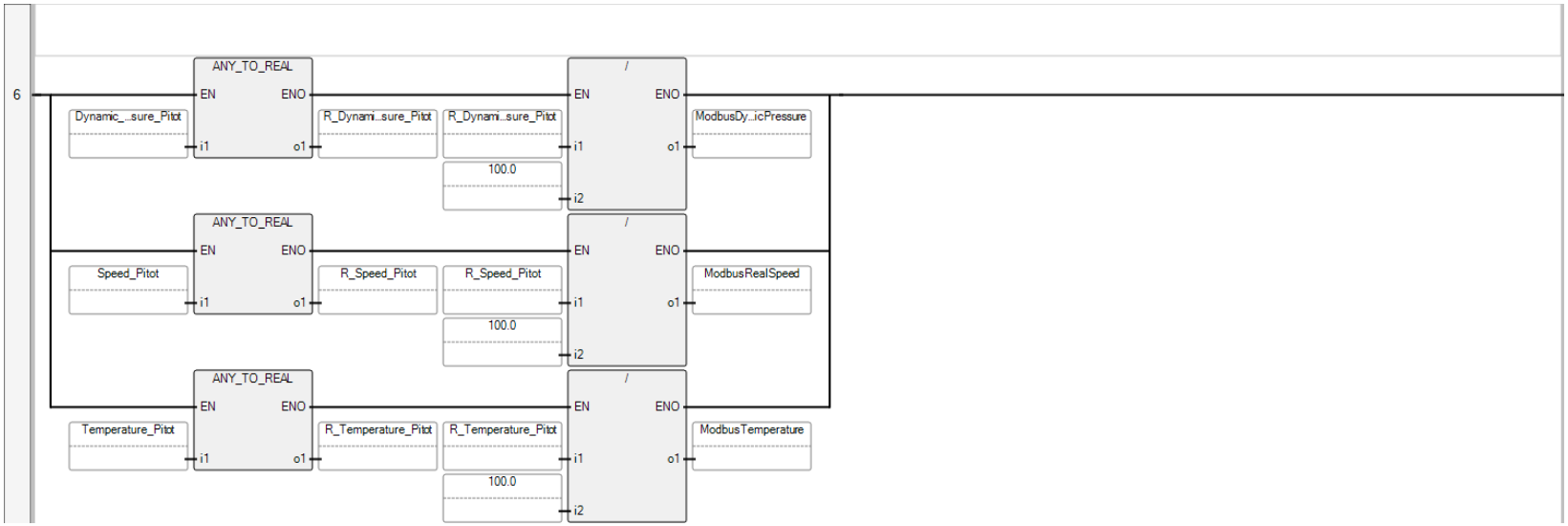
6
ANY_TO_REAL
EN
ENO
Dynamic_...sure_Pitot
i1
o1
R_Dynami...sure_Pitot
/
R_Dynami...sure_Pitot
100.0
i2
ModbusDy...icPressure
Speed_Pitot
R_Speed_Pitot
R_Speed_Pitot
ModbusRealSpeed
Temperature_Pitot
R_Temperature_Pitot
R_Temperature_Pitot
ModbusTemperature

Controller.Micro850.Micro850.TEMPERATURE

```
TempDirectRead:= _IO_P1_AI_00;
TempCelsiusResult3:=(ANY_TO_REAL( TempDirectRead)*(200.0/52428.0)*(21.52/21.42))- 50.62;
```

Controller.Micro850.Micro850.FAN_CONTROLER

```
done := FALSE;

FOR i := 0 TO 7 DO
   IF ((xSpeedIn >= anemometer_speed_table[i]) AND
     (xSpeedIn <= anemometer_speed_table[i+1])) THEN

      x0 := ANY_TO_REAL(anemometer_speed_table[i]);
      x1 := ANY_TO_REAL( anemometer_speed_table[i+1]);
      y0 := ANY_TO_UINT( raw_data_table[i]);
      y1 := ANY_TO_UINT (raw_data_table[i+1]);

      IF (x1 - x0) <> 0.0 THEN
         interpolated_value := ANY_TO_REAL(y0) + (((xSpeedIn - x0) * ANY_TO_REAL(y1 - y0)) / (x1 - x0));
      ELSE
         interpolated_value := ANY_TO_REAL(y0);
      END_IF;

      yDrawDataOut := ANY_TO_UINT(interpolated_value); // Redondeo
      done := TRUE;
      EXIT;

   END_IF;
END_FOR;
```

12.4 Appendix 4: Data Acquisition Module Code

```
#include <ModbusMaster.h>
#include <Wire.h>


#define SENSOR_ADDR 0x28 // I2C address of the DLVR sensor
#define DE_RE_PIN 2 // DE/RE pin on your RS-485 transceiver
#define SLAVE_ID  1 // The Modbus address of your PLC
#define REG_START 0  // Where in the PLC's holding-register map you
start writing (0 → 40001)

// Create a ModbusMaster object
ModbusMaster node;

// Moving average filter parameters
const uint8_t WINDOW_SIZE = 100; // Number of samples in the averaging
window
float maBuffer[WINDOW_SIZE]; // Circular buffer to store recent
pressure values
uint8_t maIndex = 0; // Current index in the circular buffer
bool bufferFull = false; // Flag indicating the buffer has been filled
at least once


unsigned long previousMillis = 0;
const int ModbusInterval = 1000;

uint16_t reg0 = 0;
uint16_t reg1 = 0;
uint16_t reg2 = 0;


// Callback before we transmit a Modbus frame: enable driver
void preTransmission() {
  digitalWrite(DE_RE_PIN, HIGH);
}
// Callback after transmission: disable driver (enter receive mode)
void postTransmission() {
  digitalWrite(DE_RE_PIN, LOW);
```

```
}

void setup() {
  // 1) Set up hardware Serial for RS-485 (8-N-1 @ 9600)
  Serial.begin(9600, SERIAL_8N1);

  // 2) Configure DE/RE pin
  pinMode(DE_RE_PIN, OUTPUT);
  digitalWrite(DE_RE_PIN, LOW);

  // 3) Initialize the ModbusMaster object
  node.begin(SLAVE_ID, Serial);
  node.preTransmission(preTransmission);
  node.postTransmission(postTransmission);

  // --- Initialize I2C for the DLVR sensor
  Wire.begin(); // Start I2C bus as master
  pinMode(A4, INPUT_PULLUP); // Enable internal pull-up on SDA pin
  pinMode(A5, INPUT_PULLUP); // Enable internal pull-up on SCL pin

  // --- Zero out the moving average buffer ---
  for (uint8_t i = 0; i < WINDOW_SIZE; i++) {
  maBuffer[i] = 0.0f;
  }

  // Short delay to allow sensor power-up
  delay(10);
}

void loop() {

  unsigned long Now = millis();

  // --- 1) Read 4 bytes from DLVR: 2 bytes pressure, 2 bytes
temperature ---
  Wire.requestFrom(SENSOR_ADDR, (uint8_t)4);
  if (Wire.available() == 4) {
    uint8_t msb = Wire.read(); // Pressure MSB
    uint8_t lsb = Wire.read(); // Pressure LSB
    uint8_t t_msb = Wire.read(); // Temperature MSB
    uint8_t t_lsb = Wire.read(); // Temperature LSB


    // --- 2) Decode differential pressure from 14-bit reading ---
```

```
    uint16_t raw = (uint16_t(msb) << 8) | lsb;
    uint16_t counts = raw & 0x3FFF; // Mask out the status bits
    float p_inH2O = (int32_t(counts) - 8192) / 6553.0f; // Dynamic
Pressure Transfer Function
    float p_Pa = (p_inH2O * 249.08891f) - 0.982f; // Convert to Pascals
and apply calibration offset


    // --- 3) Decode temperature from 11-bit reading ---
    uint16_t t_counts = (uint16_t(t_msb) << 3) | (t_lsb >> 5);
    float temperature = t_counts * (200.0f / 2047.0f) - 50.85f; //
Temperature Transfer Function


    // --- 4) Update the moving average buffer with the new pressure
reading ---
    maBuffer[maIndex] = p_Pa;
    maIndex = (maIndex + 1) % WINDOW_SIZE;
    if (maIndex == 0) bufferFull = true;


    // Determine how many valid samples we have
    uint8_t validCount = bufferFull ? WINDOW_SIZE : maIndex;
    float sum = 0.0f;
    for (uint8_t i = 0; i < validCount; i++) {
      sum += maBuffer[i];
    }

    float p_avg = sum / validCount; // Compute the average pressure in
Pa


    // --- 5) Compute flow speed using Bernoulli's equation: v = sqrt(2
* ΔP / ρ) ---
    float speed_avg = sqrtf(2.0f * p_avg / 1.184f);


    // --- 6) Prepare scaled values for Modbus registers (to preserve
decimals) ---
    reg0 = uint16_t(p_avg * 100);
    reg1 = uint16_t(speed_avg * 100);
    reg2 = uint16_t(temperature * 100);

  }
```

```
  if (Now - previousMillis >= ModbusInterval) {
    previousMillis = Now;

    //Load them into the ModbusMaster transmit buffer
    node.setTransmitBuffer(0, reg0);
    node.setTransmitBuffer(1, reg1);
    node.setTransmitBuffer(2, reg2);

    //Send a “Write Multiple Registers” (Function 16)
    uint8_t result = node.writeMultipleRegisters(REG_START, 3);

  }


}


// --- Hardware wiring ---
// DLVR Sensor to Arduino:
//   DLVR Pin 1 → GND
//   DLVR Pin 2 → 5V
//   DLVR Pin 3 (SDA) → A4
//   DLVR Pin 4 (SCL) → A5
// RS-485 Module to Arduino UNO:
//   DI → TX (pin 1)
//   RO → RX (pin 0)
//   DE & RE → digital pin 2
//   VCC → 5V
//   GND → GND
```